

8-2019

# Integration of a High Speed Megawatt Class Induction Motor and High Frequency Variable Speed Drive System through Modeling and Simulation

Dean Reuben Nuque Millare  
Clemson University, deanrem@g.clemson.edu

Follow this and additional works at: [https://tigerprints.clemson.edu/all\\_theses](https://tigerprints.clemson.edu/all_theses)

---

## Recommended Citation

Millare, Dean Reuben Nuque, "Integration of a High Speed Megawatt Class Induction Motor and High Frequency Variable Speed Drive System through Modeling and Simulation" (2019). *All Theses*. 3167.  
[https://tigerprints.clemson.edu/all\\_theses/3167](https://tigerprints.clemson.edu/all_theses/3167)

This Thesis is brought to you for free and open access by the Theses at TigerPrints. It has been accepted for inclusion in All Theses by an authorized administrator of TigerPrints. For more information, please contact [kokeefe@clemson.edu](mailto:kokeefe@clemson.edu).

INTEGRATION OF A HIGH SPEED MEGAWATT CLASS INDUCTION MOTOR  
AND HIGH FREQUENCY VARIABLE SPEED DRIVE SYSTEM THROUGH  
MODELING AND SIMULATION

---

A Thesis  
Presented to  
the Graduate School of  
Clemson University

---

In Partial Fulfillment  
of the Requirements for the Degree  
Master of Science  
Electrical Engineering

---

by  
Dean Reuben Nuque Millare  
August 2019

---

Accepted by:  
Dr. Ramtin Hadidi, Committee Chair  
Dr. Curtiss Fox  
Dr. Johan Enslin

## ABSTRACT

With the prominence of high speed, MW class motor usage in various industries such as the petrochemical and natural gas sectors, advancements in related technologies allow for achievable benefits such as increased energy efficiency, compressed power density, and cost savings. A novel high frequency variable speed drive (VSD) and motor system is being developed by Clemson University and TECO-Westinghouse Motor Company through a Department of Energy (DOE) project. In order to test this prototype, a dynamometer setup is required, involving another induction motor, another motor drive, and a gearbox. The system is modeled and simulated through MATLAB/Simulink in order to predict system behavior, control propagation, and protection limits. Individual parts of the system are individually modeled and evaluated before integrating the entire system together in software.

Simulation of the various components involve a plethora of parameters, settings, and topologies to be researched and analyzed. V/Hz is used as the control method for the motors involved in the system. Voltage sources are modeled to represent this method and output desired waveforms. Both speed and torque outputs on the machines are managed in specific manners to evaluate desired performance. Open loop and closed loop controls are explored and expressed through the results. An equation is given to relate the V/Hz setpoints of both high speed and low speed sides of the integrated system to conduct a full load test. Through these simulation efforts, actual system test procedures can be established and safety concerns can be assessed.

## ACKNOWLEDGMENTS

I would like to thank the DOE for their funding of work on this project. This opportunity for research has been a challenging and rewarding experience.

I would also like to acknowledge TECO-Westinghouse Motor Company for providing the manufacturing and testing capabilities to achieve such a technological advancement such as this one.

Thank you to the Energy Innovation Center and its amazing engineers and researchers for all of your support ever since I started as a summer intern.

Much thanks goes to my committee for always being willing to answer my questions, leading me in the right direction, and dealing with my plethora of graphs. Thank you Dr. Enslin for all of your “what-if” suggestions and trust in being a volunteer for your conference. Thank you Dr. Fox for making sure I learned what I needed to and for always giving insight and perspective to the things I was doing. Thank you Dr. Hadidi for always being there for me and encouraging me through all of this.

Thank you to my family for all of the physical, emotional, and monetary support throughout graduate school and life in general.

Lastly, thank you to my wife, Emily, for sticking with me through the hard times and always giving me a goal to strive towards.

## TABLE OF CONTENTS

|   | Page |
|---|------|
| TITLE PAGE .....                                | i    |
| ABSTRACT.....                                   | ii   |
| ACKNOWLEDGMENTS .....                           | iii  |
| LIST OF TABLES .....                            | vi   |
| LIST OF FIGURES .....                           | vii  |
| CHAPTER   |      |
| I.    INTRODUCTION .....                        | 1    |
| Motivation.....                                 | 1    |
| High Speed Induction Motor .....                | 2    |
| High Frequency Variable Speed Drive .....       | 3    |
| Simulation Goals.....                           | 8    |
| Integration of Parts.....                       | 10   |
| Summary.....                                    | 11   |
| II.   INDUCTION MOTORS.....                     | 13   |
| Concept .....                                   | 13   |
| High Speed Induction Motor .....                | 18   |
| Low Speed Induction Motor .....                 | 21   |
| Simulation.....                                 | 25   |
| Summary.....                                    | 47   |
| III.  HIGH FREQUENCY VARIABLE SPEED DRIVE ..... | 48   |
| Theory.....                                     | 48   |
| Standards.....                                  | 52   |
| Active Front End.....                           | 53   |
| Inverter .....                                  | 54   |
| Drive Model .....                               | 56   |
| V/Hz Control.....                               | 65   |
| Simulation Results .....                        | 67   |
| Limitations .....                               | 73   |

| Table of Contents (Continued)               | Page |
|---|------|
| Summary .....                               | 74   |
| IV. INTEGRATION .....                       | 75   |
| Overview .....                              | 75   |
| Coupled IM with Ideal Voltage Sources ..... | 75   |
| Full Load Test Results .....                | 87   |
| Dynamics .....                              | 97   |
| Summary .....                               | 99   |
| V. CONCLUSIONS .....                        | 100  |
| APPENDICES .....                            | 102  |
| A: Excel Validations .....                  | 103  |
| B: No-Load Acceleration Tests .....         | 105  |
| C: MATLAB Parameter File .....              | 108  |
| D: Motor Data .....                         | 115  |
| REFERENCES .....                            | 120  |

## LIST OF TABLES

| Table |  | Page |
|-------|--|------|
| 2.1   | Ideal outputs of HSIM .....                          | 25   |
| 3.1   | Effect of carrier frequency on peak overvoltage..... | 52   |
| 4.1   | PI controller gains for torque control.....          | 83   |
| B.1   | No-load acceleration test parameters .....           | 105  |
| D.1   | HSIM parameters (95°C, 500Hz).....                   | 115  |
| D.2   | HSIM simulated full load test.....                   | 116  |
| D.3   | HSIM locked rotor test (95°C, 500Hz, 2082V) .....    | 117  |
| D.4   | LSIM simulation motor parameters .....               | 118  |
| D.5   | LSIM data .....                                      | 119  |

## LIST OF FIGURES

| Figure   | Page |
|--|------|
| 1.1 PAU topology .....   | 4    |
| 1.2 Front view drawing of new VSD.....                               | 5    |
| 1.3 Generic torque and current curves with respect to speed [1]..... | 7    |
| 1.4 Test setup for HSIM and VSD system.....                          | 8    |
| 2.1 Example torque-speed curve of an induction motor .....           | 14   |
| 2.2 Steinmetz equivalent circuit of induction motor [1].....         | 16   |
| 2.3 Thevenin equivalent circuit of induction motor [1].....          | 16   |
| 2.4 V/Hz relationship between voltage and frequency .....            | 20   |
| 2.5 Uncoupled LSIM on pedestal .....                                 | 22   |
| 2.6 V/Hz curve profile setting on HMI.....                           | 24   |
| 2.7 Asynchronous Machine block [1].....                              | 26   |
| 2.8 Preliminary Simulink model of V/Hz source.....                   | 29   |
| 2.9 Comparison of timing sources for V/Hz operation.....             | 31   |
| 2.10 Updated Simulink model of V/Hz source.....                      | 32   |
| 2.11 HSIM full load test speed output .....                          | 34   |
| 2.12 HSIM full load test speed output zoomed in .....                | 34   |
| 2.13 HSIM full load test voltage input.....                          | 35   |
| 2.14 HSIM full load test voltage input zoomed in.....                | 36   |
| 2.15 HSIM full load test current input.....                          | 37   |
| 2.16 HSIM full load test torque output .....                         | 38   |



List of Figures (Continued)

| Figure  | Page |
|---|------|
| 2.17 Open loop speed control block diagram for HSIM.....              | 39   |
| 2.18 Simulink open loop speed control.....                            | 39   |
| 2.19 HSIM open loop test torque output.....                           | 40   |
| 2.20 HSIM open loop test speed output.....                            | 41   |
| 2.21 HSIM open loop test current input.....                           | 41   |
| 2.22 Laplace domain PI control system.....                            | 43   |
| 2.23 Discrete model of PI controller using the trapezoidal rule ..... | 43   |
| 2.24 Closed loop speed control block diagram for HSIM .....           | 44   |
| 2.25 Simulink closed loop speed control .....                         | 44   |
| 2.26 HSIM closed loop test torque output .....                        | 45   |
| 2.27 HSIM closed loop test speed output .....                         | 45   |
| 2.28 HSIM closed loop test current input.....                         | 46   |
| 2.29 HSIM closed loop test voltage envelope .....                     | 47   |
| 3.1 "Cube" topology [1].....  | 48   |
| 3.2 DPT test circuit with optional snubber .....                      | 51   |
| 3.3 Experimental DPT for 1kV/400A case.....                           | 51   |
| 3.4 Sinusoidal PWM (SPWM).....  | 55   |
| 3.5 Custom blockset for drive modeling.....                           | 58   |
| 3.6 Cube model .....  | 59   |
| 3.7 Isolation transformer model.....                                  | 59   |

## List of Figures (Continued)

| Figure | Page  |
|--------|---|
| 3.8    | Controls model for a single slice ..... 61                    |
| 3.9    | AFE controls for a single cube..... 62                        |
| 3.10   | VSD model..... 63   |
| 3.11   | Updated high level control system..... 64                     |
| 3.12   | VSD output line-to-neutral voltage..... 68                    |
| 3.13   | VSD output line-to-neutral voltage zoomed in..... 68          |
| 3.14   | VSD RL load test current..... 69                              |
| 3.15   | VSD RL load test current zoomed in..... 70                    |
| 3.16   | VSD with HSIM load test speed..... 71                         |
| 3.17   | VSD with HSIM load test torque..... 71                        |
| 3.18   | VSD with HSIM load test current..... 72                       |
| 3.19   | VSD with HSIM load test line-to-line voltage ..... 72         |
| 3.20   | VSD with HSIM load test DC link voltage ..... 73              |
| 4.1    | Simplified system model..... 76                               |
| 4.2    | Effect of decreasing V/Hz value for coupled operation..... 78 |
| 4.3    | Torque control block diagram..... 80                          |
| 4.4    | Effect of $k_p$ in speed loop of torque control ..... 81      |
| 4.5    | Effect of $k_i$ in speed loop of torque control ..... 81      |
| 4.6    | Effect of $k_p$ in torque loop of torque control ..... 82     |
| 4.7    | Effect of $k_i$ in torque loop of torque control ..... 83     |

List of Figures (Continued)

| Figure  | Page |
|---|------|
| 4.8 Controls for simplified system model.....                     | 84   |
| 4.9 Trip modeling for simplified system model.....                | 86   |
| 4.10 Integrated system full load test torque control signals..... | 87   |
| 4.11 Integrated system full load test speed control signals.....  | 88   |
| 4.12 Integrated system full load test frequency reference .....   | 88   |
| 4.13 Integrated system full load test HSIM speed .....            | 89   |
| 4.14 Integrated system full load test LSIM speed.....             | 89   |
| 4.15 Integrated system full load test HSIM torque .....           | 90   |
| 4.16 Integrated system full load test LSIM torque .....           | 90   |
| 4.17 Integrated system full load test HSIM current .....          | 91   |
| 4.18 Integrated system full load test LSIM current .....          | 91   |
| 4.19 HSIM trip frequency reference .....                          | 92   |
| 4.20 HSIM trip speed control.....                                 | 92   |
| 4.21 HSIM trip torque control .....                               | 93   |
| 4.22 HSIM trip LSIM speed .....                                   | 93   |
| 4.23 HSIM trip HSIM speed.....                                    | 94   |
| 4.24 HSIM trip LSIM torque .....                                  | 94   |
| 4.25 HSIM trip HSIM torque.....                                   | 95   |
| 4.26 HSIM trip LSIM voltage.....                                  | 95   |
| 4.27 HSIM trip LSIM current .....                                 | 96   |

List of Figures (Continued)

| Figure |   | Page |
|--------|---|------|
| 4.28   | HSIM trip HSIM voltage .....  | 96   |
| 4.29   | HSIM trip HSIM current.....   | 97   |
| 4.30   | HSIM trip LSIM output torque comparison based on ramp<br>to zero speed .....      | 99   |
| A.1    | Model of equivalent circuit model in Simulink .....                               | 103  |
| A.2    | Spreadsheet for calculations and comparison of equivalent<br>circuit values ..... | 104  |
| B.1    | Torque-speed curve for 3 hp motor .....   | 105  |
| B.2    | Torque-speed curve for 50 hp motor .....  | 106  |
| B.3    | Torque-speed curve for 500 hp motor .....   | 106  |
| B.4    | Torque-speed curve for 2250 hp motor .....  | 107  |
| D.1    | Percent full load torque and current vs. percent speed .....                      | 118  |

# CHAPTER ONE

## INTRODUCTION

### Motivation

In 2013, manufacturing accounted for more than a quarter of the approximately 40% of primary energy consumption in the United States [1]. Electric motor-drive systems utilized much of this energy for industrial processes such as fans and compressors [1]. With the advancement of technologies such as wide bandgap (WBG) devices, improvements in the energy efficiency and power density of these systems can be realized. This challenge is being addressed by the Advanced Manufacturing Office (AMO) of the Department of Energy (DOE) through a Funding Opportunity Announcement (FOA) issued in 2015.

Clemson University was awarded project funding at its research facility in North Charleston, SC. This award was received in partnership with TECO Westinghouse Motor Company (TWMC). Clemson's Energy Innovation Center (EIC) provides mechanical and electrical testing capabilities for wind turbine drivetrains and variable distributed energy resources (DERs). Within the facility are medium voltage, re-engineered motor drives called Power Amplifier Units (PAUs) that are utilized to create a grid emulator for compliance to standards such as IEEE 1547 and UL 1741 [2], [3]. TWMC provides manufacturing and component testing capabilities for the project.

The goal is to create a fully integrated high speed MW class motor and high frequency variable speed drive system [4]. This would be a commercially viable system for high speed industrial applications, where the potential energy savings range from 3%

to 9% if implemented in a majority of motor applications [1]. A major benefit of this setup is that higher speeds are achievable without the use of a gearbox. This removes physical maintenance, losses, and costs to any process that integrates the drive and motor system. However, this requires state-of-the-art advancements in the design of the entire system. The project will investigate the feasibility of advanced magnetic materials, improved insulation, cooling techniques, high speed bearing design, and enhanced conducting [4].

Due to the novelty of this technology, the system may not conform to the limitations of current testing standards of motors and drives. However, the components of the system can be tested against current standards for their desired operating constraints. Complete system performance tests will be conducted at the EIC, including tests on shutdown protection functionality, speed control, loading, dynamometer characterization, and Hardware-in-the-Loop (HIL). Once the system is validated and achieves the proposed specifications, commercialization can commence to implement into the relevant industries.

### High Speed Induction Motor

A main focus area in industry for high speed motors is in the chemical and oil and natural gas sectors [1]. These energy-consuming markets project large growth in the coming future, giving impetus to this project. Conventional induction motors in these applications are limited to lower voltage, speed, and power ratings. However, with the ability to efficiently drive motors at higher voltages, frequencies, and temperatures, significant improvements can be made to these industries and more.

The proposed high speed induction motor (HSIM) is designed to achieve these operating constraints. The HSIM is rated at 1 MW, 4160 V, and 15,000 RPM with a squirrel cage structure [4]. Materials such as Litz wires are analyzed based on their common usage for high frequency applications. Ceramic bearings are considered for their mitigation of friction loss and inherent insulation. Rotor shapes are compared to achieve optimum stress levels during rotation. Combining these innovations, TECO Westinghouse has developed a prototype motor that is being tested based on industry standards. This machine will be controlled by the volts per hertz (V/Hz) method, providing relatively simple speed commands for the motor.

To observe the effects of loading on the HSIM, a dynamometer setup is used. The dynamometer includes a gearbox, a low speed induction motor (LSIM), and a torque transducer. The LSIM is specified at a nominal synchronous speed of 1800 RPM and 1.119 MW power output. This motor will operate in the generating mode to produce a torque load on the HSIM. Through V/Hz control of the PAUs, the desired load torque can be implemented. The gearbox will translate the rotor speeds between 15,000 RPM and 1800 RPM, coupling the two motors. The torque transducer will allow for data collection on the mechanical behaviors of the system. Speed and torque are the main parameters of interest to validate system operation.

### High Frequency Variable Speed Drive

The high frequency variable speed drive (VSD) is an updated iteration of the existing drives at the EIC. The standard PAU utilizes a series connected H-bridge (SCHB)

topology to act as a controllable AC source for grid emulation [5]. It is composed of 8 “slices” connected in series, each with a four-winding transformer and 3 “cubes” to produce the three-phase voltages. Each of the “cubes” contains a three-phase active front end (AFE) input, a DC bus, and a single-phase H-bridge output [6]. The PAUs are grouped into groups of 4 slices to produce a medium voltage output of 4160 V, with overvoltage capabilities. The PAU topology can be seen in Figure 1.1.

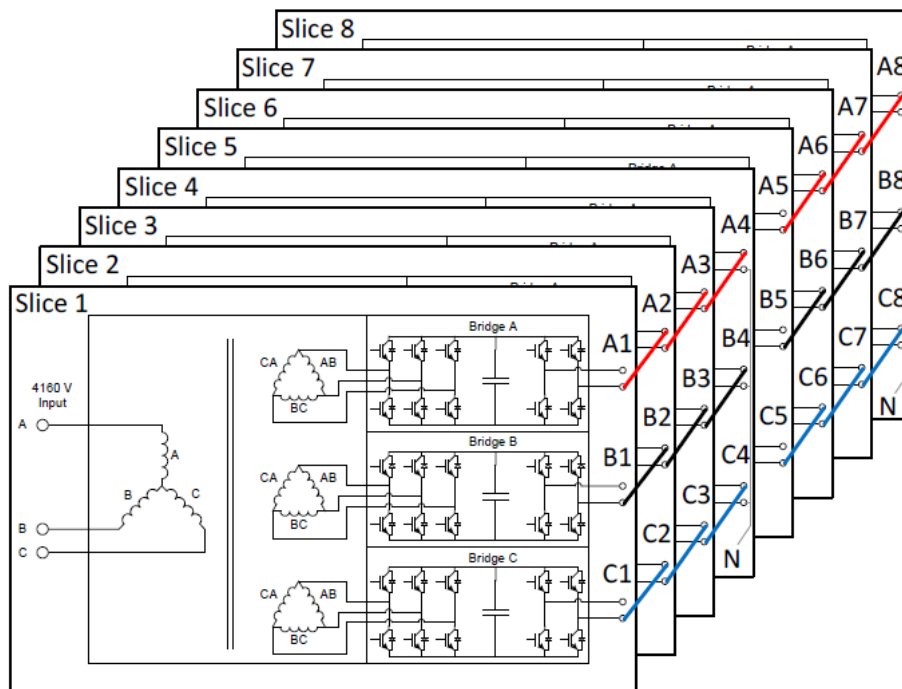


Figure 1.1: PAU topology



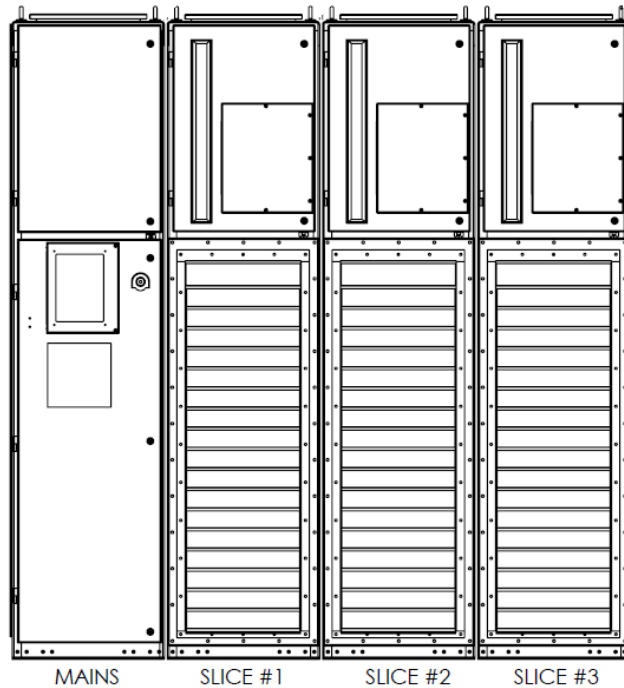


Figure 1.2: Front view drawing of new VSD

The new VSD is designed with only 3 slices, not needing excessive overvoltage functionality. A drawing of the front view of the drive can be seen in Figure 1.2. The inverter is designed to upgrade the switching devices from silicon (Si) MOSFETs to silicon carbide (SiC) MOSFETs. This allows the H-bridge topology to operate at higher voltages, switching frequencies, and temperatures. Although these improvements are applied at the device level, the modular nature of the VSD allows these benefits to be realized at the system level as well. The modularity also provides practical servicing for any issues and device failures.

Although VSDs are being used in industry today, their capabilities are rather limited in terms of voltage and power. The advancement of WBG devices, such as SiC, has created

a stronger case towards achieving more energy efficient and power dense drives. This new VSD and HSIM system will provide a substitute for many high speed applications. This VSD can also provide energy savings to other MW class motors that are normally driven by a fixed speed drive. The potential wasted energy can range from 30% to 80% in mechanical throttles for running a motor at a fixed speed [1]. Speed control with faster switching speeds will allow for decreasing these losses in any relevant application.

V/Hz will be realized in the controls for the VSD. By controlling the voltage and frequency of the input to the HSIM, a soft start to the motor can be achieved. This soft start is necessary to mitigate large inrush currents to the motor, especially with the high operational power levels. A control loop can be included in implementation to manage the frequency command based on current limits [7]. Figure 1.3 shows a family of curves representing the torque and current response at different operating frequencies. It shows that if the example drive outputs nominal voltage and frequency, the current draw of the motor will be near 600% of the rated current. However, if the operating frequency increases from zero to rated, the current draw can be limited to within 150% current.

The pulse-width modulation (PWM) technique can manipulate the voltage and frequency by changing the modulation signal. This signal is a sinusoidal waveform that provides a reference for the three-phase voltage output of the VSD. Depending on the desired speed performance, the modulation signal must be adjusted according to the motor characteristics. Since the speed of the motor is essentially proportional to the drive output frequency, the frequency signal can be changed proportionally to the desired speed. In this way, the speed of the HSIM can be regulated to better serve the load.

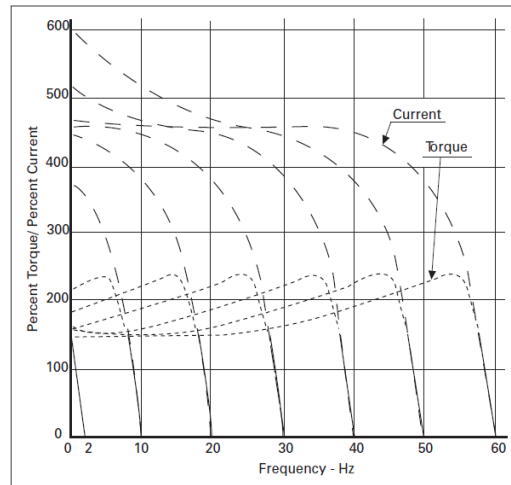


Figure 1.3: Generic torque and current curves with respect to speed [1]

Both the new VSD and the PAUs will be used in the project scope. The PAUs will provide interfaces on both sides of the test setup as shown in Figure 1.4. PAU 1 is designated as the motor drive for the dynamometer subsystem. It will be used to bring the LSIM up to speed and regenerate power to act as a load. PAU 4 will operate as the emulated grid interface for the VSD. This will allow for grid interconnect testing of the drive, evaluating its response to voltage sags, faults, etc. Everything in the dotted lines are the devices being brought to the test facility. The new VSD would normally be coupled to the step-down transformer, but for evaluation purposes, is buffered through PAU 4.

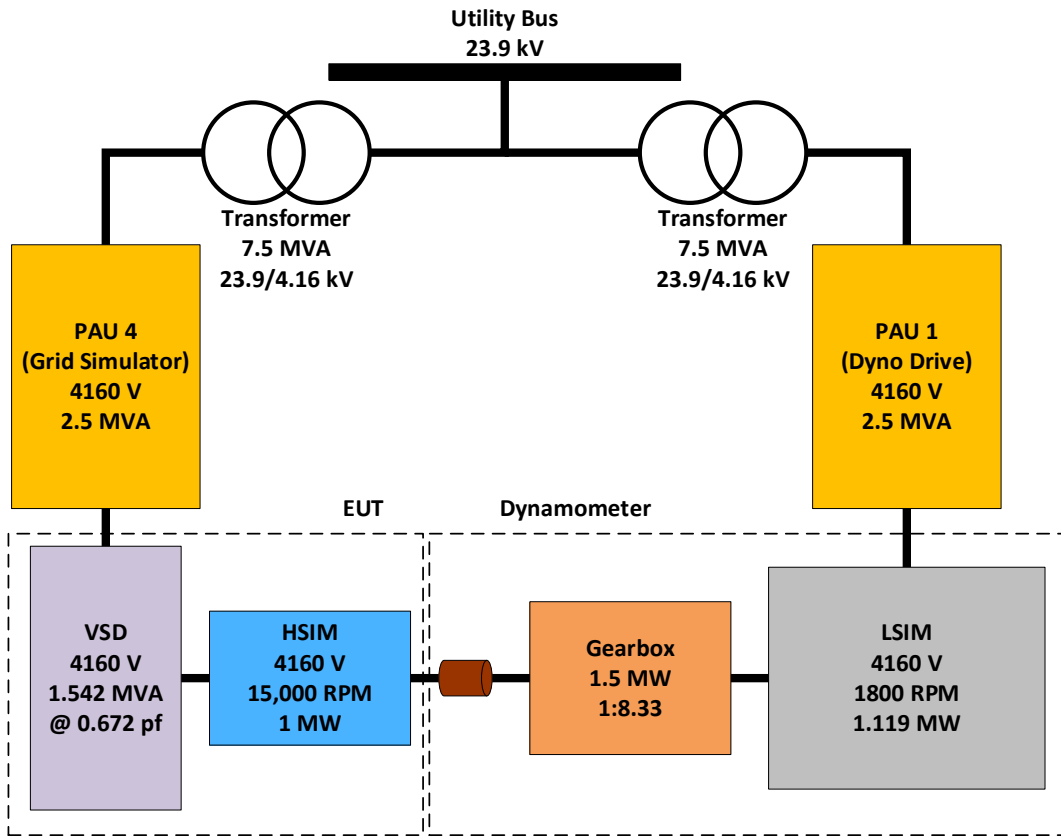


Figure 1.4: Test setup for HSIM and VSD system

### Simulation Goals

In order to predict the independent and coupled behaviors of the new motor and drive, a time-domain simulation platform is employed. MATLAB/Simulink is chosen as the software for modeling based on its capabilities and previous work experience. Integration of the two devices into a single simulation environment is necessary to identify possible operational issues, electromagnetic idiosyncrasies, safety concerns, and more. In this manner, a full system analysis can be conducted to evaluate key performance criteria of the model and be used to upgrade future iterations of the system and its operation.

Within the modeling environment, a model for the induction motor must be utilized to reflect practical applications of a motor. The high frequency voltage on the stator must be translated throughout the model without neglecting ramifications because of frequency. Included parameters for the motor model must be obtainable through standard testing of the actual motor. Initializations must be possible in order to simulate a multitude of test cases based on normal operational points.

The actual VSD design is derived from the existing PAUs at the EIC. The PAUs have existing blocks and models created for grid testing application [6]. However, due to the modular configuration of the PAU, different voltage and power levels can be achieved based on the system topology. For high speed motor operation, the VSD is designed with three modules instead of the usual four in the PAUs. This simple change requires significant inspection on the preexisting modeling endeavors to create the new three slice setup.

The gearbox provides a mechanical means of coupling the HSI and the dynamometer. In simulation this can be done through numerical means, rather than modeling the physical behaviors of the gearbox. Since the gearbox is a means of translating mechanical behaviors between the high and low speed sides of the system, it can be simplified into a gain ratio. In this way, the simulation can focus its computational resources on the actual devices under test, the VSD and HSI.

The controls for the whole system must be modeled to produce comparatively realistic operation. These considerations will exist mainly in the VSD and PAU modeling. Voltage outputs must be determined by desired test applications. Startup sequences must

be commanded to run to full speed without alarms and tripping. Speed and torque control with PI controllers are necessary features to be included for the HSIM and LSIM, respectively. Safe shutdown procedures must be observed to act within the protection limits.

### Integration of Parts

Creating the integrated simulation requires comprehensive modeling of all the necessary parts. The drive must be altered and validated, the motor model must produce accurate results, and the controls must be included in an accessible manner. The various interacting pieces to the model must be evaluated individually before complete integration. Therefore, the design process will involve iterations of assessments on the individual components to gradually develop the full model. Once the integrated model is created, test cases can be implemented to observe possible behaviors of the system as a whole.

Two main simulations are created for different purposes. One model includes the motors coupled by the gearbox ratio, a controllable three-phase voltage source, and the control loops for speed and torque control. This model is prepared for relatively short simulation times, in the range of minutes, to evaluate different iterations of testing operation. From changing PI gain values to tripping one of the drives, this model allows quick changes in parameters to observe the relevant effects. The other model is designated as the detailed model. This is because of the inclusion of the comprehensive drive modeling being used instead of the ideal voltage sources. This model is intended for simulations that have already been validated through the faster model. Transients, dynamics, and high

frequency effects can be better analyzed because of the smaller time step and faster switching activity. Both models are useful to predict behaviors of the actual system. Then, with actual data to compare against, further improvements can be made to the modeling.

This modeling endeavor serves to create a comprehensive method to predict system behaviors and issues. With both motors coupled together and connected to their respective drives, it allows for a single simulation to verify desired performance specifications for the whole system. Voltage, current, speed, and torque can be easily logged and analyzed for any anomalies due to high frequency operation. Safe startup settings can be established through simulation to use as a reference for actual testing of the system. Any test that may want to be executed on the real system can be evaluated in simulation first, to create any precautions before putting the motors and drives at risk. General troubleshooting can also be done in simulation so that the system does not have to be stressed by repeated operation. The modeling and simulation of this system provides a virtual double where much understanding, experimentation, and theorizing can be done in parallel with the actual test setup.

### Summary

This chapter establishes the scope of a DOE project for a prototype motor and drive system for high speed, MW level operation. Introductions for the advanced technologies and novel testing techniques for such a system are given. The focus of simulation is provided to express the challenges and necessities for accurate representation of the various devices under test. With all the modeling incorporated in a single simulation, system

evaluations can be done while analyzing electrical and mechanical phenomenon simultaneously.

The structure of this thesis will start with explanations and theoretical constraints on the two prototype devices, the motor and drive. In each chapter, the fundamental concepts are divulged and their modeling ramifications are given. Results are included to exhibit conformity to the overall system design. Once the motor and drive models are evaluated separately, they will be integrated into a single simulation. Realistic considerations of coupling the components are addressed and the modeling requirements that arise will be expressed. Tests of the whole system will be done through software to predict the practicality of the various control methods. Lastly, simulation results are given to support the achievability of the prescribed experiments and the system as a whole.



## CHAPTER TWO

### INDUCTION MOTORS

#### Concept

Induction motors are composed of two main parts, the stator and the rotor, separated by an air gap [9]. The rotor is mounted on bearings to alleviate friction during rotation. Two types of rotors exist for induction motors, wound and squirrel-cage. Both the stator and rotor have windings which carry alternating current (AC) during operation. Induction motors derive their name from the magnetic field of the stator windings electromagnetically inducing an opposing current in the rotor. According to Lenz's Law, this induced rotor current also creates an opposing magnetic field on the rotor [9]. This causes the rotor to accelerate in the direction of the stator's magnetic field until the induced current and torque balance against the motor load. An induction motor always operates below the synchronous speed of the motor because if the stator magnetic field and the rotor were spinning at the same speed, there would be no induced current in the rotor. This difference in synchronous and actual speed is referred to as the "slip",  $s$ , of the motor as shown in (2.1). This value of slip can be found through is normally designated as a decimal value or percentage of the nominal synchronous speed of the motor. The synchronous speed,  $n_s$ , of the motor is dependent on the frequency applied to the stator,  $f_s$ , and the number of poles,  $p$ , as shown in (2.2).

$$s = \frac{n_s - n_m}{n_s} \quad (2.1)$$

$$n_s = \frac{120f_s}{p} \quad (2.2)$$

The National Electrical Manufacturers Association (NEMA) has categorized the different types of induction motors based on their size, application, and electrical type [10]. Further categorization is made for polyphase, squirrel-cage induction motors [10]. Speed and torque of the rotor are a couple of distinguishing characteristics that make induction motors versatile in the industrial environment. The two are commonly depicted in a single plot with torque on the vertical axis and speed on the horizontal axis, as shown in Figure 2.1.

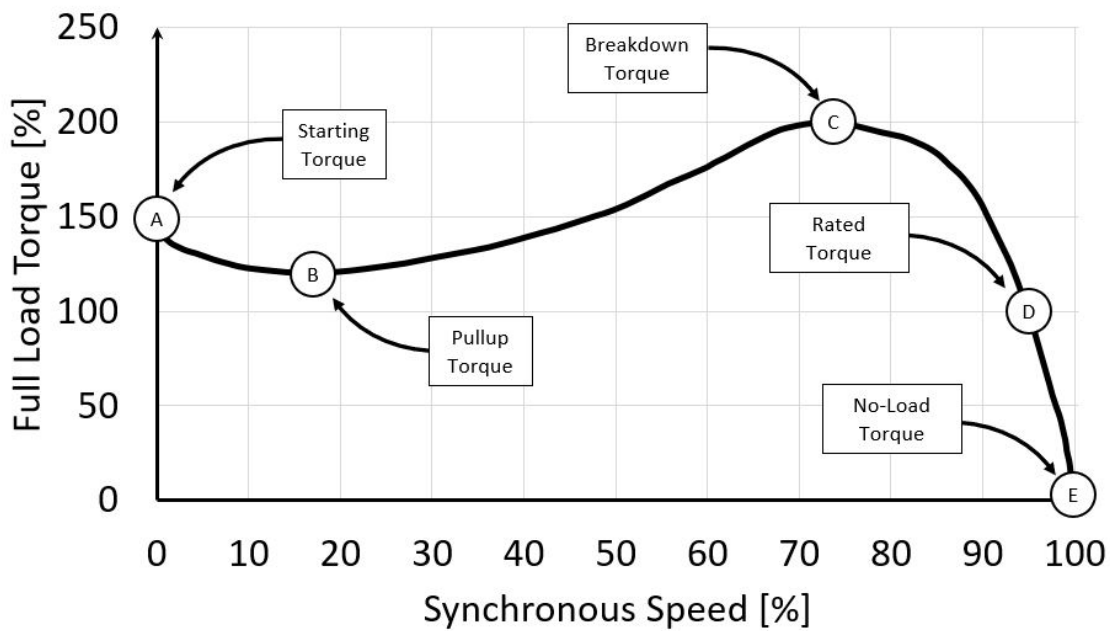


Figure 2.1: Example torque-speed curve of an induction motor

The shape of the curve has five points of significance. The starting torque is the amount needed to overcome the inertia of a still motor. Here, the slip is 100%, expressing the magnetic fields of the stator and rotor have no interaction. The pull-up torque is not always an explicit operating point, but when applicable, it is the minimum amount of torque

developed as the motor accelerates towards rated speed. The breakdown torque is the peak amount of torque the motor can produce. The rated torque is a nominal value that the motor is specified to handle at a specified nominal speed and slip. This is also the motor's upper bound for a safe operating area. Although the motor can produce more torque, it should not be operated for extended periods of time above this value. Lastly, the no-load torque expresses the condition where the motor is not coupled to any type of load. Here, the motor spins at near synchronous speed with a slip of virtually 0%.

To model the operation of an induction motor, an equivalent circuit can be used to mathematically relate the input voltage to the machine and the output slip, torque, and speed. Figure 2.2 shows this circuit representation with resistors and inductors, which is similar to that of a single-phase transformer model. All circuit components are referred to the stator, evident in the designation of components with an apostrophe. The circuit is composed of representations for the stator, core, and rotor each designated in the subscript by "s", "c", and "r", respectively. The core includes a magnetizing reactance component designated " $X_m$ " and a resistance " $R_c$ " to represent iron core losses in the machine. The stator and rotor each have a leakage reactance component as well. The slip of the motor is designated by the "s" term, thus designating the speed and torque output of the motor.

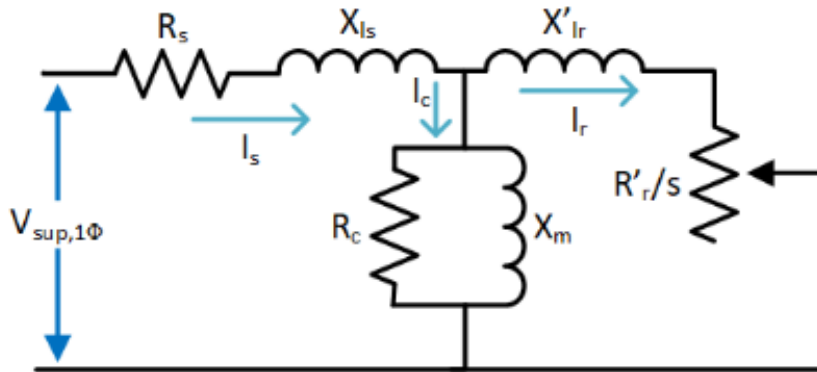


Figure 2.2: Steinmetz equivalent circuit of induction motor [1]

For additional simplifications in computations, a Thevenin equivalent circuit can be used. This circuit provides a series circuit modeling the output behaviors of an induction motor. The rotor side of the circuit remains the same, while the stator and core are combined to create the new Thevenin equivalent impedances. The circuit can be seen in Figure 2.3. Through circuit analysis the equations for  $V_{th}$ ,  $R_{th}$ , and  $X_{th}$  can be derived and are shown in (2.3), (2.4), and (2.5).

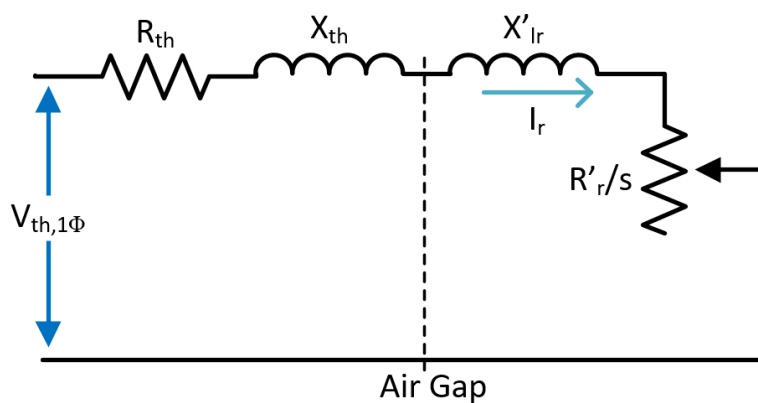


Figure 2.3: Thevenin equivalent circuit of induction motor [1]

$$V_{th,1\phi} = V_{sup,1\phi} * \frac{X_m}{[R_s^2 + (X_{ls} + X_m)^2]^{1/2}} \quad (2.3)$$

$$R_{th} = \frac{R_s X_m^2}{R_s^2 + (X_{ls} + X_m)^2} \quad (2.4)$$

$$X_{th} = \frac{X_m (R_s^2 + X_{ls}^2 + X_{ls} X_m)}{R_s^2 + (X_{ls} + X_m)^2} \quad (2.5)$$

Based on a given input voltage, frequency, and slip of the machine, calculations can be done to find the currents flowing in the machine, power output and losses, and torque outputs [9]. (2.6) expresses the single-phase mechanical output power of the motor at a given slip. The developed mechanical torque at a given slip can be found in (2.7). Both of these values can be multiplied by a factor of three to achieve the three-phase equivalent output. The expression for output torque can be manipulated to find the breakdown torque of the motor and the slip at which it occurs, as shown in (2.8) and (2.9).

$$P_{mech} = I_r'^2 \frac{R'_r}{s} (1 - s) \quad (2.6)$$

$$\tau_{mech} = \frac{30}{\pi n_s} \frac{V_{th,1\phi}^2}{(R_{th} + \frac{R'_r}{s})^2 + (X_{th} + X'_{lr})^2} \frac{R'_r}{s} \quad (2.7)$$

$$\tau_{max} = \frac{15}{\pi n_s} \frac{V_{th,1\phi}^2}{R_{th} + [R_{th}^2 + (X_{th} + X'_{lr})^2]^{1/2}} \quad (2.8)$$

$$s_{\tau_{max}} = \frac{R'_r}{[R_{th}^2 + (X_{th} + X'_{lr})^2]^{1/2}} \quad (2.9)$$

Using these theories, equations, and modeling considerations, simulation of the HSIM and LSIM can be achieved. These equations provide an evaluation for standard values that will occur in the motors. Both electrical and mechanical references can be used to verify dynamic simulation of these devices.

## High Speed Induction Motor

Through Maxwell 3D Transients simulations, parameters for the induction motor model are found. Using the design constraints aforementioned, this electromagnetic domain solver provides values of the HSIM operating at full load. Also, the equivalent circuit parameters are derived using the locked rotor impedance test [11]. The values are referred to the stator and calculated at a condition of 95°C and 500Hz. The parameters found for the HSIM can be found in Appendix D.

These values are used as a benchmark to assess the simulations of the HSIM. Due to limitations of modeling, various assumptions will be made in order to obtain a reasonable simulation of the system as a whole. An example will be in the losses of the machine itself. The total amount of losses may have to be manually added towards any power loss calculations made in the simulation. Since these values are given during a certain operation of the HSIM, they are technically only valid during such conditions. Assumptions made to interpolate behaviors will be addressed to have as accurate a model as possible.

It is advantageous to model the HSIM through use of the dq reference frame. This change of variables eliminates all time-varying inductances by referring motor variables to a frame of reference that may or may not rotate [12]. In the dq reference frame, variables such as three-phase voltages can be represented as constant, DC signals instead of sinusoidal AC signals because of the new reference. This makes computations and controls more straightforward. Conversions from the abc to the dq reference frames can be generalized by a matrix transformation as shown in (2.10). This transformation is to an arbitrary reference frame rotating at some speed,  $\omega$ . Here, “f” represents any three-phase

machine variable such as voltage or current. The angular displacement of the reference frame is represented by  $\theta$ .

$$\begin{bmatrix} f_{qs} \\ f_{ds} \\ f_{0s} \end{bmatrix} = \frac{2}{3} \begin{bmatrix} \cos \theta & \cos\left(\theta - \frac{2\pi}{3}\right) & \cos\left(\theta + \frac{2\pi}{3}\right) \\ \sin \theta & \sin\left(\theta - \frac{2\pi}{3}\right) & \sin\left(\theta + \frac{2\pi}{3}\right) \\ \frac{1}{2} & \frac{1}{2} & \frac{1}{2} \end{bmatrix} \begin{bmatrix} f_{as} \\ f_{bs} \\ f_{cs} \end{bmatrix} \quad (2.10)$$

The reference frame speed,  $\omega$ , is important for observation of induction motors. If  $\omega$  equals zero, then the abc values are referred to the stationary reference frame, not providing much simplification. However,  $\omega$  can be set to rotate at the same rate as the stator electrical frequency, which would express the stator variables as DC signals if balanced. Rotor variables can also be observed as DC signals if the reference frame rotates at the same rate as the rotor shaft. Depending on which variables are of most interest, the reference frame can be set accordingly.

Given the topology of an induction motor, various control schemes can be implemented to achieve certain operations and outputs of speed and torque. Volts per hertz (V/Hz) is used in this case to simplify the system level control method of the induction motor. The efficiency of speed control for the HSIM is relatively negligible with respect to the fact that the applications of such a motor will generally be constant operation at rated speed and load. However, this modeling exercise in control is presented to show the capability of such a system.

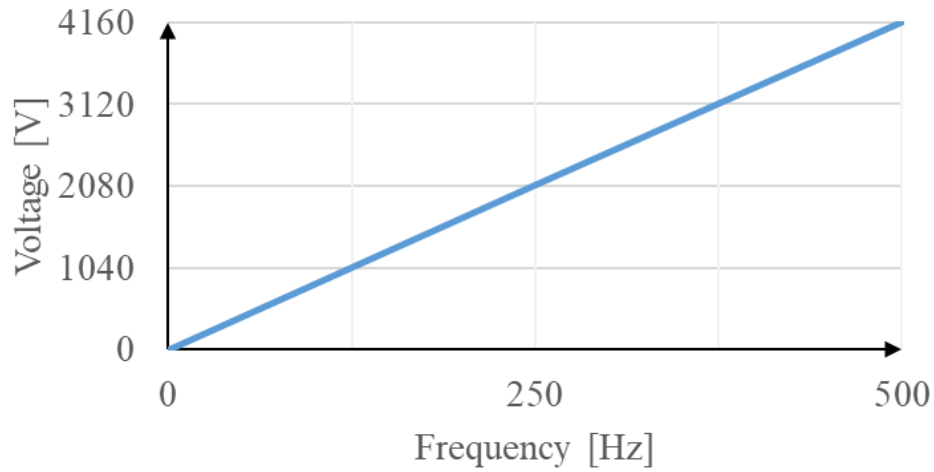


Figure 2.4: V/Hz relationship between voltage and frequency

The V/Hz method is derived from the desire to maintain the torque of a machine at a constant value [13]. This is achieved by applying a constant ratio of voltage magnitude and frequency to the stator of an induction motor as shown in Figure 2.4. The source thus provides a nearly constant magnetic field in the stator, inducing a constant electromagnetic force (EMF) in the air gap in the normal operating range of the V/Hz curve.

Given the relationship in (2.2) between the synchronous speed of the machine and the source frequency, it is shown that the two are directly proportional. In addition to the frequency, the voltage applied to the stator must also be changed to keep the air gap flux from saturating.

$$E = K_b \varphi_{max} f_s \quad (2.11)$$

Since the stator impedance is relatively small, in order to achieve greater efficiency of the HSI, the induced EMF is approximately equal to the supply phase voltage. In this case, (2.11) can be rewritten as (2.12).



$$\varphi_{max} = \frac{V_{\phi}}{K_b f_s} \quad (2.12)$$

Since  $K_b$  is a constant based on the stator winding factor and the number of turns per phase in the stator, the air gap flux can be clearly seen as proportional to the ratio of source voltage and frequency. Through understanding this scalar control of the HSI, the model of the motor can be evaluated based on an idealized source representing the VSD.

### Low Speed Induction Motor

The LSIM is part of the dynamometer subsystem. This motor will run in a generating mode when coupled to the HSI for full system tests to create a controllable load torque. This motor was procured from Stanley Electric Motor Co., Inc, chosen for its ability to handle MW class power flow. Originally built by Siemens as a tri-rated, dual voltage machine, the LSIM is rated to operate at 1500 hp (or 1.119 MW), 4000 V, 193 A, and 1784 RPM. Other relevant data from Siemens and a torque-speed curve are given in Appendix D.



Figure 2.5: Uncoupled LSIM on pedestal

Before testing the HSIM with the dynamometer, the LSIM must be commissioned by itself. The machine seen in Figure 2.5 is setup on its pedestal, connected to PAU 1 through its terminal box, given control power, and programmed to spin at full speed without any load. Operation of the motor is conducted based on Siemens instruction manual for induction motors and generators [14]. The manual provides important protection settings that are considered in the configuration of the PAU. Examples include temperature alarms and trips, overcurrent trips, and voltage and frequency deviation limits. Other significant information such as initial starting procedure and troubleshooting are used to work through issues that occur in commissioning.

To drive the LSIM, the PAU must be reconfigured to operate as a motor drive. This was the initial purpose of the drives by design and the HMI has existing programmable motor drive settings with a keypad input. Physical cabling for the motor terminals is run

from the PAU room through conduit to the test bay. The PAUs are normally connected to a Master that controls each set of PAUs in parallel for grid tests. However, the mains system control board in the PAU requires a direct connection from the control room PC for motor drive application. Once connected, drive configuration settings are established for the motor, the inverter, protections, and controls.

The procedure of spinning the motor to full speed involves the V/Hz method to ramp up the voltage and frequency output of the PAU from zero to rated values. However, issues arose in the form of trips in the system, unexpected noises, and axial movement of the shaft or “endplay”. Different tests were conducted to solve these issues and achieve a smooth ramp to full, no-load speed. Various parameters had to be reset because of mistaken values. The control settings and regulations had to be cycled through to observe which modes would cause a trip in the system. An approach was used to circumvent trip conditions and allow manual increasing of the stator voltage amplitude while at full rated frequency. This unorthodox method achieved the goal of full speed, albeit through experimental means. It essentially was a softened version of “line starting” a motor, because the voltage amplitudes increased in steps instead of ramps. This experiment leads to creating the V/Hz curve seen in Figure 2.6 that could be automated to start the motor from a stalled condition to full speed without manual intervention. Although, once the machine is properly coupled to the gearbox, the issues of “endplay” will be mitigated with an established magnetic center of the shaft axially.

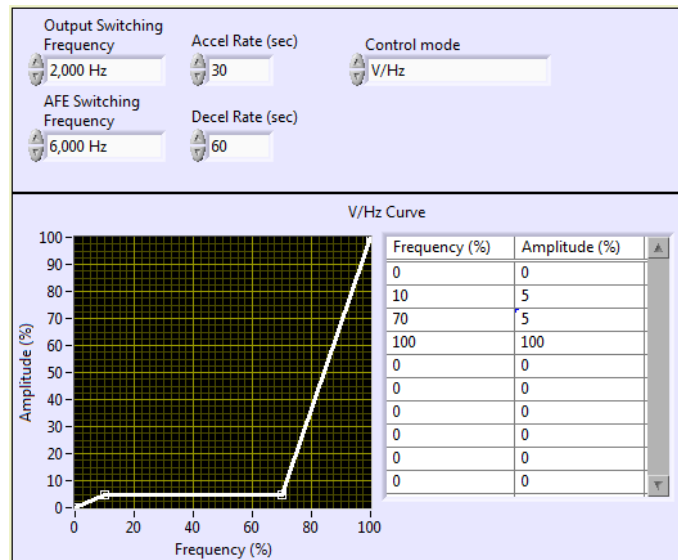


Figure 2.6: V/Hz curve profile setting on HMI

Controlling the LSIM to achieve full speed at no-load condition is a precursor to torque control of the dynamometer. Through V/Hz motor control, the HSIM can be tested with various forms of loads such as constant, fan, and pump loads. Given actual experimental data, the modeling of these machines can become more representative of actual operation. The iterative process of modeling and experimenting is mutually conducive, where one process improves the other. Modeling and simulation is done before and after experimental endeavors such as commissioning of the LSIM. Therefore, the actual machine behaviors can be predicted more accurately and lead to further design enhancements.

## Simulation

With the given parameters of the two induction motors, preliminary calculations are done to estimate the various outputs of the machine during steady-state operation. These calculations are done using the equations aforementioned through a spreadsheet to allow for manipulating variables easily and obtaining an output. Circuit analysis is conducted to obtain the voltages and currents of the stator, core, and rotor. The calculations are further verified by simulation of circuit components using Simulink. All of the values under consideration are compared against each other to show close agreement. An example case of the spreadsheet and circuit model can be seen in Appendix A. Both

The values obtained for the full load case are important for verification of steady-state operation of the motors. Total three-phase powers, rotor speed, slip, and load torque are significant variables that determine the accuracy of simulation outputs. There are discrepancies between the ideal values in Table 2.1 and those of Table D.2 due to unmodeled behaviors such as friction and windage losses, stator copper losses, and rotor cage losses. Table 2.1 uses the equivalent circuit representation while Table D.2 has detailed physical design of the HSIIM.

Table 2.1 Ideal outputs of HSIIM

| <b>Variable</b> | <b>Input <math>P_{3\phi}</math></b> | <b>Input <math>Q_{3\phi}</math></b> | <b><math>n_m</math></b> | <b><math>s</math></b> | <b><math>\tau_{load}</math></b> |
|-----------------|-------------------------------------|-------------------------------------|-------------------------|-----------------------|---------------------------------|
| <b>Value</b>    | 1090 kW                             | 942 kVAR                            | 14983.5 RPM             | 0.0011                | 685 Nm                          |

Despite differences between specific values, the mechanical outputs are comparable. Considering the high level of simulation for this system, as long as the

induction motor model can achieve reasonable mechanical and electrical behaviors, then the model can be validated based on scope. However, due to the high frequency operation of this motor, care must be taken to observe behaviors and issues that occur because of high frequency operation. To address this, both HSIM and LSIM must be modeled and tested through software.

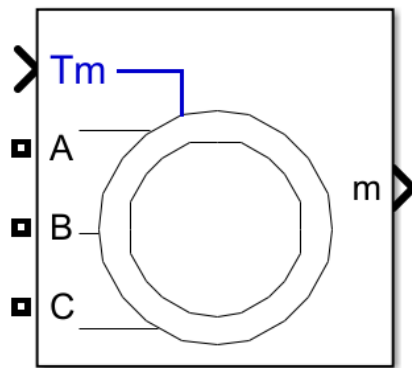


Figure 2.7: Asynchronous Machine block [1]

The Simulink model of an induction motor is given through the “Asynchronous Machine” block as seen in . This block allows the user to simulate an induction motor based on its Steinmetz equivalent circuit parameters, all referred to the stator. Mechanical parameters such as inertia and a friction factor are incorporated to provide some electromechanical interactions in simulation. Physical inputs are considered for loading effects of torque or speed. The mechanical and electrical modeling are separated in the block, coupled together by the electromagnetic torque, rotor angle, and rotational rotor speed of the machine. Output measurements for the electrical and mechanical behaviors of the motor can be extracted from the output port on the block. This includes voltages, currents, and fluxes of both the stator and rotor as well as output speed, torque, and angle.

Other features of modeling include three different rotor topologies and their respective dq equivalent circuit representation. This allows the user to choose the reference frame in which the dq waveforms can be observed in, whether stationary, rotor, or synchronous. Depending on where the voltages are unbalanced, either stator or rotor, the application reference frame will be chosen to rotate at the nominal rate of the unbalanced side [15].

The dq equivalent circuit is implemented in the induction motor block. The block applies the state-space equations used to derive the voltage, current, and flux linkages [12]. Since the equations reference the dq values of the variables, they are identically utilized for all three reference frames. The distinction between each of the frames is made with abc-to-dq and dq-to-abc transformations. The input three-phase voltage is converted from two line-to-line values to four dq values representing the stator and the referred rotor. The output three-phase current is converted from four dq values representing the stator and rotor to three phase values. These reference frames dictate a relative angle and speed of the rotor that can be extrapolated to behaviors at a higher frequency and speed. This capability supports the usage of the Simulink block for modeling the HSIM and LSIM.

Given the integrated system setup of a HSIM and LSIM coupled through a gearbox, the two motors are be driven in two distinct “modes”. Since the HSIM requires high speed operation, it will be driven by speed control. On the other hand, the LSIM, acting as part of the dynamometer, will be torque controlled. These two capabilities are possible based on the input parameter selected in the Simulink block. Therefore, the HSIM will require a speed output given a torque input while the LSIM will require a torque output with a speed input. Both configurations of the block must be validated to observe simulation integrity.

No-load acceleration tests from a stall condition are performed through Simulink using example cases provided in [12]. Each case is simulated to evaluate accurate operation of each respective set of motor parameters. This test applies rated voltage to the terminals of an induction machine to observe the acceleration behavior. The motors used in this study are all 60 Hz, 4 pole machines, thus all have a nominal synchronous speed of 1800 RPM. Albeit being relatively low speed machines, this test verifies feasibility of the dynamic model for the HSIM. There is a MW class machine included in the example cases to provide insight into torque-speed behaviors of the HSIM. The Simulink model shows agreement with the plots provided in [12], thus substantiating the usage of the block for this system. The parameters used and results obtained can be reviewed in Appendix B.

To conduct further validation on the HSIM and LSIM, a variable voltage source emulating the VSD must be created. This is due to the normal Simscape Power Systems library three-phase programmable voltage source only being able to manipulate amplitude or frequency separately during a single simulation. Signals for the three single-phase voltages are created through an idealized sinusoidal function.

$$v_{\varphi} = V_m \sin(2\pi ft + \theta) \quad (2.13)$$

Using (2.13), a three-phase, V/Hz controlled voltage source is made possible by manipulating the frequency,  $f$ , and voltage magnitude,  $V_m$ . To execute a constant ratio of voltage and frequency, the repeating table block is used to create a ramp from zero output to full rated voltage followed by a constant output, as shown in Figure 2.4. The outputs are generated through a set of arrays in the model's parameter file based on the time and output desired. At the minimum, three setpoints must be designated to express the start of



operation, the end of ramping, and a steady-state value. If desired, additional setpoints can be added to incorporate operations such as changing V/Hz of one of the induction motors or voltage and frequency boost [16]. Due to the usage of single-phase controllable voltage sources, the voltage magnitude is given as a peak, single-phase value as opposed to the three-phase, RMS value designated by the V/Hz ratio. However, because the proportionality between voltage and frequency is maintained, the V/Hz ratio is essentially a scaled value of the voltage and frequency arrays' ratio. The time vectors are coordinated between the frequency and voltage blocks to change at the same time, i.e. start, ramp, and steady-state. This preliminary model can be observed in Figure 2.8.

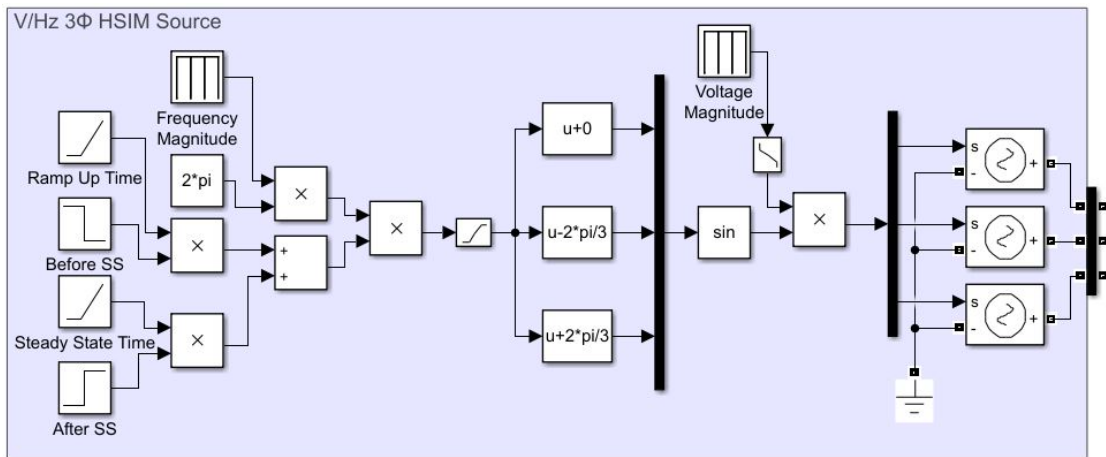


Figure 2.8: Preliminary Simulink model of V/Hz source

An interesting behavior of the model is the design of the timing source. Due to the way that the frequency is modeled, a ramp followed by a constant, it is actually a time dependent source. Therefore, when multiplied by a clock timer output, the input to the sine function block will have a  $t^2$  term that doubles the rate at which the frequency is increased during the V/Hz ramp. This creates a discontinuity when the frequency has reached its desired value. The ramp condition's quadratic behavior will obtain a value that is twice as large and a slope that is twice as steep as desired. When the frequency block outputs a constant after its ramp, a linear input to the sine function block will be obtained.

In order to consolidate the two modes of operation, ramp and constant, a new timing source is created. This time will output at half rate while the frequency is ramping up, and then output at full rate when the frequency is maintained as constant. Therefore,  $t$  will follow the piecewise linear function given in (2.14). A comparison between timing sources can be observed in Figure 2.9.

$$t = \begin{cases} t/2, & t < t_{ramp} \\ t, & t \geq t_{ramp} \end{cases} \quad (2.14)$$

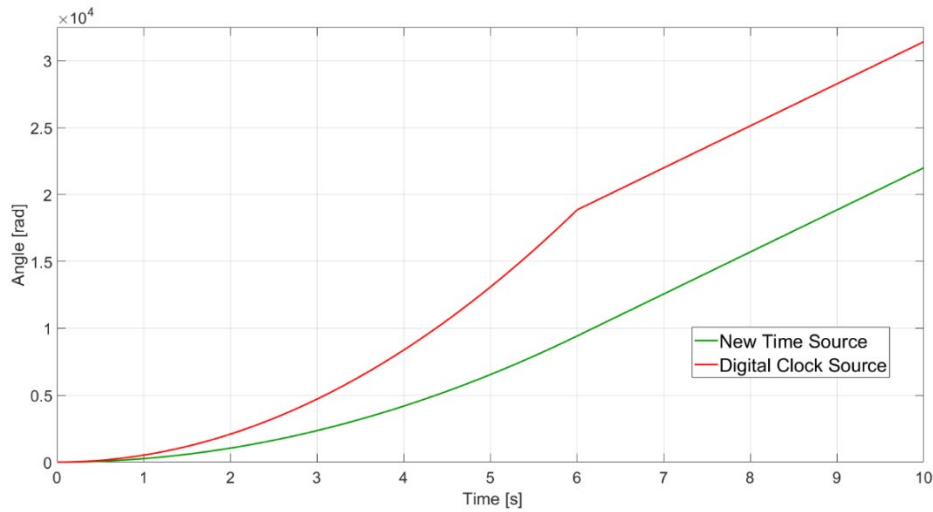


Figure 2.9: Comparison of timing sources for V/Hz operation

This new timing source is implemented in Simulink through two ramp blocks and step functions to designate the timing rate at the specified time. As shown in Figure 2.9, the discontinuity is removed while keeping the same steady-state frequency. The point at which the discontinuity is observed, at  $t = 6$  s, shows the problem of having a value that is double what is desired. Careful attention must be given to the initial value of the second ramp block that returns the time input to a normal rate. Since the input time occurs at a half rate while the ramp is occurring, the duration of the ramp will determine the initial value that the normal rate timing block must start.

However, due to further operations of the induction motor model, the voltage source must be able to account for any change in the frequency input. Therefore, a discrete-time integrator is incorporated into the model. This block takes an input of the angular frequency and outputs the angle to be sent to the trigonometric function block. In this way, only one time dependent function is utilized and the effect of time is still used. To be sure

of correct operation, the derivative of the angle is taken and observed against the reference frequency. These two signals should be comparable, albeit with a filtered version showing the smooth frequency change. The new model can be observed in Figure 2.10.

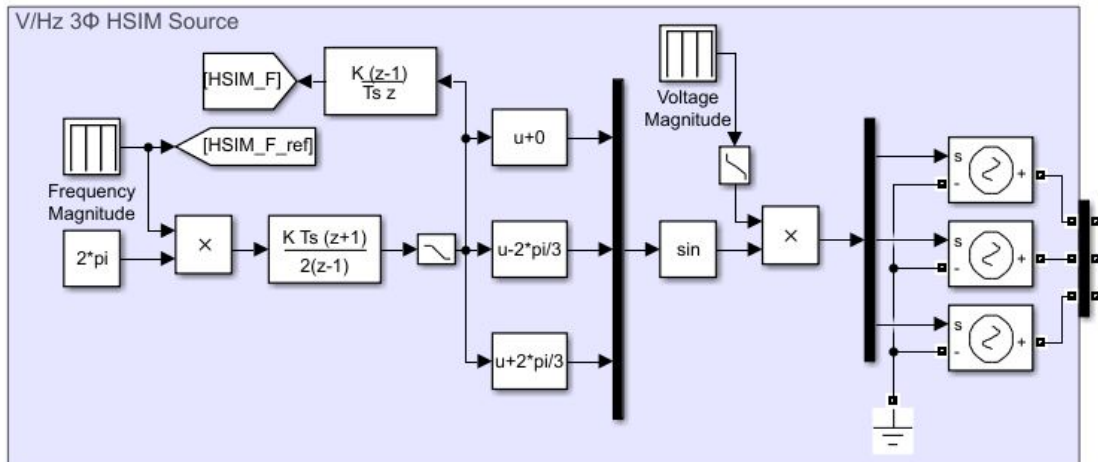


Figure 2.10: Updated Simulink model of V/Hz source

Low pass filters are included in the V/Hz source to mitigate the effects of discontinuities on the induction machines. The filters are applied to both the frequency and voltage inputs, since these blocks create piecewise linear functions. The damping ratios are set to a value of 1 to obtain smooth function outputs. This modeling consideration is done to mimic the actual controlled output of the induction motors, where voltage and frequency setpoints are changed through a controller. However, when controls are included, these filters are commented out to allow the controller to maintain the desired operation.

Given this new voltage source and parameters to model the induction machines, full load tests are done to observe conformity to desired behaviors. This test uses the V/Hz source to ramp up voltage and frequency to nominal values. Once the machine settles at near synchronous speed, a torque load is applied to the machine. These tests are done to

validate steady-state values. Additional tests will be done to address startup behaviors such as inrush current.

The V/Hz source is connected to the HSI<sub>M</sub> and LSI<sub>M</sub> models in separate simulations. The respective parameters are inputted to each machine through a MATLAB parameter file to easily change variables. The output measurements are logged in scopes to observe electrical and mechanical behaviors simultaneously. For the HSI<sub>M</sub>, the voltage is set to increase from zero to nominal in six seconds. This is found through experimentally changing the ramp time in the simulation and observing the speed data. With a ramp time of less than five seconds, the machine does not have enough time to overcome the torque-speed characteristics of the machine. In this case, the motor stalls and does not achieve the desired speed. The LSI<sub>M</sub> is simulated in the same way, and is found to actually be able to operate with a line start, albeit with very large starting currents and torque oscillations. Due to the similarity in simulation procedure, only the HSI<sub>M</sub> outputs will be presented for the full load test.

The speed plot of the HSI<sub>M</sub> for this full load test can be seen in Figure 2.11 with a zoomed-in version in Figure 2.12. The overall view of the speed output shows a resemblance of the standard V/Hz curve. This follows the proportional relationship between the nominal synchronous speed and stator frequency. The V/Hz increases voltage and frequency and the speed of the machine follows a similar pattern. Once the machine reaches near nominal synchronous speed, oscillations occur from the sudden change from ramp to a steady-state source input. A step load change is provided after eight seconds of simulation time. Again, more oscillations are observed due to the sudden mechanical load.

After this transient settles out, the machine speed resolves to near the expected full load speed of 14,983.5 RPM or a slip of 0.0011. Thus, the desired steady-state speed behavior is achieved. However, the oscillation that occur must also be considered. This will be resolved in the use of PI controllers for the speed regulation.

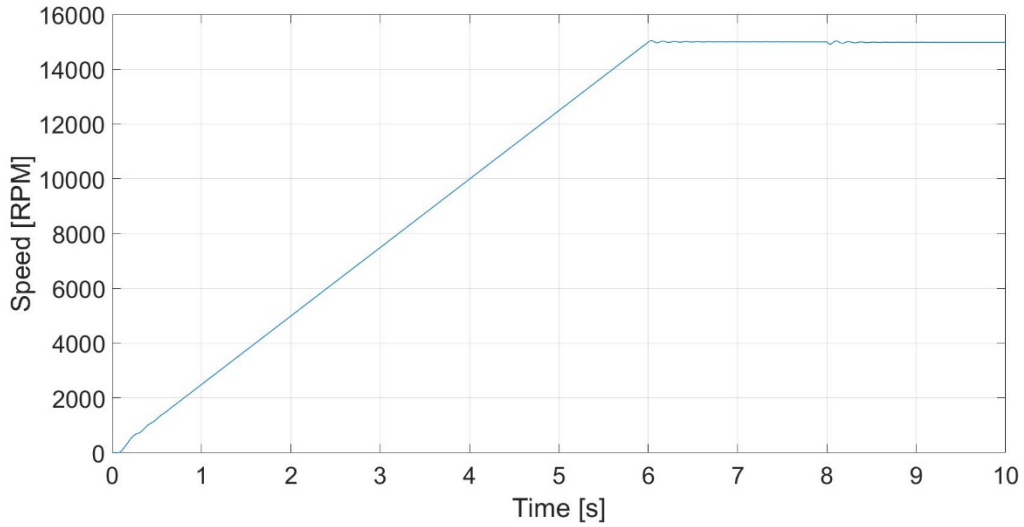


Figure 2.11: HSIM full load test speed output

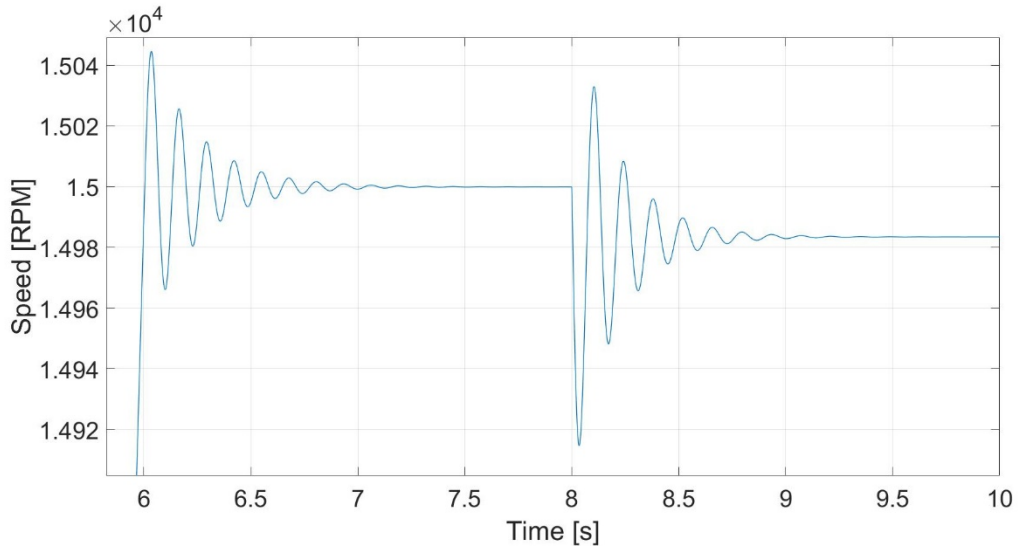


Figure 2.12: HSIM full load test speed output zoomed in

Observing the voltage in Figure 2.13, there is a similar shape to the speed output. This voltage is modeled in an ideal fashion, creating a balanced and increasing amplitude and frequency as shown in Figure 2.14. This input is a simplified version of the actual motor drive, which is more detailed and requires extensive time to fully simulate. Although the modeled voltage source is a basic three-phase source, the overall steady-state behaviors of the motor are validated. This supports further usage of the motor model and encourages the comprehensive modeling of the VSD.

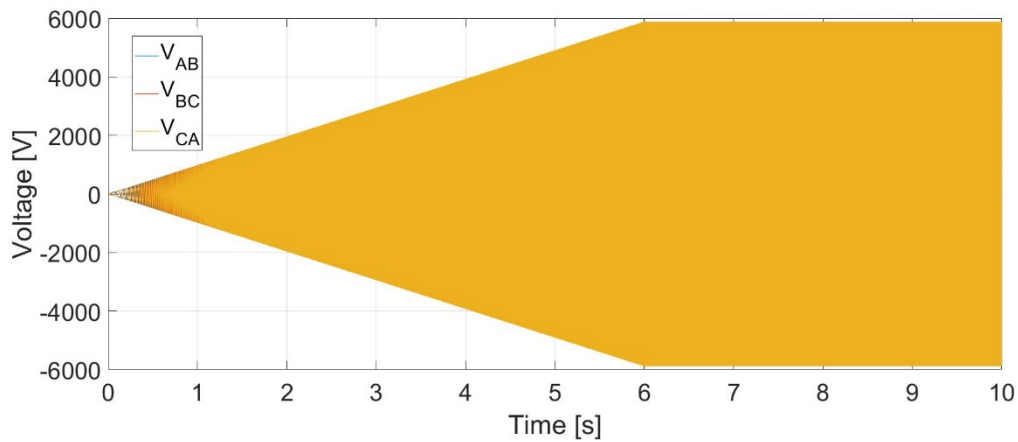


Figure 2.13: HSIM full load test voltage input

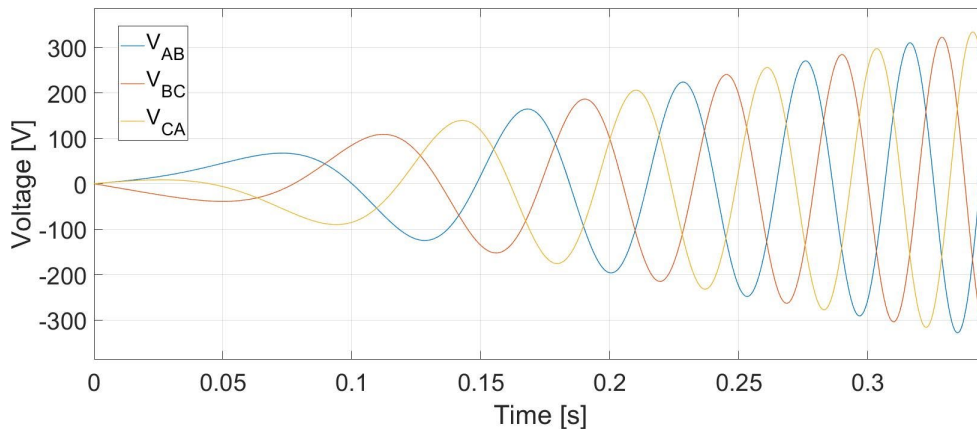


Figure 2.14: HSIM full load test voltage input zoomed in

The source current in Figure 2.15 shows several issues that must be addressed during testing of the actual motor. Inrush current approaches  $800 A_{\text{peak}}$ , even with the V/Hz soft startup. This is more than twice the expected full load current rating, which is only 220 A ( $311 A_{\text{peak}}$ ). This will affect how the HSIM is started during actual testing. Whether having a slower V/Hz ramp or a variable V/Hz curve similar to the method seen in Figure 2.6, the voltage source must be altered to avoid system failures. Another consideration is manipulating the protection settings of the PAU giving power to the VSD. Even though the large current magnitudes are not desirable, if the HSIM can handle the currents without any physical consequences, this inrush may be tolerable. These settings will have to be altered to allow for alarms and trips to occur that disregard the inrush condition.



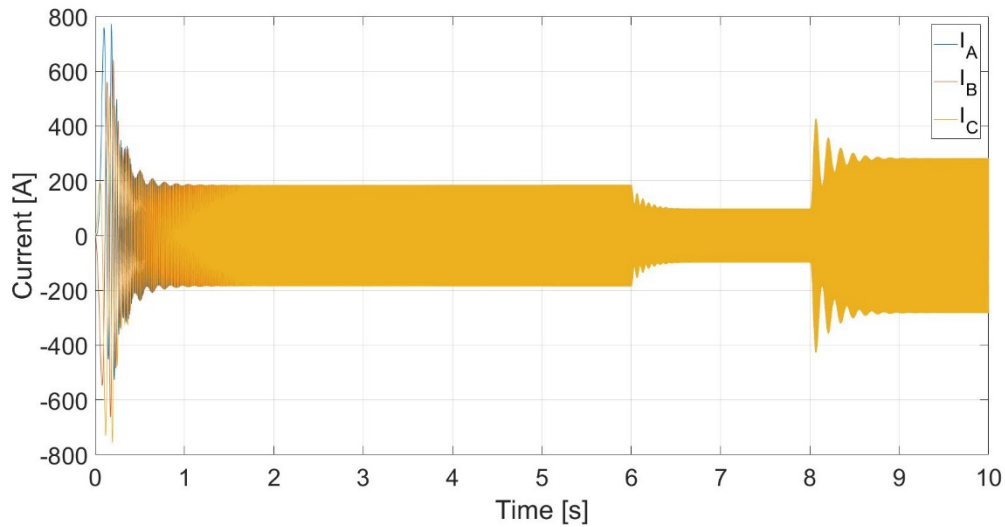


Figure 2.15: HSIM full load test current input

Another consideration are the low frequency oscillations during the transients to no-load full speed and to full load speed. This phenomenon exists because of the relationship between the current and power generalized in (2.6). Power is also related to torque by a factor of the rotational speed as shown in the equation (2.15). This is why the torque oscillations seen in Figure 2.16 resemble the current oscillations. Although the transients are relatively quick, the realizations of this test on the actual HSIM would mechanically stress the machine. With the mechanical fabrication of the prototype HSIM already finished, the mitigation must occur in the motor drive output. This is why controls for the motor must be implemented.

$$P = \tau * \omega \quad (2.15)$$

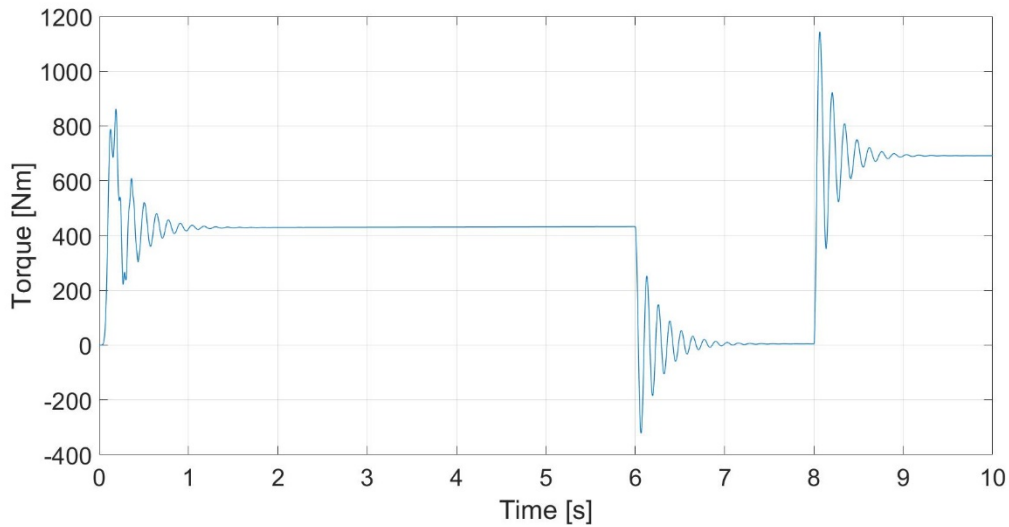


Figure 2.16: HSIM full load test torque output

For the HSIM, speed control is implemented based on its application to achieve high speeds at the MW level. Open and closed looped simulations are conducted to observe motor response and establish limits for actual motor operation. Open loop control has an input of speed and output of voltage magnitude and frequency. This control method is applicable when the HSIM is not loaded. Closed loop control includes a PI controller to adjust the voltage and frequency references based on feedback from the motor speed. This allows for regulation of the speed based on a desired value. Control modeling for the LSIM with become more relevant when the two motors are coupled.

A simple block diagram of the open loop control is shown in Figure 2.17. The parts of the diagram in green are designated as control signals. The VSD and HSIM are outlined in black to show that they are physical devices. A given input of speed in RPM is given through  $n_H^*$ , where the subscript expresses that the variable is on the high speed side of the system and the asterisk expresses it as a reference value. This speed reference is converted

from a rotational speed value to a frequency value through usage of (2.2). From this frequency reference, the voltage reference can be found by applying the desired V/Hz curve. Often, this conversion can be simply expressed by a ratio of the nominal voltage and frequency for the motor. However, depending on the startup constraints for the HSIM, this may be altered and applied as a lookup table. Lastly, the voltage and frequency references are sent to the VSD to output the desired voltage.

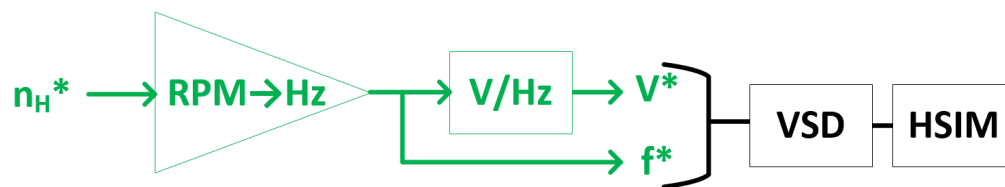


Figure 2.17: Open loop speed control block diagram for HSIM

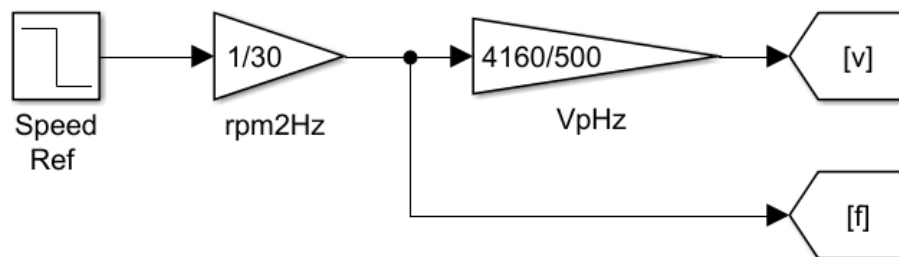


Figure 2.18: Simulink open loop speed control

For this test, the same V/Hz source is used to drive the HSIM. The difference is the addition of the Simulink implementation shown in Figure 2.18. The model is run to full, no-load speed and then terminated. The final state of the simulation is saved as a dataset in MATLAB, and is used as an initial condition to run the open loop speed control test. Then, the speed reference is changed from 15,000 RPM to lower values to observe the machine response. Changes in the speed reference are made instantaneously, thus creating

oscillations in the torque, speed, and current. Through experimentation, it is found that a step change of 120 RPM will cause the current to rise to the full load rating of 311 A<sub>peak</sub> as seen in Figure 2.19, Figure 2.20, and Figure 2.21. Therefore, the speed reference for controlling the HSIM should not be instantaneously changed more than this value to operate within the machine ratings.

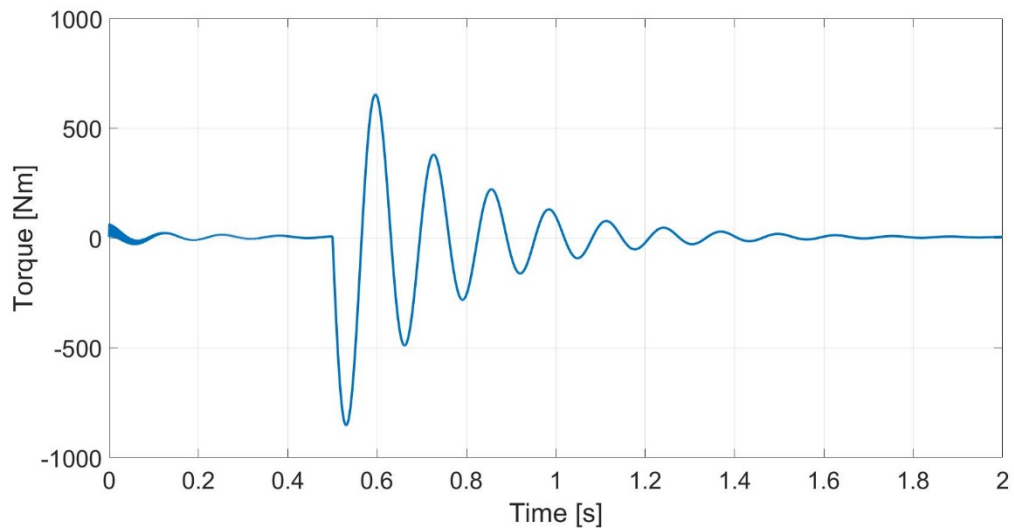


Figure 2.19: HSIM open loop test torque output

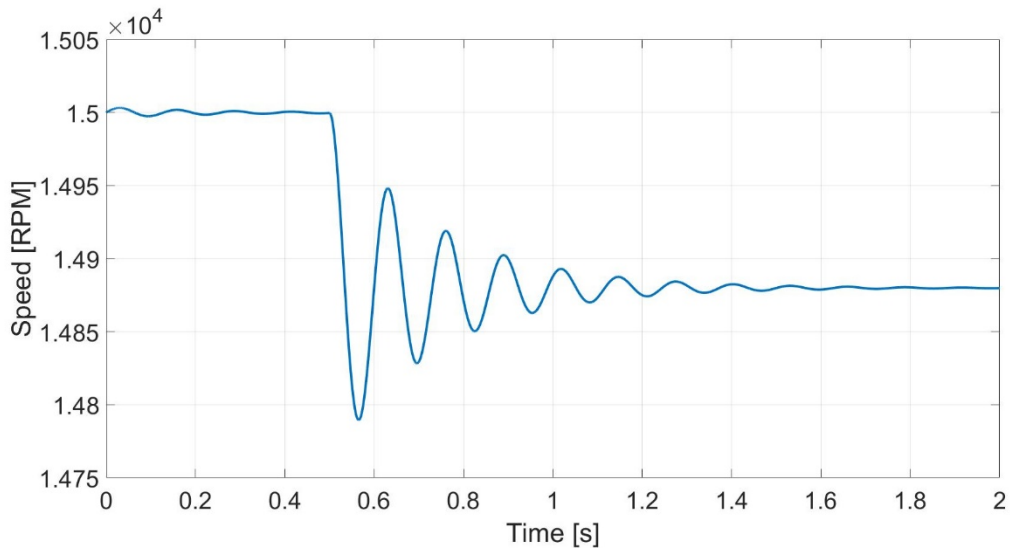


Figure 2.20: HSIM open loop test speed output

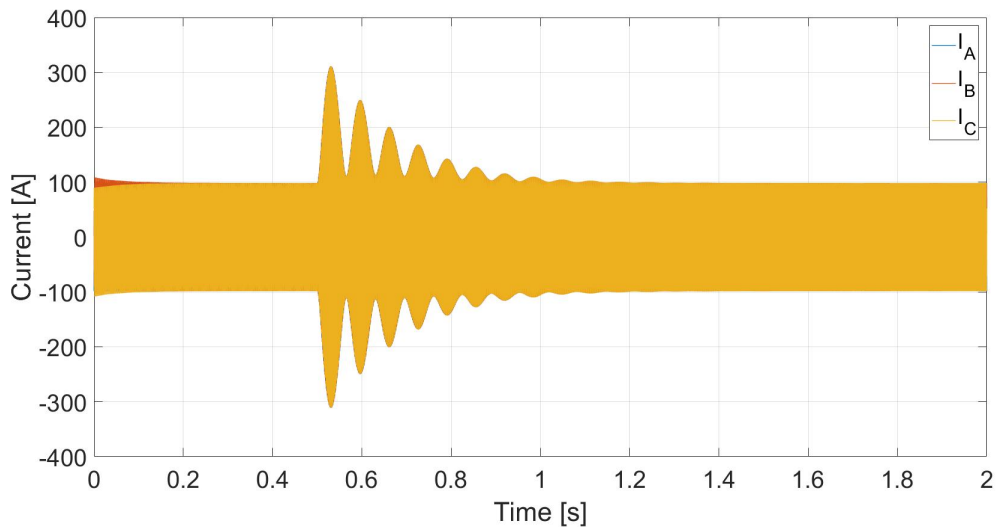


Figure 2.21: HSIM open loop test current input

However, limitations to the rate of change for the reference speed can be implemented by the “Rate Limiter” block. The smaller the slew rate, the smaller the oscillations. Since the current draw of the machine is a determining factor for protection

settings, it can be used as a guideline for changing the slew rate. Depending on how much current is deemed to be safely present in the system, this rate can be changed in simulation to predict current behavior in the actual motor. However, the mitigation function of the “Rate Limiter” can be achieved through the closed loop control of the HSI. Through tuning the added PI controller, the VSD references can be changed in a smoother fashion, creating an S curve. This will reduce the oscillations and keep the current within reasonable limits.

In order to implement a PI controller, a discretized version must be modeled. Based on a standard Laplace domain block diagram of a PI controlled system seen in Figure 2.22, a relationship can be found between the error signal,  $e$ , and the plant input,  $u$ . The other variables such as the reference,  $r$ , and the plant output,  $y$ , are negligible during this study. The expression of (2.16) resembles a transfer function from the error signal to the plant input using the PI gain values  $k_p$  and  $k_i$ . A transformation into the Z domain based on the trapezoidal rule given by (2.17) is made to create an evaluation of  $u$  based on current and previous states. Since the system is discrete, a variable for the sample period,  $T$ , is necessary to include. Note that  $z^{-n}$  in the Z domain refers to a value that is  $n$  delays old. Using (2.18), the PI controller can be modeled in Simulink as shown in Figure 2.23.

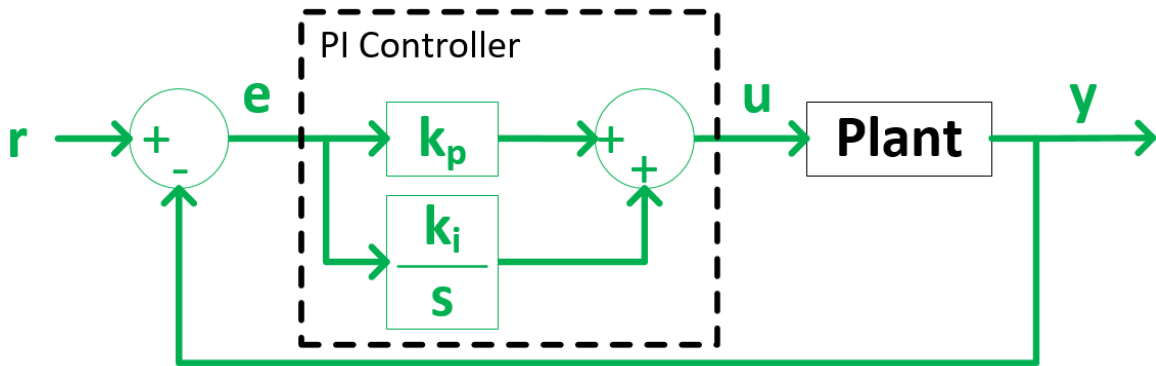


Figure 2.22: Laplace domain PI control system

$$\frac{u}{e} = \frac{k_p s + k_i}{s} \quad (2.16)$$

$$s \rightarrow \frac{2z - 1}{Tz + 1} \quad (2.17)$$

$$u = uz^{-1} + \left(\frac{T}{2}k_i - k_p\right)ez^{-1} + \left(\frac{T}{2}k_i + k_p\right)e \quad (2.18)$$

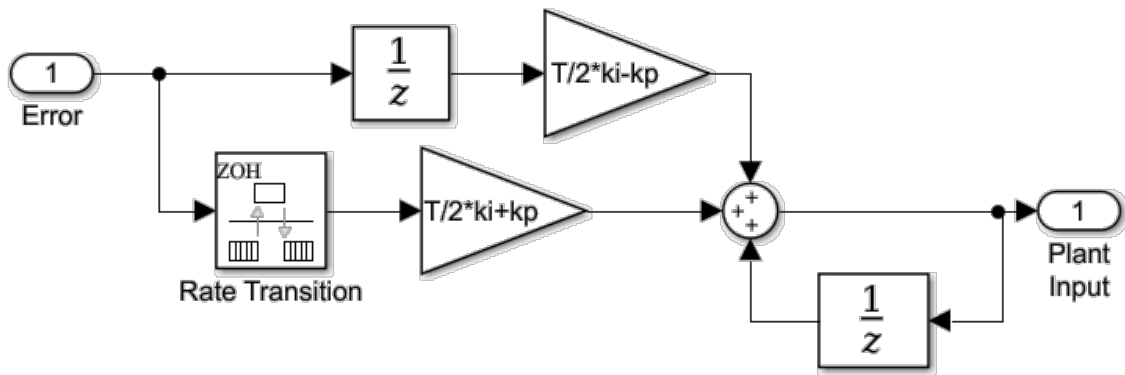


Figure 2.23: Discrete model of PI controller using the trapezoidal rule

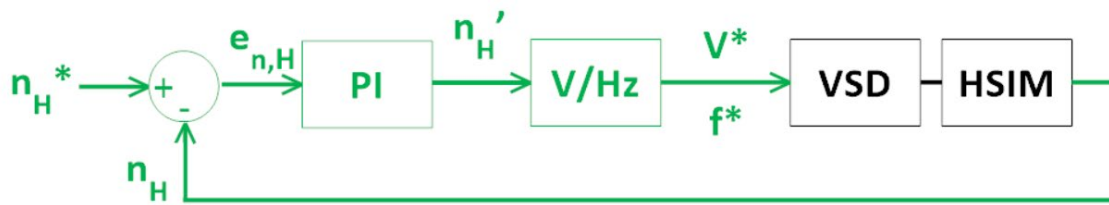


Figure 2.24: Closed loop speed control block diagram for HSIM

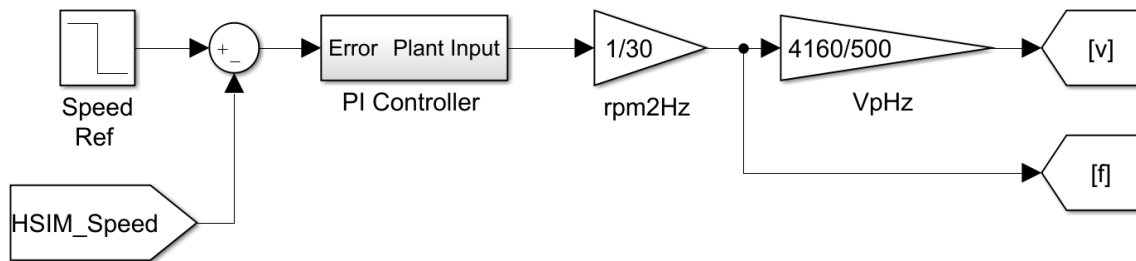


Figure 2.25: Simulink closed loop speed control

With the PI controller included, the feedback loop must be added as well to receive the HSIM speed output and create an error signal as shown in Figure 2.24. The Simulink modeling of the controls can be seen in Figure 2.25. Conducting a similar speed test to the open loop control, the reference is changed from 15,000 RPM to 14,900 RPM. With a controller sample period of 1 ms, different combinations of  $k_p$  and  $k_i$  are simulated to observe effects on the motor. Increasing  $k_p$  produces similar oscillations from the open loop test while increasing  $k_i$  mitigates the oscillations. However, increasing  $k_i$  too much results in control instability. To compare the improvement, plots are given for the torque, speed, and current of the closed loop test in . Here,  $k_p = 0$  and  $k_i = 5$  with the same modeling for the VSD and HSIM as the open loop test.



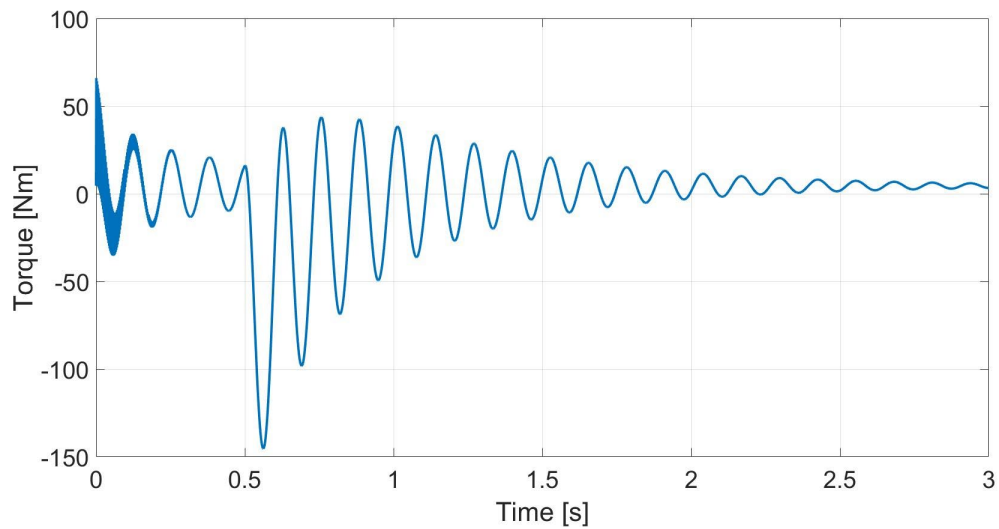


Figure 2.26: HSIM closed loop test torque output

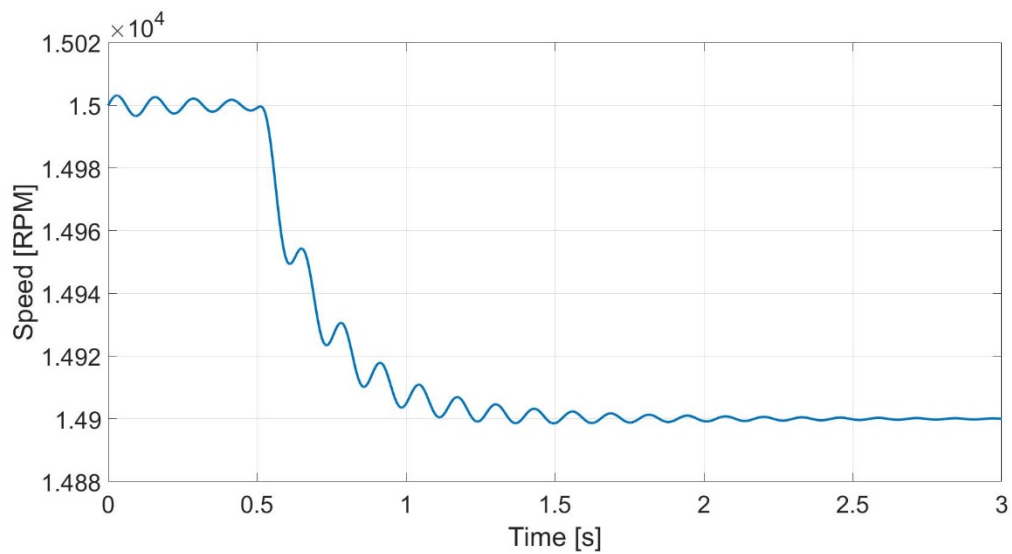


Figure 2.27: HSIM closed loop test speed output

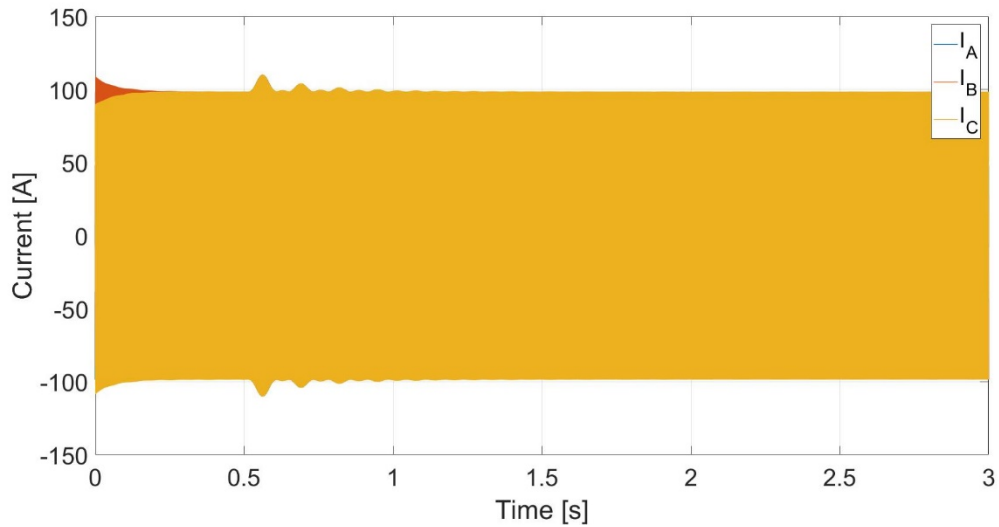


Figure 2.28: HSIM closed loop test current input

The dramatic change in the current drawn from the voltage source is significantly improved. This change is also reflected in the smaller oscillations of the torque and speed. Another motor characteristic that is beneficial to observe is the input voltage. With added controls, the voltage is not produced manually, but through the plant input given by the PI controller. The distinction of the voltage can be observed by its envelope, which, by modeling design, is proportional to the frequency, thus following the V/Hz control method. This graph is presented in Figure 2.29. Also, through experimentation, it is found that with the aforementioned gain values, the motor can have a speed step change of 600 RPM and be within the full load current rating. Further tuning of the PI controller to obtain tighter and smoother response from the HSIM can be done. However, the prospect of speed control has been validated for the VSD and HSIM subsystem. Closed loop control enhances the capabilities of open loop control.

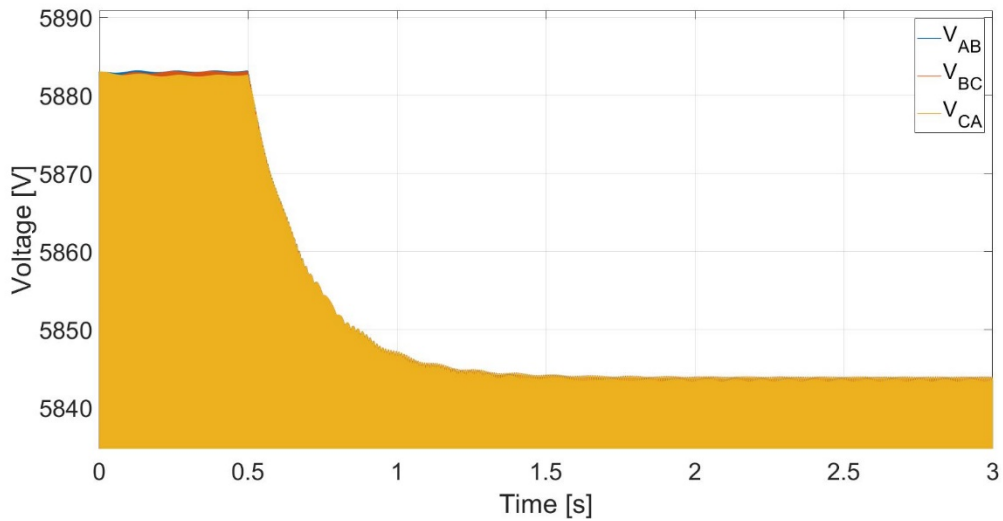


Figure 2.29: HSIM closed loop test voltage envelope

### Summary

This chapter indicates the basic operation and structure of an induction motor. Through understanding of the electromechanical relationships within the machine, source voltage requirements are specified in order to achieve desired operations. Both of the motors are modeled and simulated through Simulink, where outputs of the system can be analyzed. The V/Hz control method is used to exhibit the motor response and allows for iterative testing to achieve reasonable performance in both open and closed loop configurations. The actual LSIM has also undergone preliminary testing at the facility to reach full, no-load speed. Through various simulations of the motors offering reasonable data, efforts can be taken towards the drives.

CHAPTER THREE  
HIGH FREQUENCY VARIABLE SPEED DRIVE

Theory

VSD applications enhance the usage of induction motors in industry. The added control enables potential energy consumption and cost savings through suitable operation. The three main physical parts of a VSD are the rectifier, DC link, and inverter [17]. Through a modular configuration, the PAUs and high frequency VSD are built to have their respective electrical ratings. The “cubes” are the fundamental building blocks of both inventions, each having the three physical parts of a VSD as shown in Figure 3.1. Connecting them in a combination of series and parallel groups provide the capabilities of a MW level drive with the modularity for maintenance and testing purposes.

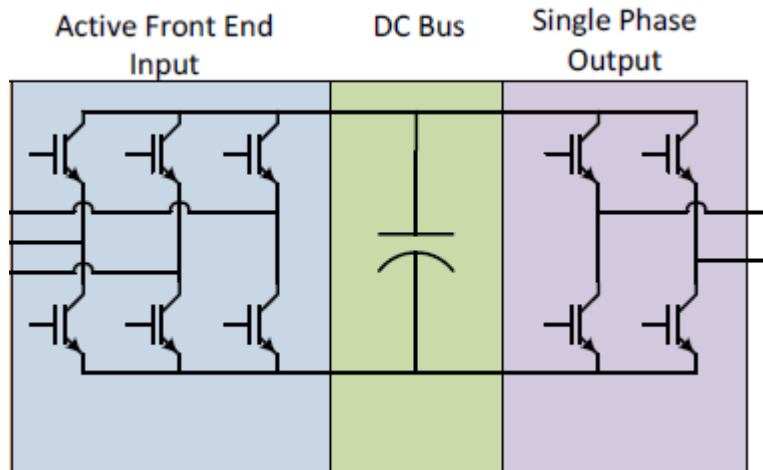


Figure 3.1: "Cube" topology [1]

The high frequency VSD's SCHB topology provides an effective means of providing an output at medium voltage, high frequency, with low total harmonic distortion (THD). Due to the structure of the system, individual switching devices can operate at lower voltage levels. Instead of experiencing the entire 4160 V across the devices, each will experience around 1100 V from each "cube's" DC link. With three "slices" connected in series, each set of three phase voltage outputs from the "slices" will sum to the seven-level VSD output phase voltages according to (3.1) [18]. The number of levels in the line-to-line voltage output can be found through (3.2) [18]. Phase shifted carrier signals in the PWM distribute the "information" of the modulation wave evenly across the "slices". Since there are three "slices," the phase shift is 60° instead of the normal 45° for the PAUs to distribute the half cycle of the carrier wave period. The modulation wave is multiplied by a factor called the modulation index, M, which affects the output three-phase voltage of the VSD according to (3.3).

$$L_{LN} = 2(\# \text{ of slices}) + 1 \quad (3.1)$$

$$L_{LL} = 2(L_{LN}) - 1 \quad (3.2)$$

$$V_{3\phi} = M(\# \text{ of slices})V_{DC}\sqrt{\frac{3}{2}} \quad (3.3)$$

The substitution of SiC MOSFETs into the inverter allows the switching frequency to be increased to more than 5 kHz as targeted by the FOA [1]. The proposed system specifications are designed to operate up to 10 kHz. This range for the device translates into an apparent switching frequency of 30-60 kHz. This relationship between the device and system level switching frequencies comes from the number of series connected "slices" and the H-bridge inverter topology having two phase legs. Therefore, the VSD will have an apparent switching frequency that is 6x the device switching frequency. These higher

switching frequencies allow the VSD to drive the HSIIM past its nominal speed, up to 18,000 RPM, by having a higher fundamental output frequency up to 600 Hz.

The DC link is managed by a capacitor to inherently maintain the desired DC voltage between the inverter and rectifier. The rectifier is designed as a four-quadrant AFE, allowing for a controllable regulation of the DC link, reduction of THD, and power regeneration [5]. This bi-directional power flow is not intended for use by the VSD in this current project. However, future work will be done regarding the AFE for an awarded DOE project on combined heat and power (CHP) [19].

SiC MOSFET half-bridge modules have undergone extensive modeling and double pulse testing (DPT). DPT uses a simple circuit setup, seen in Figure 3.2, for observing the turn-on and turn-off characteristics of the switching device. Of particular interest are the drain-source voltage,  $V_{DS}$ , and the drain current,  $I_D$ , as shown in Figure 3.3. Due to the high switching frequency of these devices in the VSD, considerations in the parasitic inductances and capacitances must be addressed [20], [21]. Possible solutions such as snubber circuits and a novel intelligent gate driver (IGD) have been researched and evaluated [22]. A test bench setup was used to implement the DPT through a National Instruments' FPGA and LabVIEW. Modeling efforts were done to reflect the parasitic effects on the switching actions. Results of simulating a simplified VSD with parasitic components included an operational concern for higher switching frequencies as shown in Table 3.1. For overall system modeling, these considerations are not as critical.

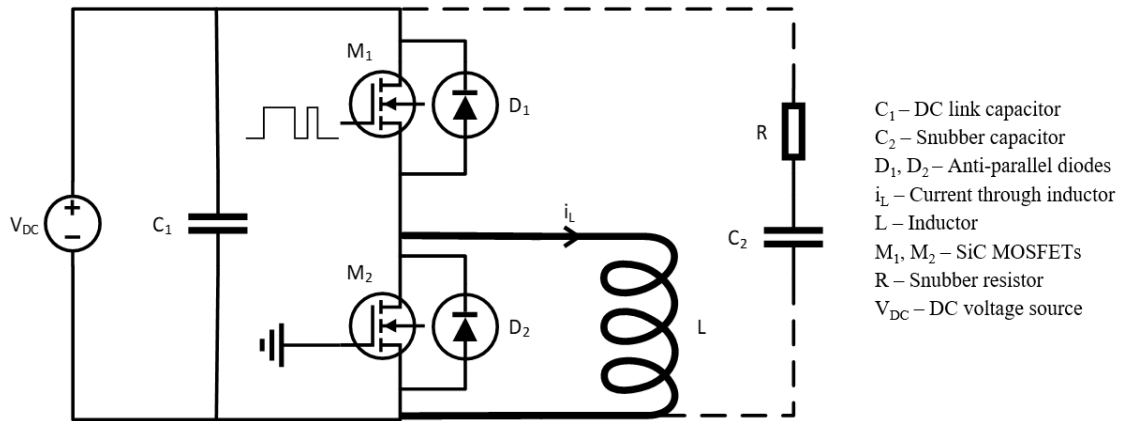


Figure 3.2: DPT test circuit with optional snubber

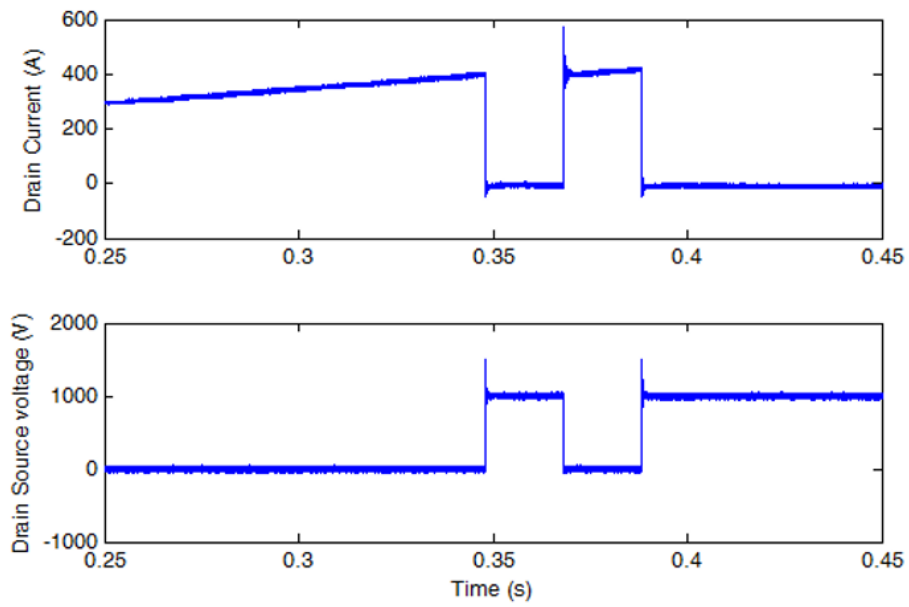


Figure 3.3: Experimental DPT for 1kV/400A case

Table 3.1 Effect of carrier frequency on peak overvoltage

| <b>Carrier Frequency [kHz]</b> | <b>Peak Transient Overvoltage [V]</b> |
|--------------------------------|---------------------------------------|
| 6                              | 1717                                  |
| 5                              | 1676                                  |
| 4                              | 1602                                  |
| 3                              | 1570                                  |
| 2                              | 1563                                  |
| 1                              | 1563                                  |

### Standards

System performance tests will be conducted at the EIC facility. These tests will utilize the standards based on VSDs and IMs [11], [23], [24], [25], [26], [27]. Along with evaluating the system according to the primary and secondary targets of the FOA, the standards will be used to characterize the dynamometer, determine the speed control functionality of the HSI, conduct speed-load tests, as well as HIL testing [1]. One of these tests involves inducing voltage sags on the system, which is possible through the grid simulator of the eGRID center.

Extensive work has been done to characterize voltage profiles based on desired sag conditions at the terminals of a solar inverter [28]. Based on various conditions such as transformer connection, voltage levels, and specific phase sag magnitudes, the grid simulator can evaluate and output the needed voltages on the grid side of the transformer to induce the expected sag condition at the terminals of the inverter [28]. The same principle applies to this system because the VSD must be interfaced with the grid through a transformer. Various sag conditions, both single-phase and double-phase, can be tested on the system to observe the VSD's ride through capability and ability to restart motor



operation. Defining these protection settings will be necessary in commercializing the prototype system.

According to IEEE 1566, the largest voltage sag that the VSD must ride through is 65% of nominal for a duration of 500ms [23]. Although a three-phase fault is one of the worst possible conditions this drive can experience on the grid side, single-phase and double-phase faults are more common. Given a trip table for the prototype VSD, the grid simulator can impose various sag conditions to validate the drive's ability to ride through a multitude of different conditions. These tests can be done through simulation before the actual device commissioning.

Shutdown operations are imperative for the integrated system. With the voltage and power levels that the system will experience, in the event of a fault, the system must be able to shut down in a safe manner. Since there are two sides to the system, high speed and low speed, each must have the capability to bring the system to a safe stop if the other side trips. Both drives can either let the mechanical systems coast to a zero speed or run in a regeneration mode to bring the remaining potential energy out of the test equipment.

### Active Front End

The AFE for the high frequency VSD is not of particular interest for the scope of this project. Since normal operation of the VSD is to drive the HSM, power flow will go through the motor. The AFE has a passive operating mode that uses an innovative phase shifting technique in the isolation transformers to create a 54-pulse rectifier [29]. This allows the adherence to any possible stringent input power quality requirements.

However, the PAU driving the LSIM will have to utilize the AFE for regeneration purposes. The power will flow from the HSIM to the LSIM, as the LSIM will operate in the generating mode to apply a load on the system. With the AFE, the PAU can regulate the internal DC bus voltage as well as operate at a commanded power factor. During trip tests for the two sides of the system, the AFE will allow the drives to dissipate the mechanical energy back into the grid. Further tests are conducted to observe any limitations that the drives must adhere to during these emergency situations.

### Inverter

The SCHB topology allows the DC voltage to become the AC voltage driving the motors. This is done through switching the SiC MOSFETs in the H-bridge at specified instances to output a PWM waveform that represents the desired sinusoid. The H-bridge can be viewed as two phase legs, where each phase leg contains two switching devices connected in series. Standard SiC MOSFET modules house one phase leg, requiring gate signals to control the two switching devices. The two should never be turned on at the same time. Otherwise, the DC link will be shorted, causing failure of the “cube”. This is mitigated by applying a “dead time” in the PWM control scheme, delaying the gate signal so the devices cannot be shorted unintentionally.

The switching scheme is based on the modulation wave, provided by sinusoidal waveforms. These waveforms are compared to the phase shifted carrier waves, which are triangle waves representing the number of “slices” in the VSD. Unipolar PWM is used for control, thus a “negative” version of the modulation wave must also be analyzed. This

“negative” modulation wave is the reflection of the regular modulation wave across the horizontal axis. When the positive modulation wave is greater than the specific phase carrier wave, an active signal is given. When the negative modulation wave is less than the specific phase carrier wave, an active signal is also given. The positive action signals are provided to one phase leg of each “cube” while the negative action signals are provided to the other phase leg of each “cube.” In this way, the control signals are distributed to the respective “cubes” to provide their portion of the phase voltage. An example switching configuration is created in PLECS and shown in Figure 3.4.

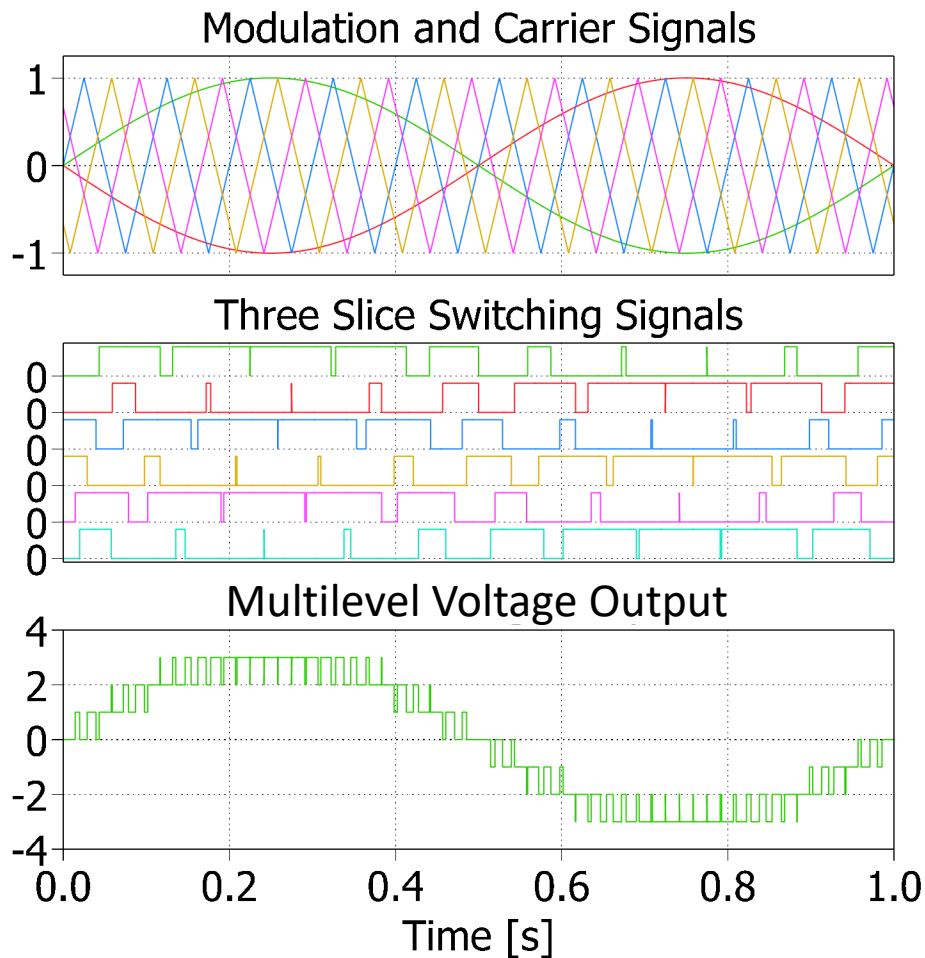


Figure 3.4: Sinusoidal PWM (SPWM)

Since there are three slices with DC voltages of 1100 V, the VSD output would normally have a maximum three-phase voltage output of 4042 V according to (3.3). To achieve the desired 4160 V, overmodulation of the SPWM must be done. This nonlinear region of control will not be able to precisely utilize (3.3) since the controller is saturated. To overmodulate the PWM method, a third-harmonic component can be added to the modulation wave or space vector modulation can be used [30]. Using Figure 2.4 as a reference, the V/Hz curve can be shifted such that the endpoints still include the zero voltage and frequency point, but the full frequency of 500 Hz has a voltage value slightly above nominal. Since the necessary gain to achieve the 4160 V output from the normal three slice output of 4042 V is 1.029, the linear region can still be assumed for preliminary simulations. Pragmatic actions will have to be taken in order to achieve a stable voltage output at the designated ratings of the HSIM.

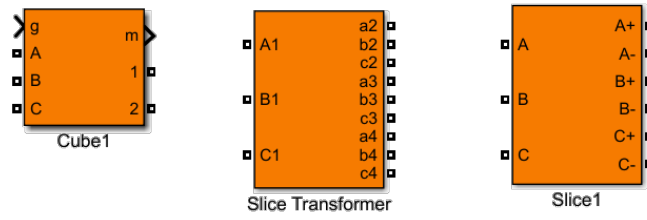
### Drive Model

Modeling of the high frequency VSD is done based on previous work modeling the PAUs [6]. The library mainly used for this modeling is the Simscape Power Systems. Although this library contains Simscape specific components, the “Specialized Technology” subdirectory is chosen because of interface capabilities with Simulink blocks. Simscape components have distinct signal connections which must be converted into Simulink signals to interface with controls and mathematics. Using the blocks in the “Specialized Technology” subdirectory allow for additional Simulink modeling without the need for conversion blocks all throughout.

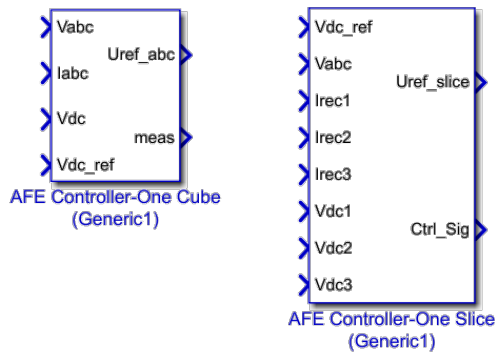
The original model represents an 8-slice PAU with grid connections, an LCL output filter, and a load [6]. This discrete model operates at a sample time of  $416.\bar{6}$  ns to precisely include the high frequency operation of switching devices. This value is chosen to have 50 data points for a cycle of the fastest apparent switching event which is 48 kHz due to the four slice topology and 6 kHz device switching frequency. Parameterization for the model has been used to expedite simulation and ensure consistent variables. The model has subsystem blocks containing the output scopes and control systems respectively to easily navigate the model.

A custom library has also been created to reuse blocks for modeling future drives such as the high frequency VSD. The blocks can be seen in Figure 3.5. Following the modularity of the PAUs and VSD, this custom library can connect the power modules in varying series and parallel combinations to achieve varying operating levels. The cube model contains the AFE, DC link, inverter, and control and measurement signals as shown in Figure 3.6. The slice transformer contains the multi-winding isolation transformer to connect to the cubes within a slice as shown in Figure 3.7. The slice block contains one slice transformer block and three cube blocks, conforming to the structure shown in Figure 1.1.

----- Power Models -----



----- Control Systems -----



----- PWM Generators -----

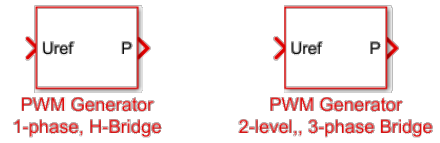


Figure 3.5: Custom blockset for drive modeling

**Cube Model - TECO Power Module**

---

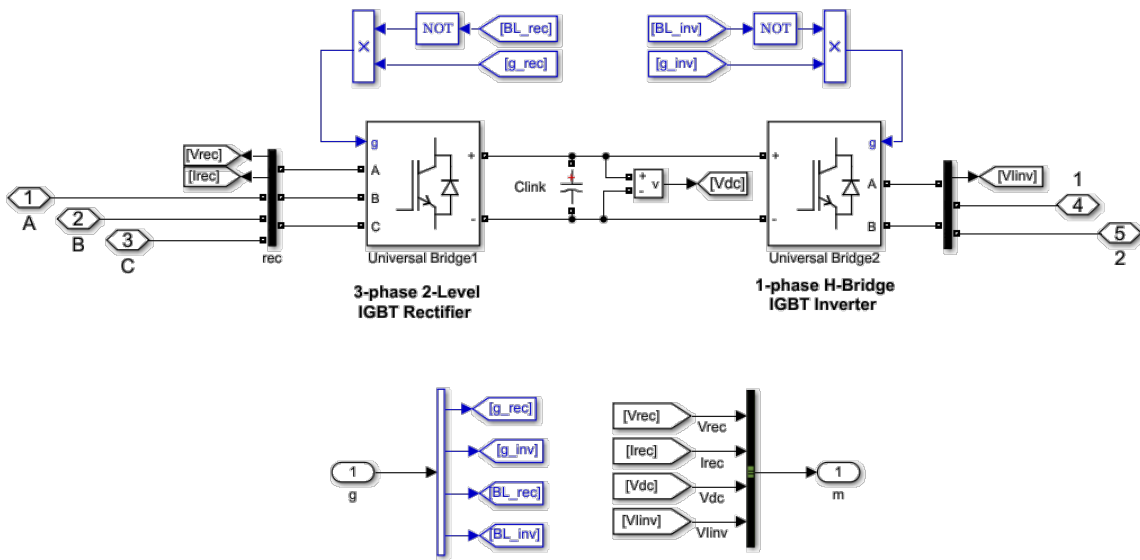


Figure 3.6: Cube model

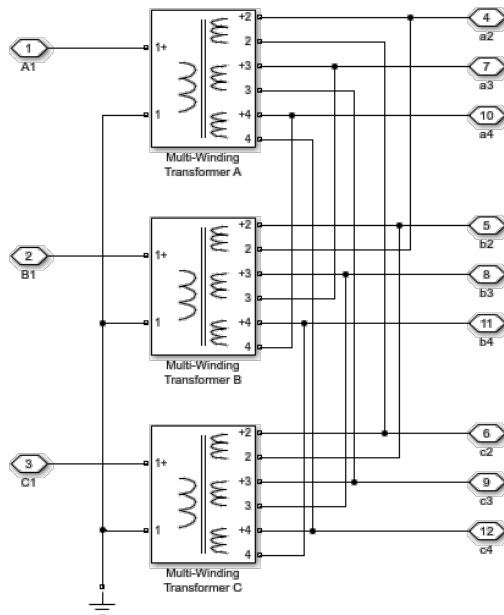


Figure 3.7: Isolation transformer model

The custom control system and PWM blocks are used within a separated subsystem in the original PAU model. This subsystem block contains controls for each slice that is modeled by receiving inputs of the slice input voltage, output slice measurements, and blocking signals for the rectifier and inverter. The output of each of the slice controls provides switching signals for each cube in the slice as well as measurements for the AFE. The blocking signals are used to delay operation of either the rectifier or inverter. In the original PAU model, the inverter is blocked until the DC link voltage is near the nominal value of 1000 V. The controls for each of the slices is shown in Figure 3.8, using the custom blocks. The AFE controller block for one slice is composed of three AFE controller blocks for one cube. Within each of the AFE blocks for a cube, there is voltage regulator, a current regulator with feedforward, a phase-locked loop, filters, conversion blocks, and measurements as shown in Figure 3.9. Both of the PWM generator blocks are composed of three major sections, “Carrier Generation,” “Uref Sampling,” and “Pulses Generation.” The main difference is within the “Pulses Generation” section, where the inverter uses a single-phase output while the rectifier uses a two-level output.



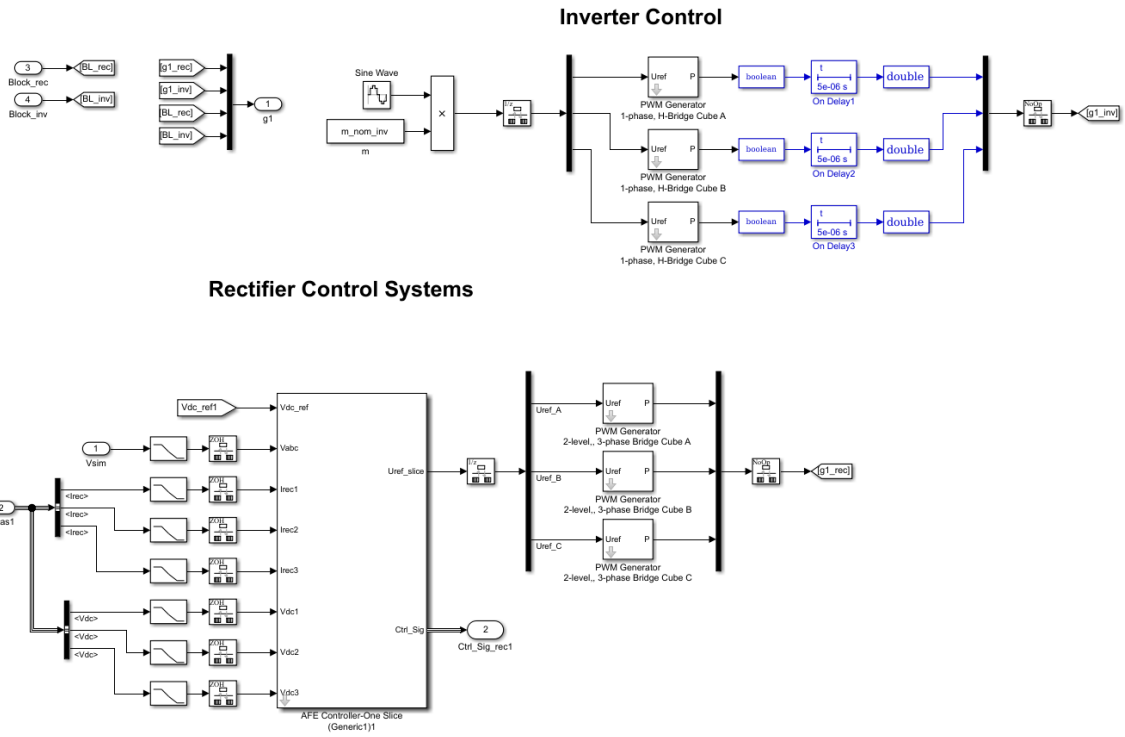


Figure 3.8: Controls model for a single slice

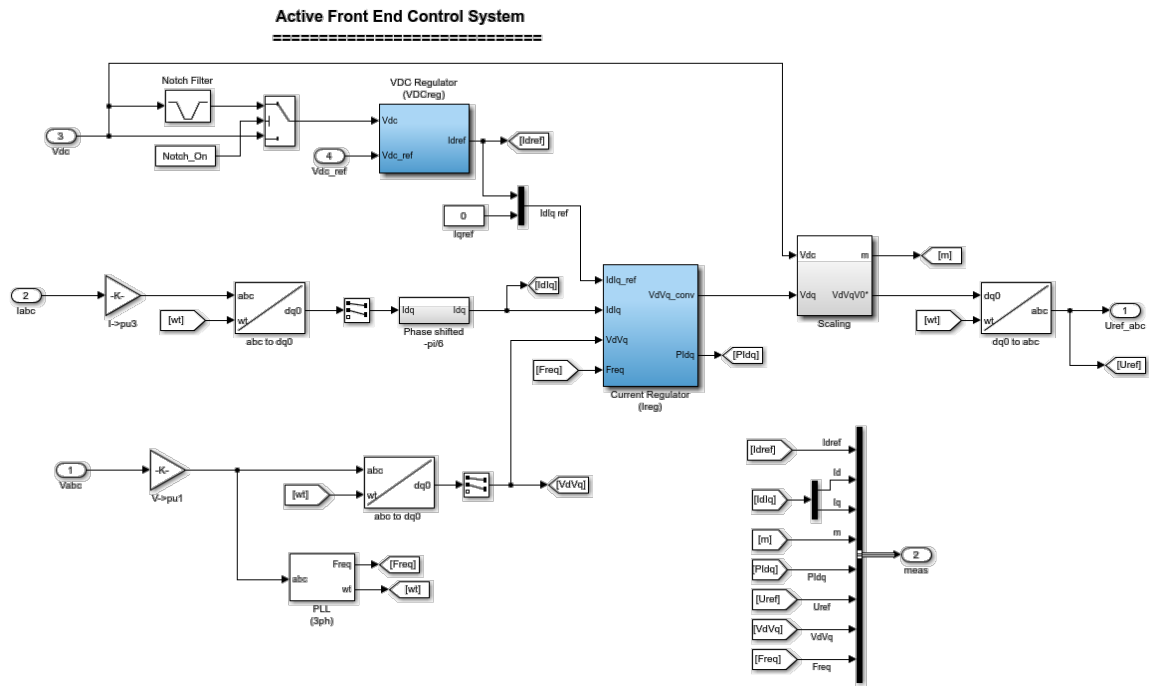


Figure 3.9: AFE controls for a single cube

In order to create the three slice VSD, the original PAU model is modified greatly. The PAU model is reduced to an ideal voltage source block and three slice blocks as seen in Figure 3.10. The grid components between the voltage source and the PAU are not within the scope of the project and are removed. The balancing reactors are also removed because there is only one group of series connected slices as opposed to the original two groups. The LCL filter, transformer, and load are removed because they are not relevant to the project. These components are also used for grid testing purposes, not motor drive testing. At the high level, the VSD model is first simulated with an open circuit to observe voltage output. Then, it is simulated with an RL load to confirm electrical operating conditions and validate the magnitude of power. Once, the RL load is confirmed, the HSM model will be connected to the drive to conduct analysis on motor and drive behaviors.

powergui

Discrete  
4.167e-07 s.

Double-click  
to open  
parameters file

Double-click  
to see  
Slice picture

Double-click  
to see  
schematic

**CLEMSON University - Duke Energy eGRID  
TWMC (Modified) Power Amplifier Unit**

SimPowerSystems Model, October 2015  
Hydro-Quebec and Clemson University Proprietary Information  
Edited by: Dean Millare

**High Speed Motor Model: Drivetrain System**

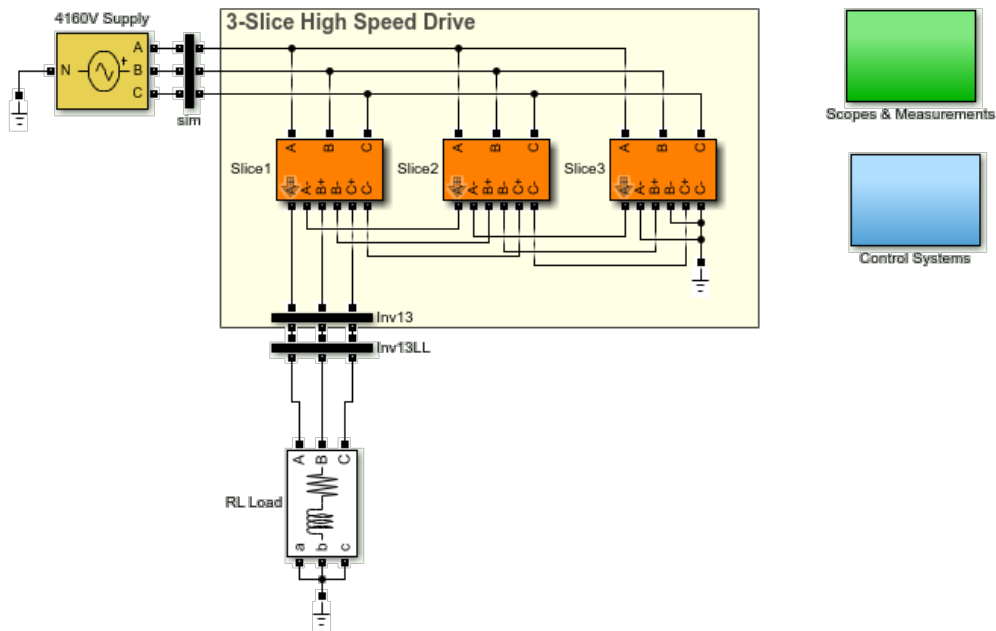


Figure 3.10: VSD model

With the slices physically modeled, the measurements for the multitude of signals in simulation must be observed. During the study of the VSD model, many variables are used to troubleshoot and debug the simulation. The voltages in the input, output, transformer secondary, DC link, and more are all logged in Simulink scopes to progressively model the novel three slice drive. AFE and inverter control signals are logged to check conformity to desired behaviors. Current limit indicators are used at one point to express whether the output currents would cause an alarm or trip in the system.

The control systems are changed to control both drives. Each control system for each slice must be replicated and designated to only control its specified slice. Included at the level of modeling with all of the control systems is the V/Hz control block shown in Figure 2.10. There are two distinct V/Hz blocks, one for each drive. This is done at the described level because the control systems for each of the slices of the respective drives all reference the same modulation signal. Instead of modeling the V/Hz block in each control system for each slice, only two blocks are needed. The updated control subsystem can be seen in Figure 3.11. Within each control system, the modeling is similar to that of the PAU model. The inclusion of the input for a modulation signal is the main difference.

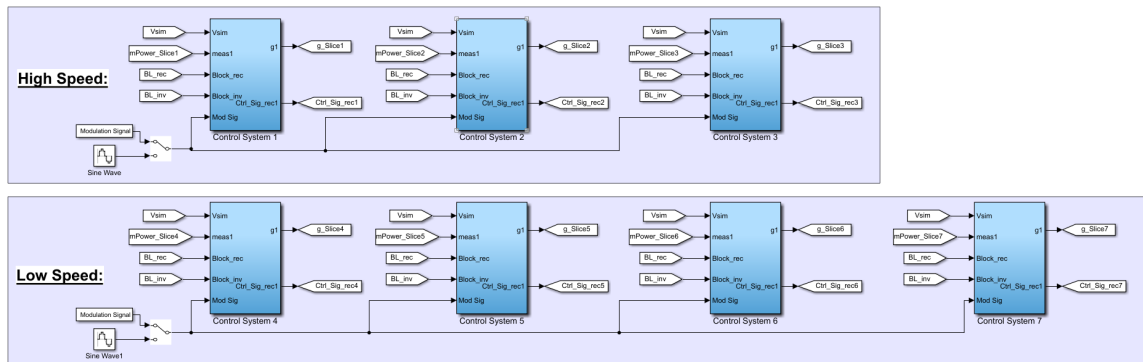


Figure 3.11: Updated high level control system

The last major modeling consideration for the VSD is the MATLAB parameter file which can be found in Appendix C. This file is updated from the file used for the PAU model to include most of the significant variables for the VSD model. For future simulations with the integrated system, all of the variables for both motors and drives are included. Variables that are used by both the high speed and low speed drives, but different in value are indicated by the suffix, “\_G”. This designates the variable being intended for

inclusion in the low speed, or generating, side of the integrated simulation. Examples include the respective motor parameters and the number of slices for the drive. This simplifies the manipulation of variables within the Simulink block that are changed based on the nomenclature. An initial condition dataset is optionally included to run tests on the system operating at full speed. The DC link voltage reference for the VSD is changed to 1100 V instead of the usual 1000 V in the PAU. The phase shifted carrier wave is setup as an array of values depending on the number of slices in the group. A manual V/Hz curve is setup through arrays representing the time, voltage, and frequency values for the lookup table block. RL load values are programmed to be determined based on the desired real and reactive power. The LPF going into the AFE control systems are increased from 1000 Hz to 2000 Hz because of harmonic distortion in cube C of slices 1 and 3 of the VSD. This comes from the double frequency harmonic of switching at a fundamental frequency of 500 Hz. The carrier frequencies are updated to 6 kHz to conform to the proposed design specifications, but can be easily changed based on the desired switching frequency. The blocking signals for the rectifier and inverter sides of the cubes are parameterized to ease in test repeatability. These revisions have all been enacted after observation of the VSD model and simulation.

### V/Hz Control

Due to the topology of the VSD, the modulation signal in simulation can be altered to achieve the desired V/Hz behavior. This is done through implementing the created V/Hz source to produce controllable, three-phase, per unit sinusoids. In this way, the inverter is

essentially replicating the sinusoidal waveforms through the phase shifted PWM. Therefore, controlling the frequency and amplitude of the modulation signals controls the output voltages to drive the motors.

The modulation signal is produced on the level of modeling with the control systems for each of the slices. In each control system block of the original PAU model, there is an inverter section with a default sine wave generator. This sine wave is defined by standard parameters such as frequency and amplitude. To become variable during simulation, this constant modulation signal is substituted with the V/Hz signal, making the control scheme a matter of changing the frequency and voltage values in the block.

However, in the existing HMI for the PAU designated for the LSIM, there is a different means of programming the drive for V/Hz control. The settings for the V/Hz control include values of rated voltage and frequency, acceleration and deceleration times, as well as a table relating frequency and voltage. The table manages the reference voltage needed for the given reference frequency, creating the V/Hz curve similar to Figure 2.4. Therefore, a V/Hz curve can be explicitly given for a set of points with interpolated values. This provides the reference for the PAU to develop the input voltage to the LSIM. Similar capabilities are expected to control the high frequency VSD.

Depending on safety and protection considerations, the rate at which these changes occur can be dictated as well. Since the frequency reference for the PAUs is controlled by a keypad on the HMI, any change is executed immediately. The acceleration and deceleration times are used to mitigate harmful effects of phenomenon such as inrush current and regenerative braking. Making sure these settings protect the motors and

gearbox is imperative for all tests. The modeling and simulation efforts to represent the VSD will serve to predict electrical and mechanical behaviors before actual testing. Settings for the VSD and PAU can be derived from analysis done through the various simulations.

### Simulation Results

Simulations are done to observe the startup procedures and steady-state behaviors of the VSD for three types of output connections: open circuit, RL load, and motor model. Both motor drives models are tested based on standard V/Hz procedure to achieve the desired output. The open circuit test shows the seven levels of a single-phase voltage output, up to 3300 V, in Figure 3.12. The V/Hz looks very angular because of how the PWM outputs the voltage. The VSD outputs voltages in increments of the DC link voltage. Since there are three slices, there are three voltage levels going positive and negative in the envelope. However, the pulse duration during each of these levels goes from short to long and resets when another level is added. By the end of the V/Hz ramp, the output voltage resembles a balanced sinusoidal waveform as shown in Figure 3.13. A modulation index of 1 is used in this case to provide the maximum voltage output within the linear region of control for SPWM.

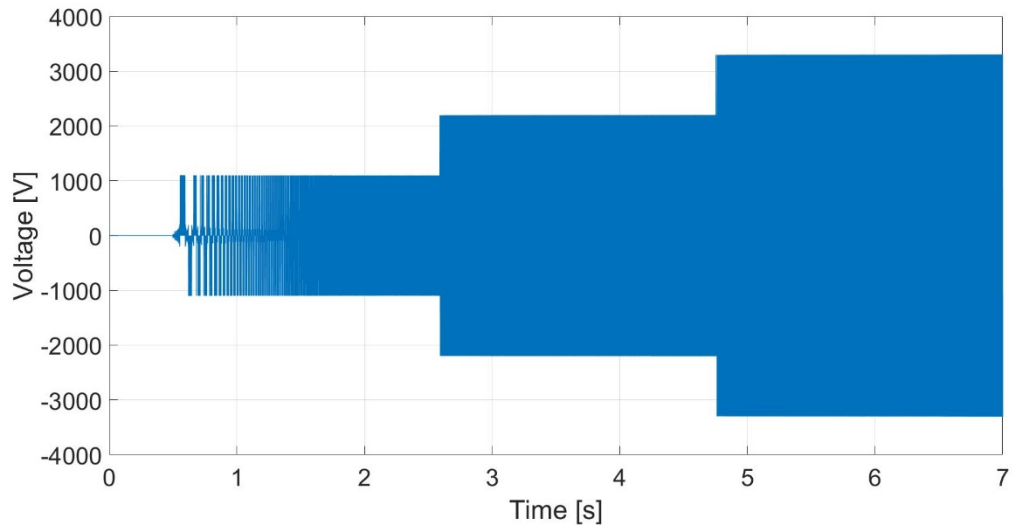


Figure 3.12: VSD output line-to-neutral voltage

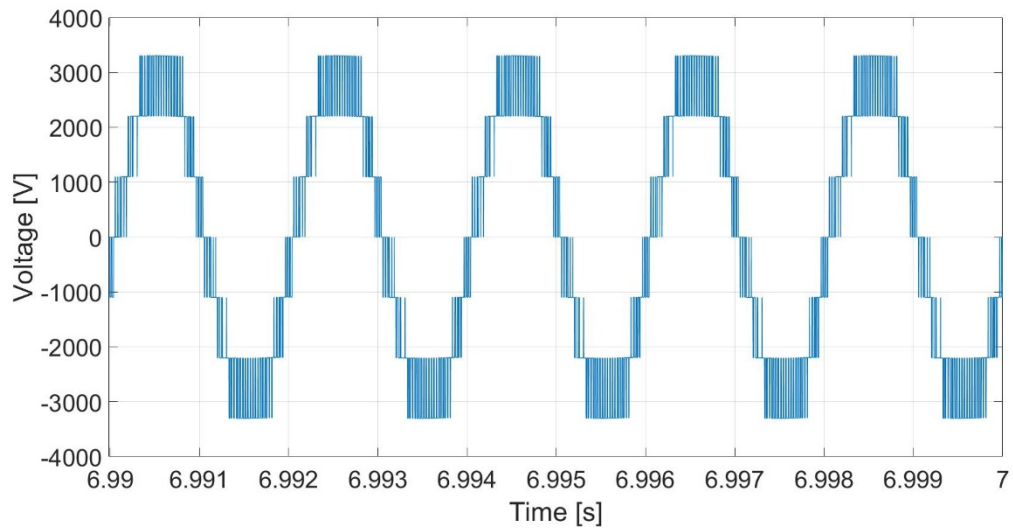


Figure 3.13: VSD output line-to-neutral voltage zoomed in

The RL load test is started in the same manner as the open circuit test. A load is connected to represent the motor operating at 4160 V, 220 A, with a 0.6 pf lagging. Using (3.4), values for the modeled resistor and inductor can be found. Since the same voltage



output is used, the current is more significant. The RL load creates a smooth current increase to the steady-state value as seen in Figure 3.14. Figure 3.15 shows that the current is also sinusoidal, supporting the use of the high frequency VSD for the HSIM. Although the peak current is not quite the designated value, the proximity provides support towards the validity of the drive model. This discrepancy stems from the use of a modulation index of 1, which creates an RMS voltage slightly under 4160 V.

$$R + jX = \frac{|V|^2}{S^*} \quad (3.4)$$

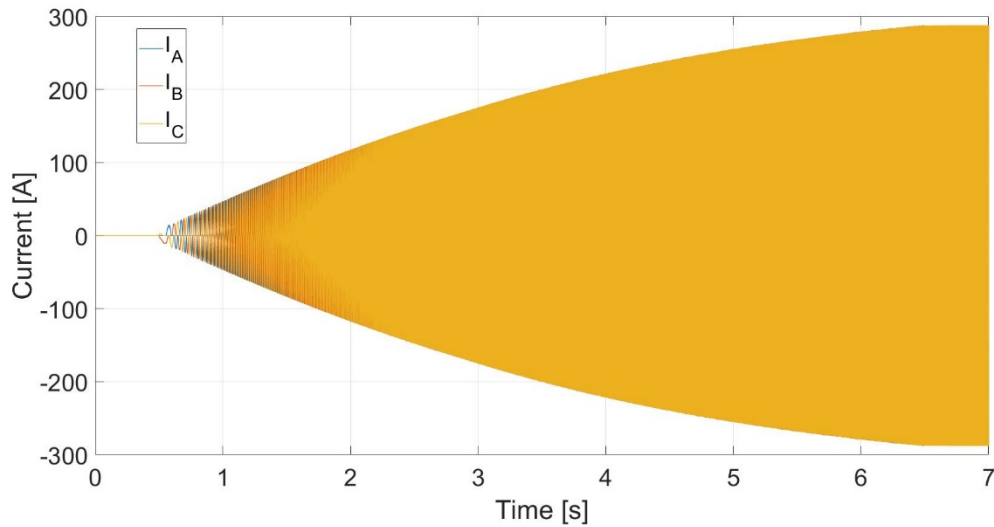


Figure 3.14: VSD RL load test current

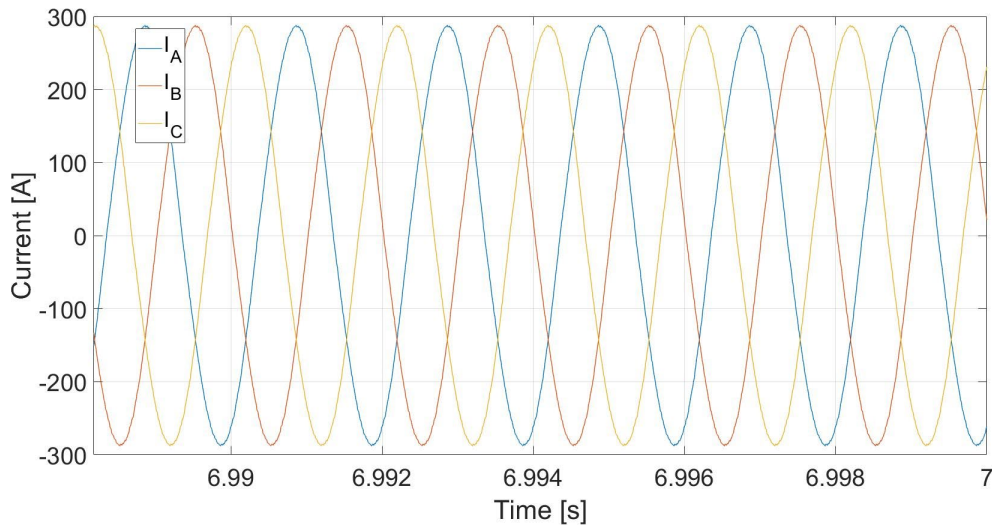


Figure 3.15: VSD RL load test current zoomed in

To simulate the VSD with the motor model, more realistic electromagnetic behaviors must be addressed. At low frequencies, V/Hz control has less effective performance in maintaining the desired flux due to the voltage drop across the stator [16]. This is due to the voltage drop that occurs from the stator terminals to the air gap in the IM. At lower frequencies, this voltage drop is more significant than at nominal frequencies. Therefore, in order to start the motor, a voltage boost is provided at the start of simulation to provide more torque without saturating the flux [8]. Through experimentation a voltage boost of 7.5% provides enough torque to start the motor for a 6 second ramp to full no-load speed. The mechanical behaviors can be observed in Figure 3.16 and Figure 3.17. The significant electrical behaviors can be observed in Figure 3.18, Figure 3.19, Figure 3.20.

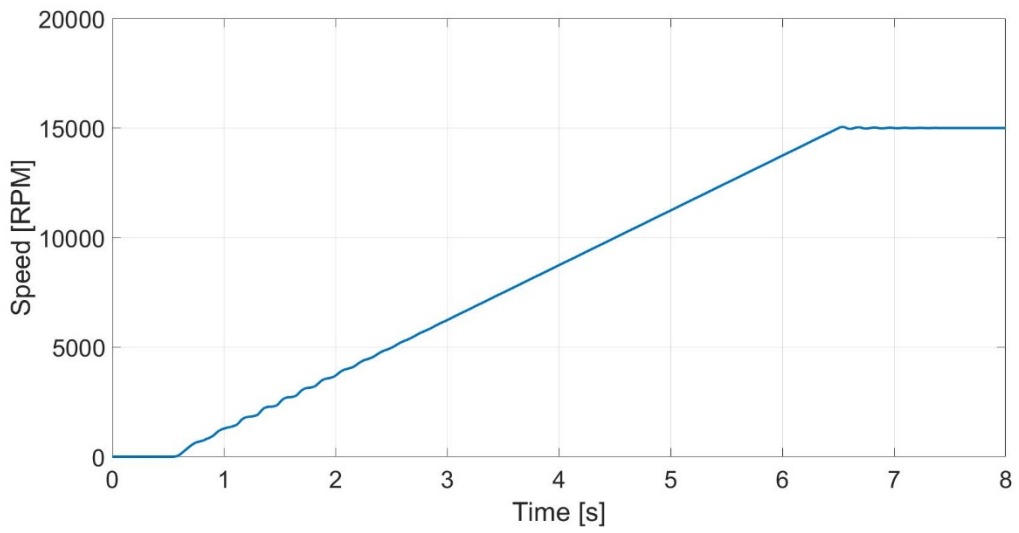


Figure 3.16: VSD with HSIM load test speed

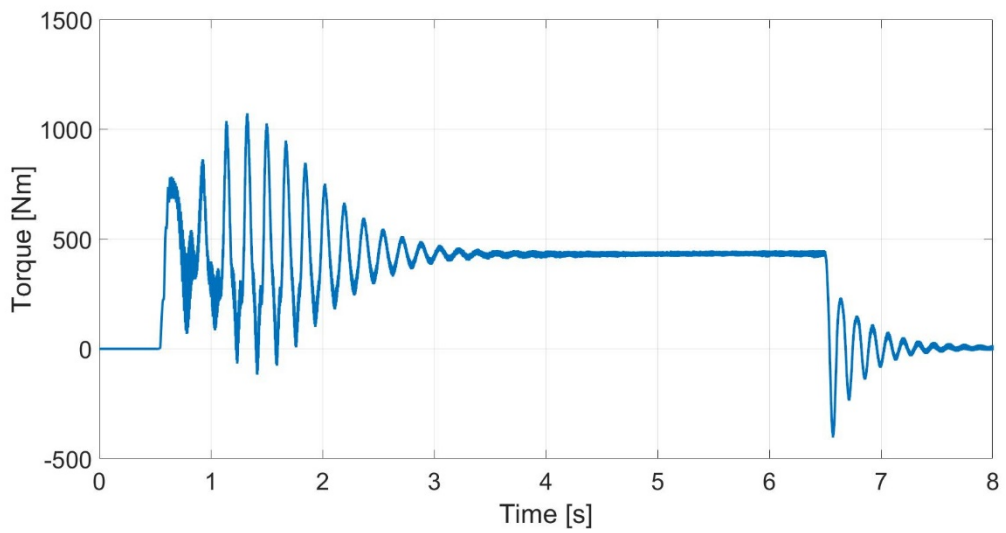


Figure 3.17: VSD with HSIM load test torque

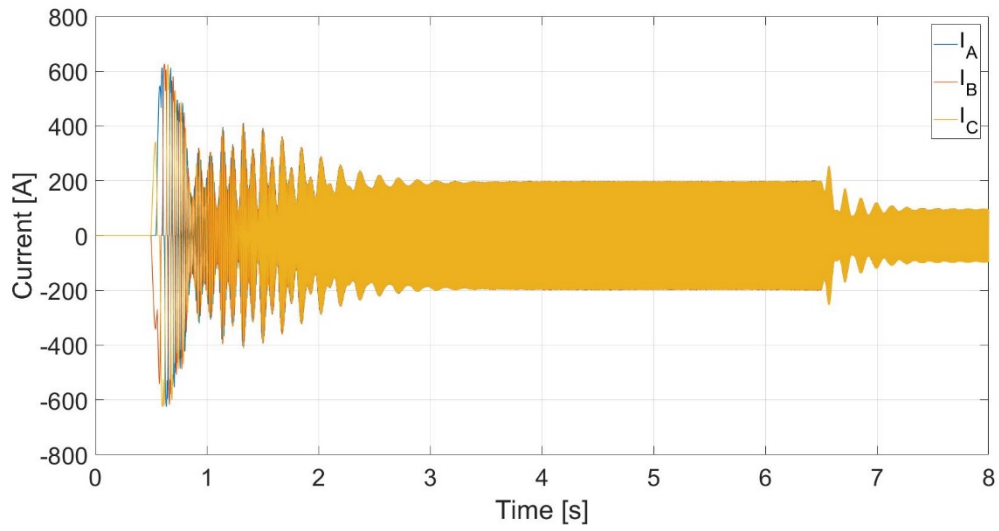


Figure 3.18: VSD with HSIM load test current

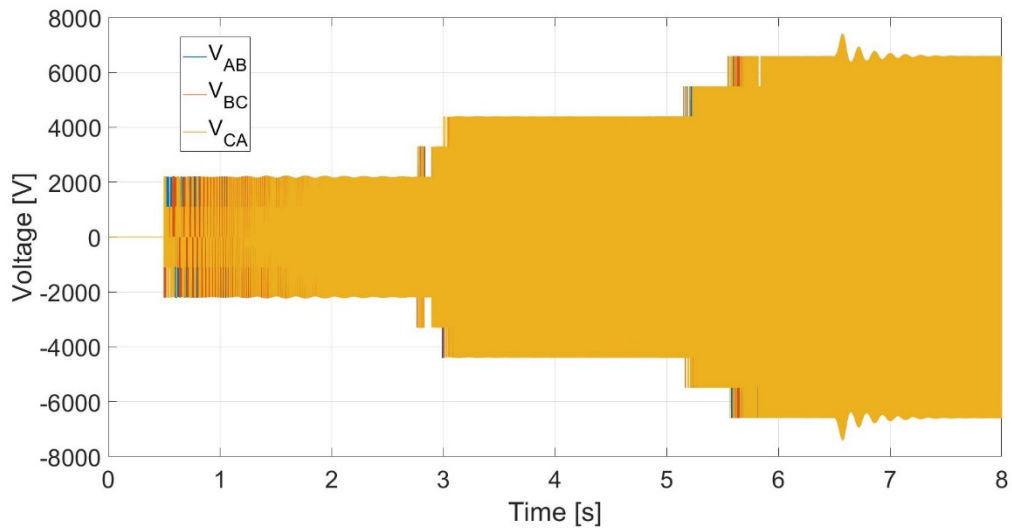


Figure 3.19: VSD with HSIM load test line-to-line voltage

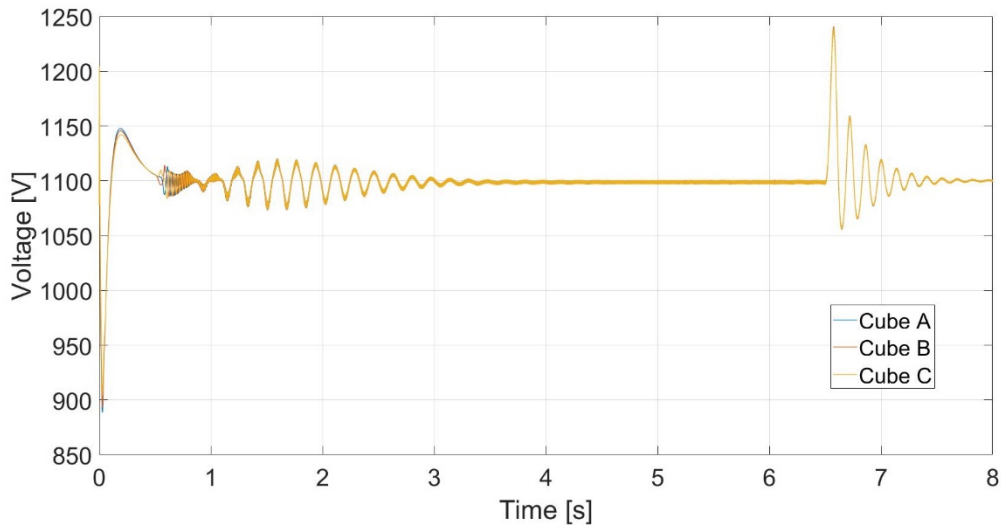


Figure 3.20: VSD with HSIM load test DC link voltage

### Limitations

The simulations provide accuracy to a certain degree. Actual testing issues that arise will change the validity of the simulation with varying magnitude. Although general behaviors have been modeled, certain minutiae will be absent from the software representation. Electrical limits are idealized in Simulink. The voltages and currents that may be observed throughout the model may not be achievable or realistic. When establishing the settings for controls, protections, and device specifications, caution must be taken when using the simulated data as a reference. Test procedures must be done systematically and gradually to avoid catastrophic failure of the test equipment. The VSD and PAU will operate at medium voltage and MW power levels so any faults during operation will have consequences for the system and the test facility. This is why settings for warnings, trips, acceleration, and deceleration must be made at the minimal setpoint

that achieves the desired action. Causing the test to shut down because of protective action is preferable to shutting down for device destruction.

### Summary

This chapter details the parts of a standard VSD and relates them to the project specifications. The techniques used for the operation of the PAU and high frequency VSD allow for command of the LSIM and HSIM. Relevant work done on testing of SiC modules and calculations for voltage sag are included. The detailed model of the precursor drive is explained as well as how it is changed to reflect the new VSD topology and performance. Simulation results of the new VSD with different loading conditions expresses its functionality. The model includes extensive details on the controls, allowing for more improvements to be made for future testing endeavors. After modeling the motors and drives separately, they can be combined together for system tests.

## CHAPTER FOUR

### INTEGRATION

#### Overview

With models developed for the motors and drives, the two are coupled together for integrated testing. This includes startup, loading, and trip scenarios. Due to the iterative process of simulation for this novel system, simulation execution time must be relatively short. Simplification is done by using the ideal V/Hz voltage source instead of the detailed drive model for the VSD and PAU. The integrated system model follows the block diagram found in Figure 1.4. The transformers and utility bus are replaced with ideal voltage sources. The gearbox will be modeled as an ideal ratio between the two machines. Controls for each drive will be evaluated simultaneously based on previous control modeling for each drive. The dynamics of the system will be analyzed and used in actual testing of the project.

#### Coupled IM with Ideal Voltage Sources

The simplified model includes the ideal drives, gearbox ratios, motor models, and controls. The drives are modeled through the V/Hz source model in Figure 2.10, each with its respective voltage and frequency input. Although the inputs are separate blocks in Simulink, they are still proportional to one another. The induction motors are configured to have a torque input to the HSIM block and a speed input to the LSIM block. Ideal gear ratios are incorporated as gain blocks to model the torque and speed coupling.

Measurements are made throughout the model to make observations on the various behaviors of the system. LPFs are included in the model to emulate smooth control of the voltage output, even though it is run in open loop. This model can be seen in Figure 4.1.

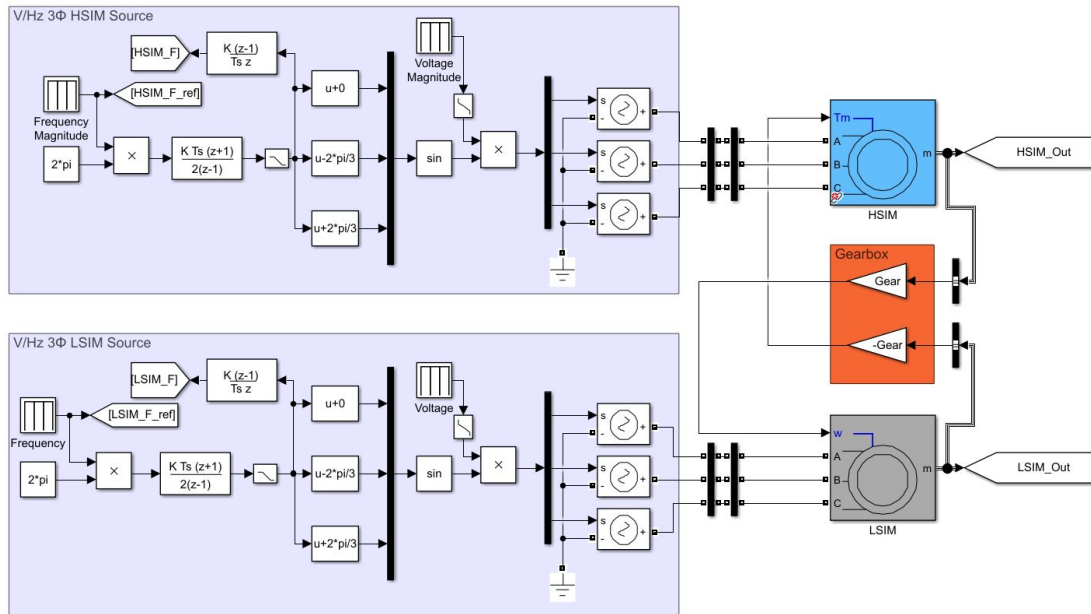


Figure 4.1: Simplified system model

This model is run in an open loop fashion to observe the startup and steady-state behaviors of the system. The open loop sequence starts by both V/Hz sources ramping up to nominal no-load conditions. Ideally, given the constant V/Hz ratio of both VSDs respectively, they should increase their voltage and frequency at the same rate, which, across the gearbox, should result in a ramping up of both motors without significant electromechanical interactions between the two. Once the two motors reach a state of equilibrium, the V/Hz of the LSIM will be decreased slightly to apply a load torque on the HSIM. This sequence will be examined in terms of steady-state and dynamic behaviors.



In order to find the V/Hz value that the LSIM must use to achieve a desired torque load, relationships must be established between the HSIM and LSIM across the gearbox. This V/Hz value is per unitized representing the proportion of voltage and frequency reference to the nominal value. Using the concept of how V/Hz affects the torque-speed curve of an induction motor, it is understood that decreasing the V/Hz value of the LSIM will effectively cause the operating torque-speed curve shift to the left as shown in Figure 4.2. This decrease does not affect the ratio between the voltage and frequency, but rather decreases the two values according to the V/Hz ratio. Since the two induction motors are coupled by a gearbox, there is a strict relationship between the operating speeds. This gear ratio of  $8.\bar{3}:1$  allows conversions to be made across the gearbox, obtaining ideal correlations between the high and low side torques and speeds. With the desired goal of obtaining a specific load on the HSIM, an equation can be derived to obtain the new V/Hz value. Since the operating point is near the synchronous speed of the machines, a linear region is assumed for the torque-speed curves.

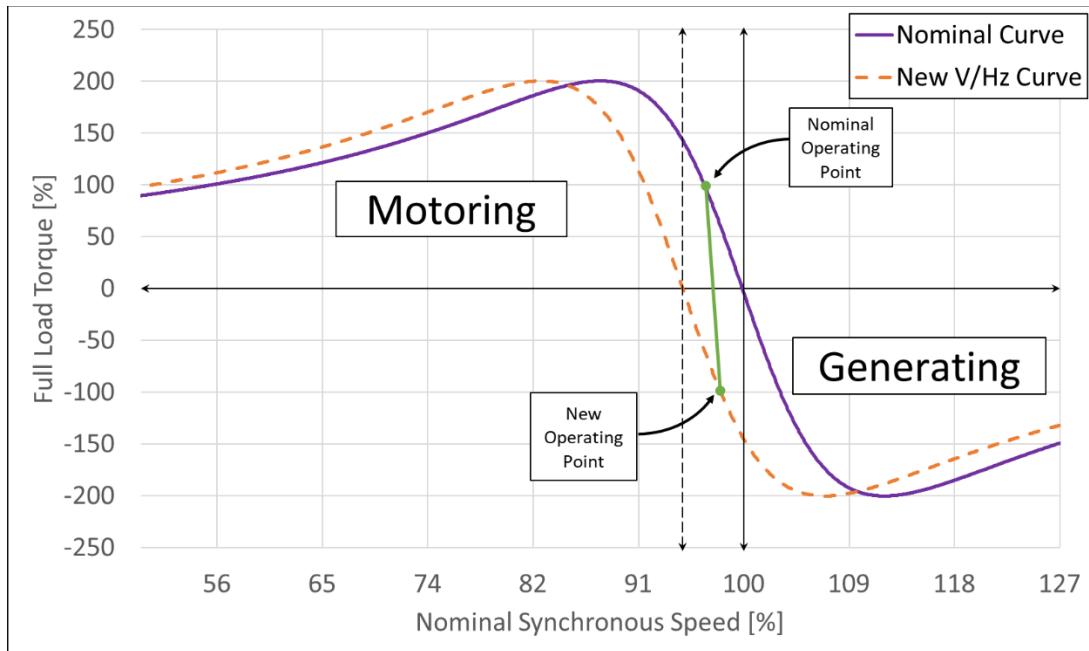


Figure 4.2: Effect of decreasing V/Hz value for coupled operation

Given a desired torque load, the speed of the HSIM can be found using a linear equation based on the rated slip speed of the machine. With the torque and speed of the HSIM, both can be translated into their LSIM counterparts by the gear ratio in the respective orientation. Speed will decrease from the HSIM to the LSIM while the torque increases. Knowing the necessary torque of the LSIM, the speed at which that torque will be achieved in a decoupled fashion can be found. This torque is not exactly the same as the nominal torque of the LSIM, thus providing the need for these additional calculations. Then, knowing the speed that the HSIM will drive the LSIM to and the speed that is necessary from the LSIM to achieve the desired load torque, the synchronous speed at which the V/Hz ratio should drive the LSIM can be found. This new speed can then be per unitized by dividing by the nominal synchronous speed of the LSIM to obtain a decimal

value, which can be used as the new operating per unit V/Hz value. This simple multiplication is possible because of the relationship between frequency and speed in (2.2).

Ideally, if both machines in the system are rated to proportionally equivalent torque values, this derivation is simplified to (4.1). This is due to the assumption of a linear operating region that would have a slip on the LSIM that approaches the same desired load torque value. Thus, the datasheet for the motors will provide the necessary information in the rated slip of the motors without needing further calculations. However, because the full rated torques of both machines are not related by the gear ratio, a general formula is derived in (4.2). This utilizes the known information from an induction motor datasheet and, based on the desired load torque, can give the amount of decrease for the V/Hz ratio. Further simplification can be observed in (4.3).

$$(V/Hz)_{\%} = \left(1 - (Load\ Torque_{pu})(s_{nom,H} + s_{nom,L})\right) * 100\% \quad (4.1)$$

$$(V/Hz)_{\%,new} = \left[1 - \tau_H \left(\frac{n_{s,L}^2 \tau_{nom,L} (n_{s,H} - n_{nom,H}) + n_{s,H}^2 \tau_{nom,H} (n_{s,L} - n_{nom,L})}{n_{s,H} n_{s,L}^2 \tau_{nom,H} \tau_{nom,L}}\right)\right] * 100\% \quad (4.2)$$

$$(V/Hz)_{\%,new} = \left[1 - \tau_H \left(\frac{s_{nom,H}}{\tau_{nom,H}} + \frac{s_{nom,L}}{\tau_{nom,L}} \left(\frac{n_{s,H}}{n_{s,L}}\right)\right)\right] * 100\% \quad (4.3)$$

The control scheme for the LSIM is incorporated to provide torque control for the dynamometer as shown in Figure 4.3. The green blocks and connections represent control signals while the black blocks and connections represent physical devices. This closed loop control scheme resembles the HSIM speed control with an outer torque control loop. The inner speed loop operates with a bandwidth that is at least a decade larger than the outer torque loop. This control allows for an input of desired load torque to obtain a new speed

control reference, which is propagated through to output voltage and frequency references to the LSIM drive.

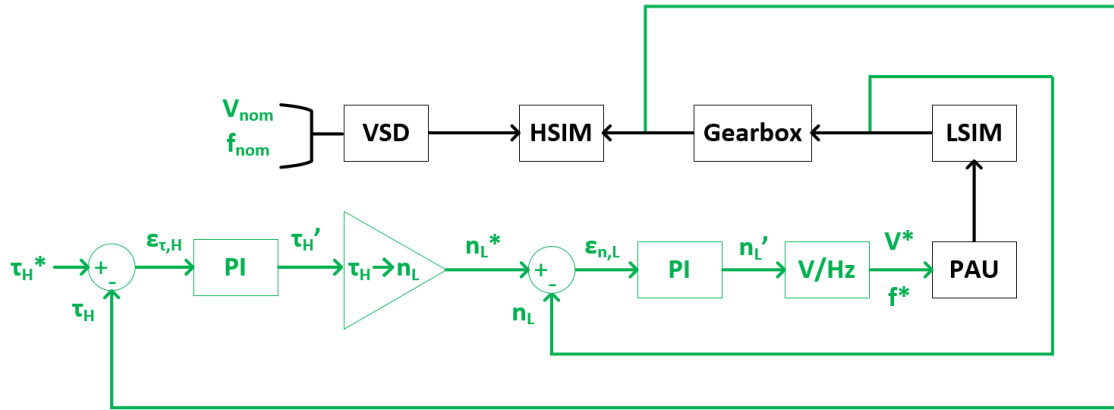


Figure 4.3: Torque control block diagram

PI controller tuning of the gain values for the LSIM drive requires established controls for the high frequency VSD. Since the purpose of the torque control of the LSIM is to provide a load for the HSIM, the HSIM does not need to be speed regulated. Also, since the HSIM is operating at a high speed with a small slip, the change in speed will be minimal. Therefore, the high speed drive V/Hz will remain at nominal values while the low speed drive will create the change. This allows multiple tests to be run to tune the gain values for the torque control.

Since there are two loops to consider, the fastest loop must be tuned, then the two loops can be tuned together. The inner speed loop is observed for the effects of changing  $k_i$  and  $k_p$  separately. These results can be seen in Figure 4.4 and Figure 4.5. Similar to the HSIM speed control test, the increasing proportional gains create increasingly large

oscillations. The increasing integral gain causes some oscillation, but not as dramatic. It also gets to the desired speed faster.

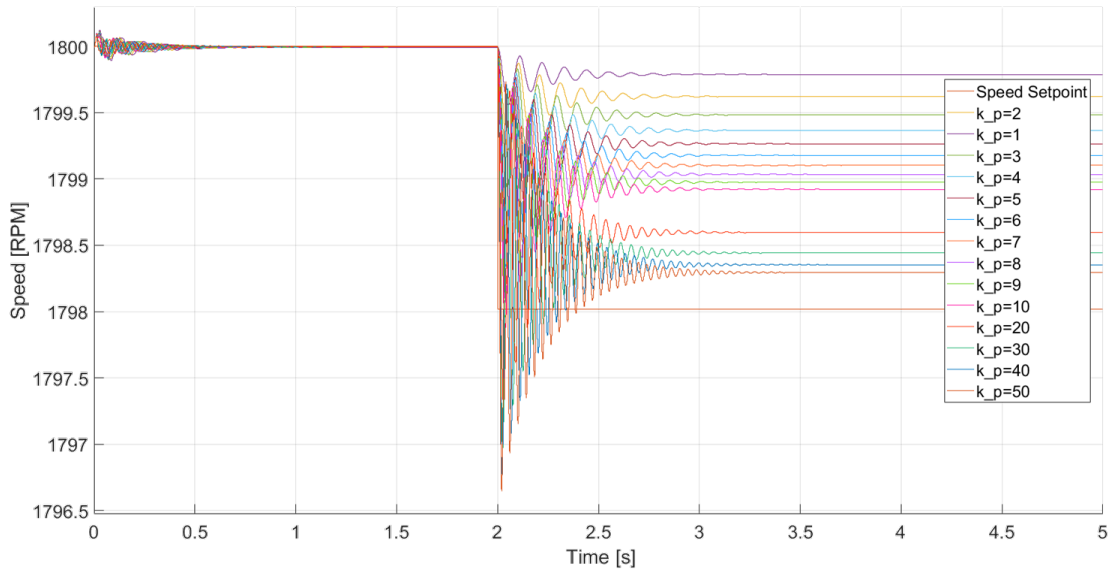


Figure 4.4: Effect of  $k_p$  in speed loop of torque control

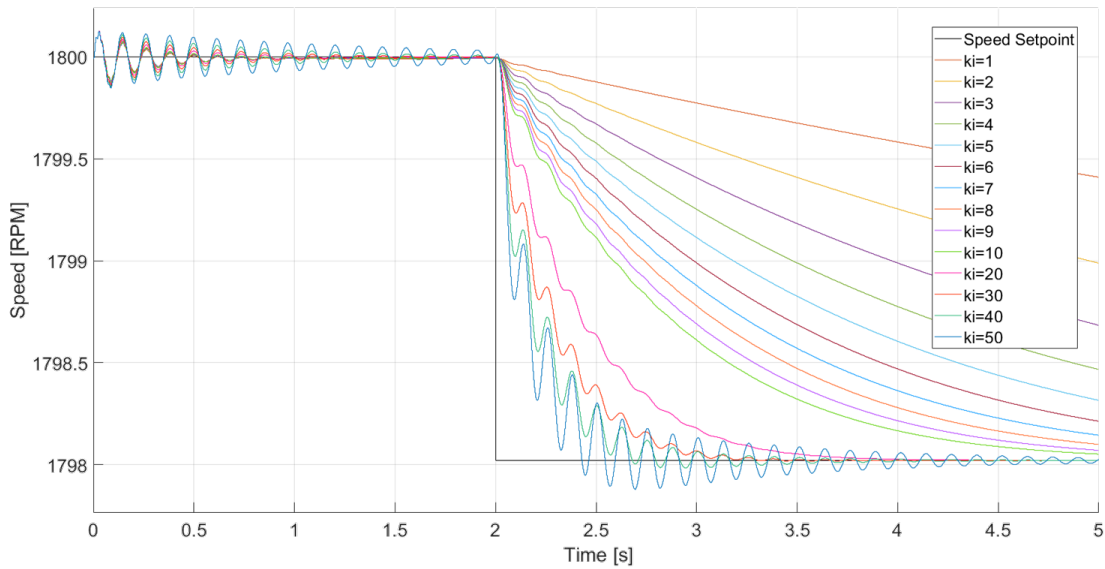


Figure 4.5: Effect of  $k_i$  in speed loop of torque control

The torque loop is also observed based on the effects of  $k_p$  and  $k_i$  in the torque PI controller. To do this, the speed loop PI controller is circumvented in simulation. This still provides the V/Hz reference signals for the low speed drive. For this study, the torque is observe referred to the high speed side of the gearbox. Increasing the proportional gain increases the overshoot but always has steady-state error. Increasing the integral gain also has overshoot behaviors but starts to oscillate more. These behaviors can be seen in Figure 4.6 and Figure 4.7. Using these behaviors as reference, the two loops are tuned in the with the coupled simulation. The gain values with good response for a full load step change and ramp can be found in Table 4.1.

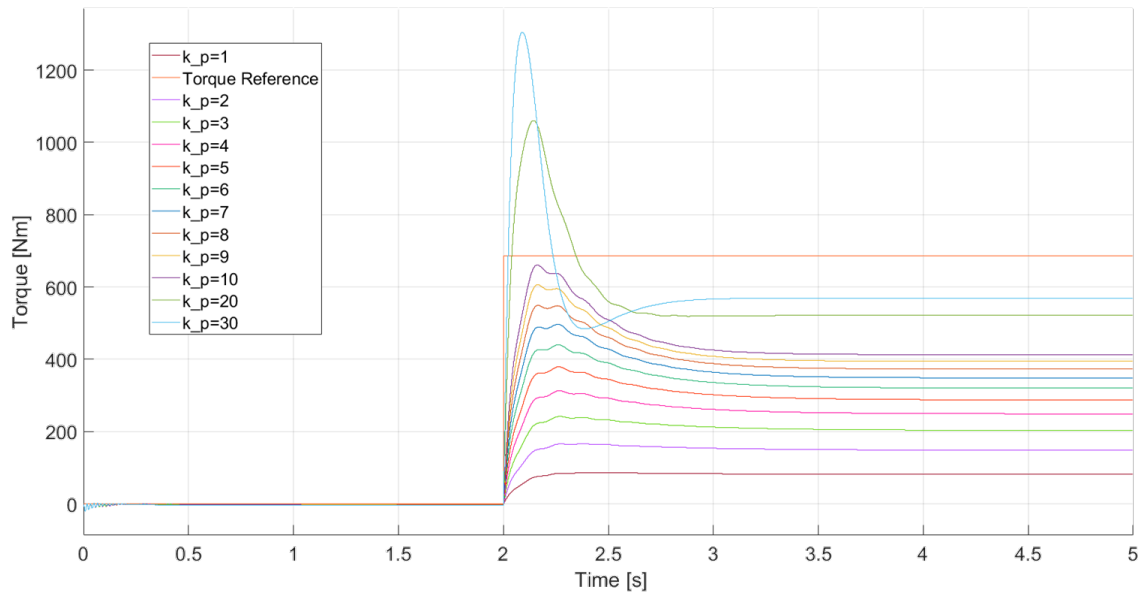


Figure 4.6: Effect of  $k_p$  in torque loop of torque control

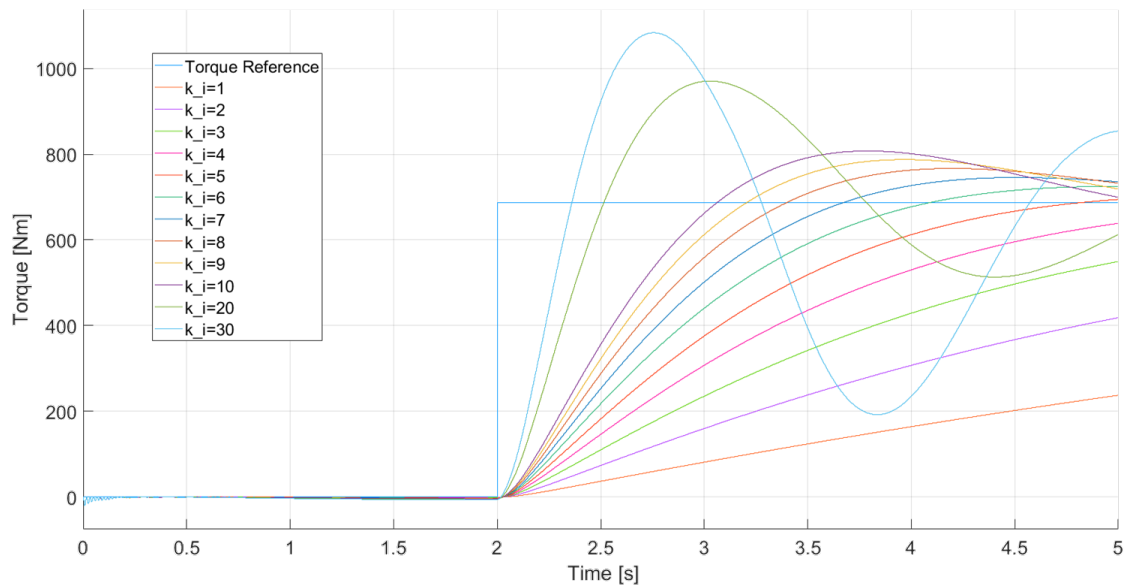


Figure 4.7: Effect of  $k_i$  in torque loop of torque control

Table 4.1 PI controller gains for torque control

|   | Speed Loop | Torque Loop |
|---|------------|-------------|
| <b>Proportional Gain (<math>k_p</math>)</b> | 7.5        | 1.5         |
| <b>Integral Gain (<math>k_i</math>)</b>     | 12.5       | 20          |

With the torque control established, the V/Hz closed loop control system can be modeled into the simplified integrated model as shown in Figure 4.8. The colors in the model represent the different sample time associated with the blocks. Since the controls are being tested after the motors reach near nominal synchronous speed, an initial condition dataset is created by the open loop, simplified system model. The speed control for the HSIM is included to simulate the feasibility of the VSD bringing the system to rest if the low speed drive trips during full load. Previous modeling iterations can be seen in the HSIM speed control blocks such as manual speed inputs and rate limiters. Switch blocks are

included to change the control from a constant frequency reference to the PI controller reference during the trip condition. The torque control for the low speed drive includes an inner speed loop, similar to the closed loop speed control for the HSIM. The outer torque loop applies closed loop feedback on the load torque of the HSIM. This error signal goes through a separate PI controller to create a plant input into conversion blocks that translate high side torque to low side speed. This conversion block essentially calculates the slip that the HSIM is expected to experience based on the load torque and imposes that slip on the low speed side to create a speed reference for the LSIM. Switching blocks are included in the torque control as well in the event that the high frequency VSD trips offline.

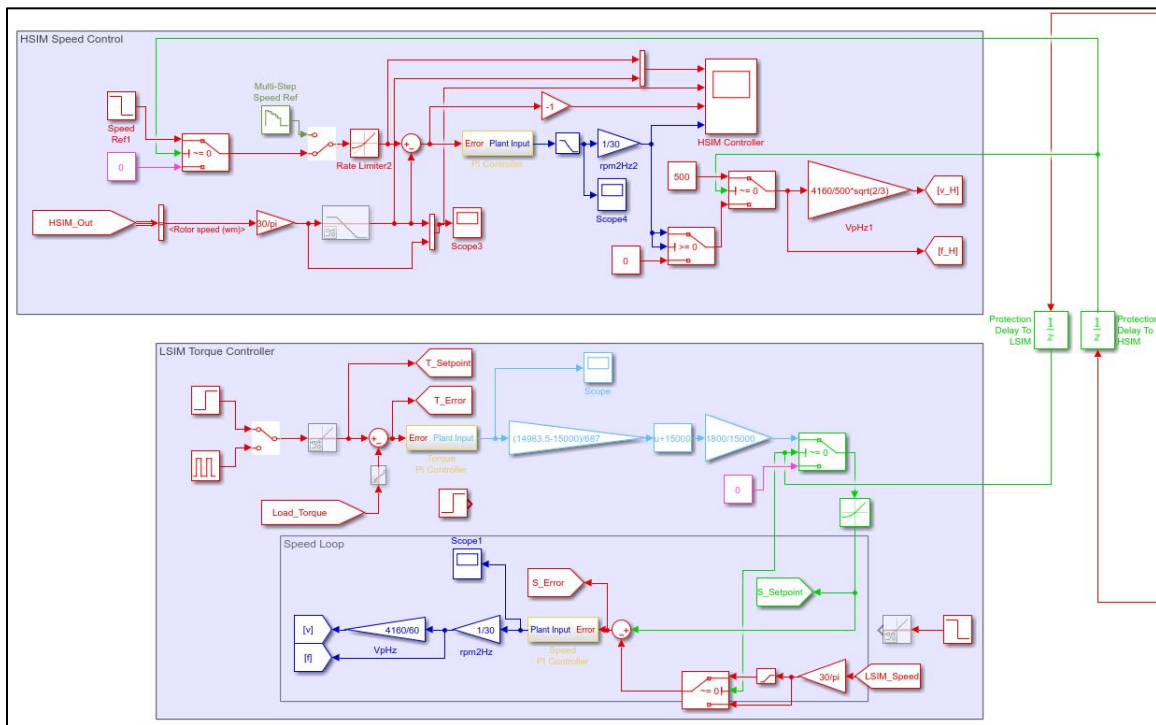


Figure 4.8: Controls for simplified system model



For simulating trip conditions, the model must include switches of some sort between the drives and the motors. Ideal switch blocks are added with a negligible internal resistance to the simplified model as shown in Figure 4.9. However, since both the switches and the IM blocks are modeled as current sources, they cannot be connected in series without a large parallel resistance. This is the reason for the 1000 pu resistors connected to the stator terminals of both motor blocks. However, when the switch opens to simulate a trip in the drive, the current that was flowing in the stator windings travel back through the load, causing a large, unrealistic power flow through the large resistance. This is why another set of ideal switches is included with 0.001 pu resistance to effectively short the stator terminals of the motor experiencing the trip. Although this process of tripping with connected loads and shorts will not be practically realized, the simulation reflects what the motor will experience. With a disconnected drive on one side of the system, emergency actions can be taken to predict shut down behaviors.

Additionally, the trip condition between the VSD and HSIM requires the dynamometer control to be altered. Since the main concern of the system during a trip scenario is to approach a state of rest in a prescribed period of time, the outer torque loop is circumvented, and a speed reference of zero is given to the inner speed loop. A slew rate limiter is imposed to control the rate at which the dynamometer brings the system to a zero-speed state. This change in control is required because the tuning of the low speed subsystem is set for loading conditions, not for tripping. Although the dynamometer would naturally bring the system to rest because of the V/Hz control method in a generating mode for normal loading procedure, the low speed controls would saturate and cause undesirable

behaviors when the HSIM shaft is not rotating. The difference in loading and trip situations require distinct control behaviors, thus the need for alteration. However, with the dynamics of the LSIM continuing operation in a torque generating mode, this emergency function is beneficial to consider.

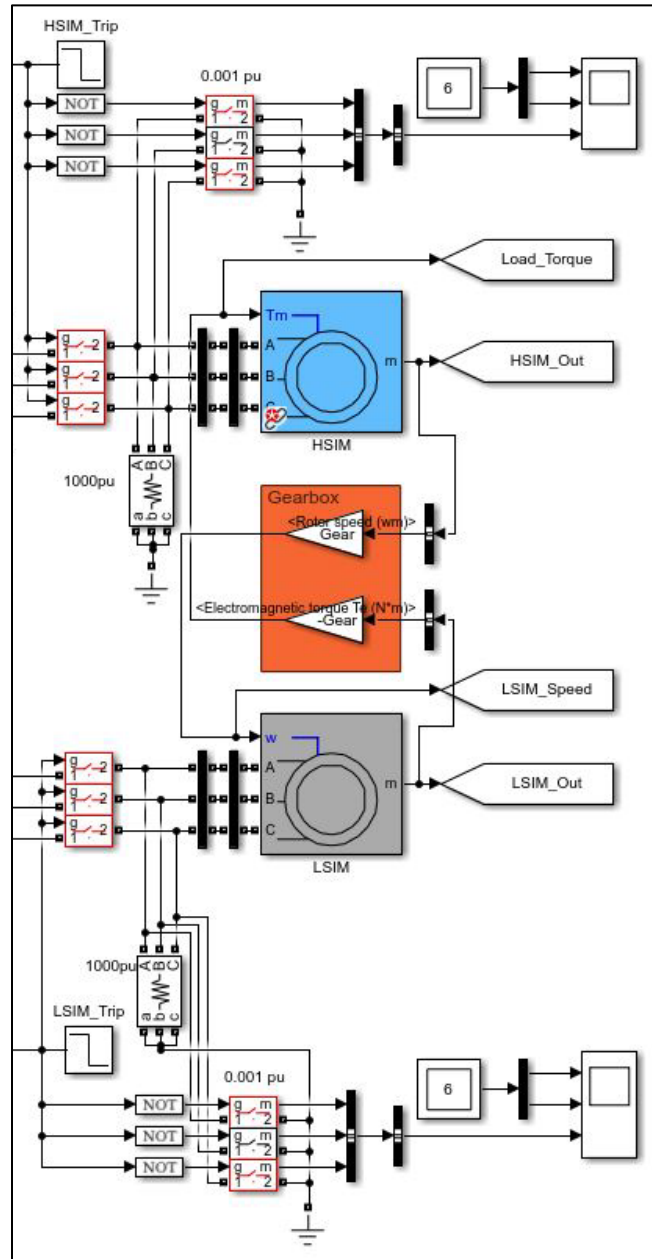


Figure 4.9: Trip modeling for simplified system model

### Full Load Test Results

With the controls, ideal drives, motors, and gearbox, a full load test is executed for the entire system. This full load test is conducted while the system is running at a full no-load condition where both machines are spinning at near their nominal synchronous speed and the drives are outputting their nominal voltage and frequency. Several control behaviors are given in Figure 4.10, Figure 4.11, and Figure 4.12.

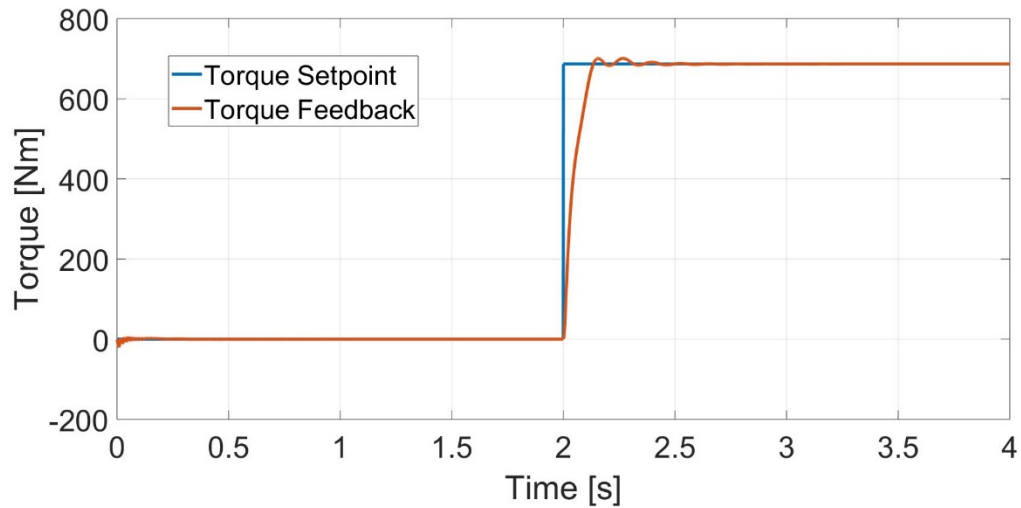


Figure 4.10: Integrated system full load test torque control signals

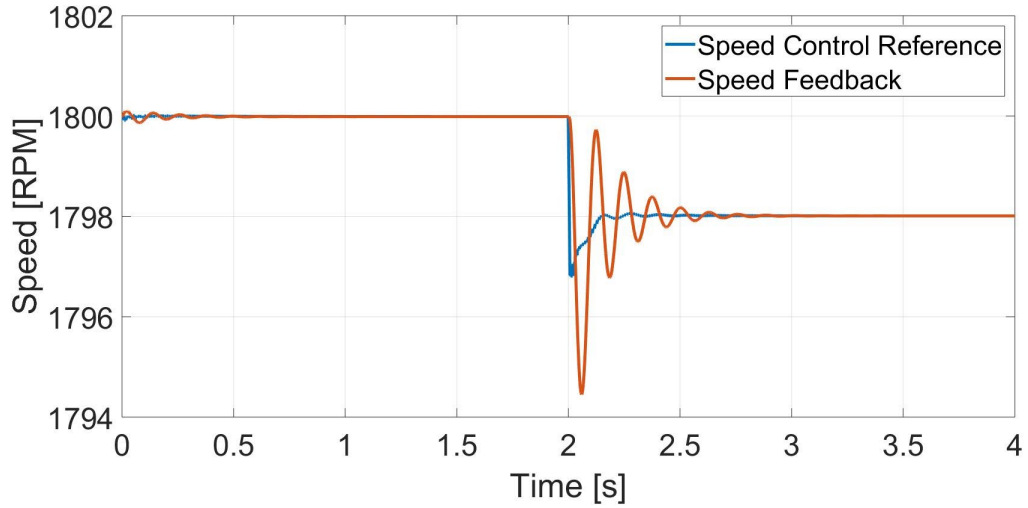


Figure 4.11: Integrated system full load test speed control signals

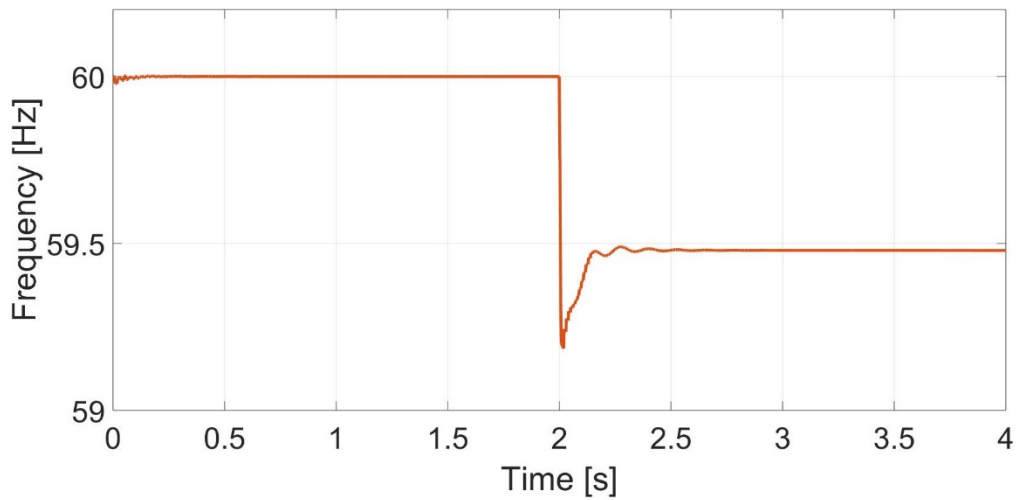


Figure 4.12: Integrated system full load test frequency reference

In response to these control actions, the HSIM and LSIM are driven to the nominal slip of the HSIM. The speeds are related by the gearbox, thus being proportional to each other. The speeds of both motors during loading can be seen in Figure 4.13 and Figure 4.14. The torques produced by both machines are also related by the gear ratio, but are

negative of each other because of their operating modes as shown in Figure 4.15 and Figure 4.16. Lastly, the current drawn from each drive approaches the rated value during this full load test as exhibited by Figure 4.17 and Figure 4.18.

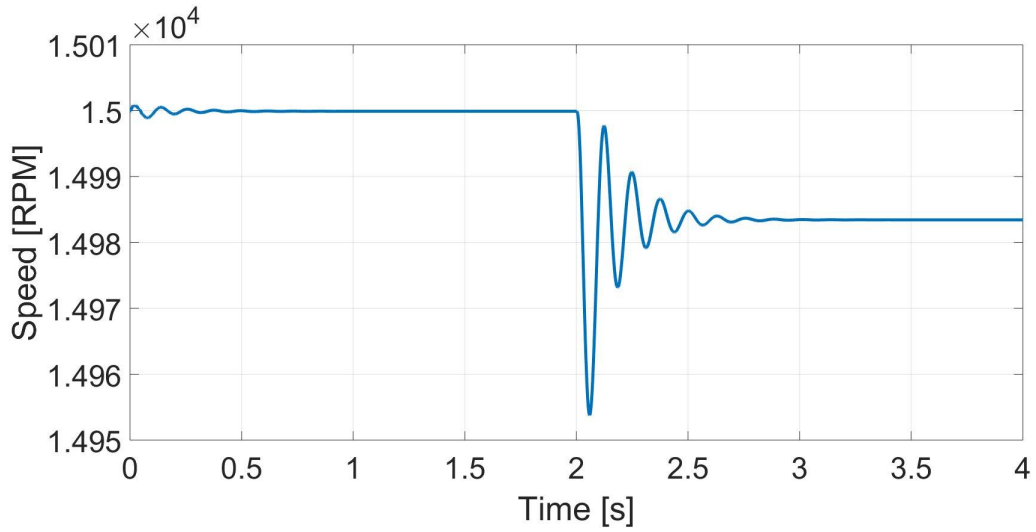


Figure 4.13: Integrated system full load test HSIM speed

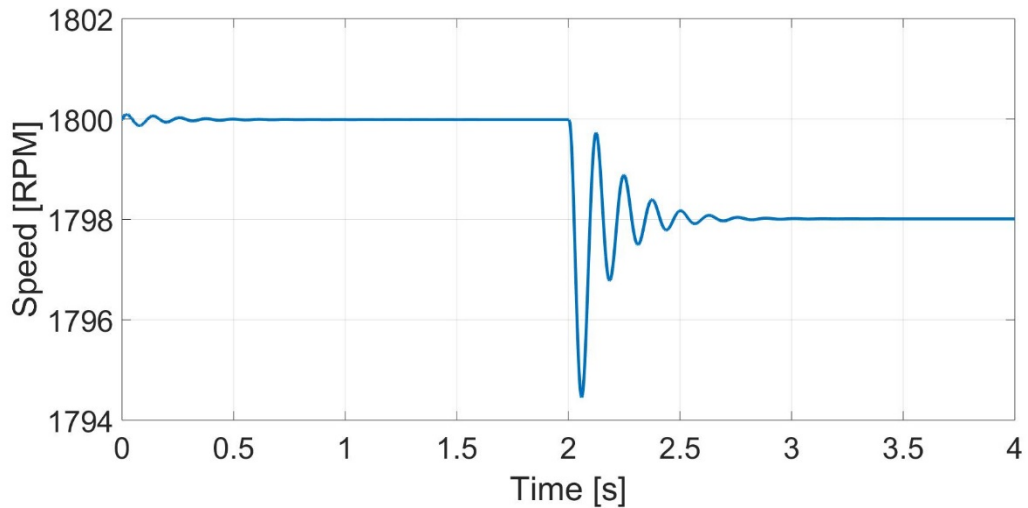


Figure 4.14: Integrated system full load test LSIM speed

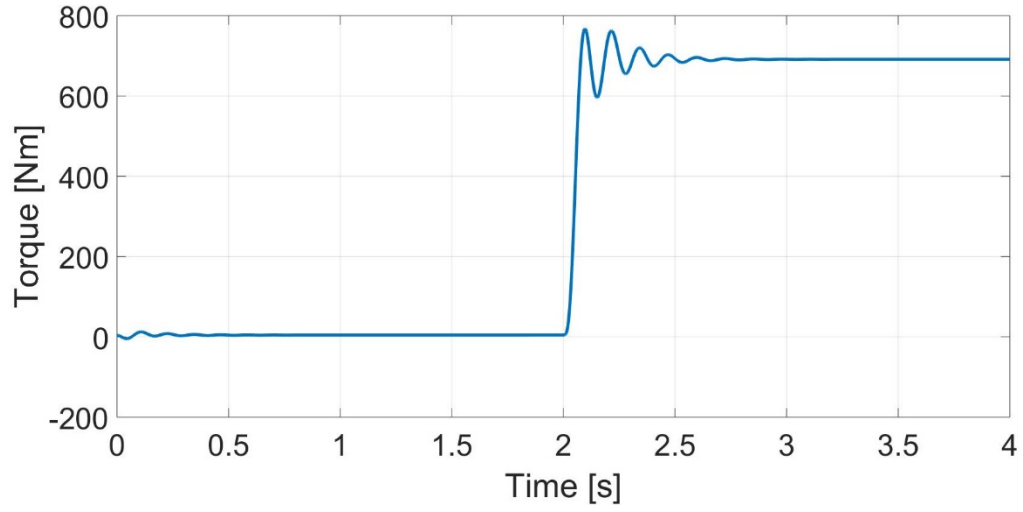


Figure 4.15: Integrated system full load test HSIM torque

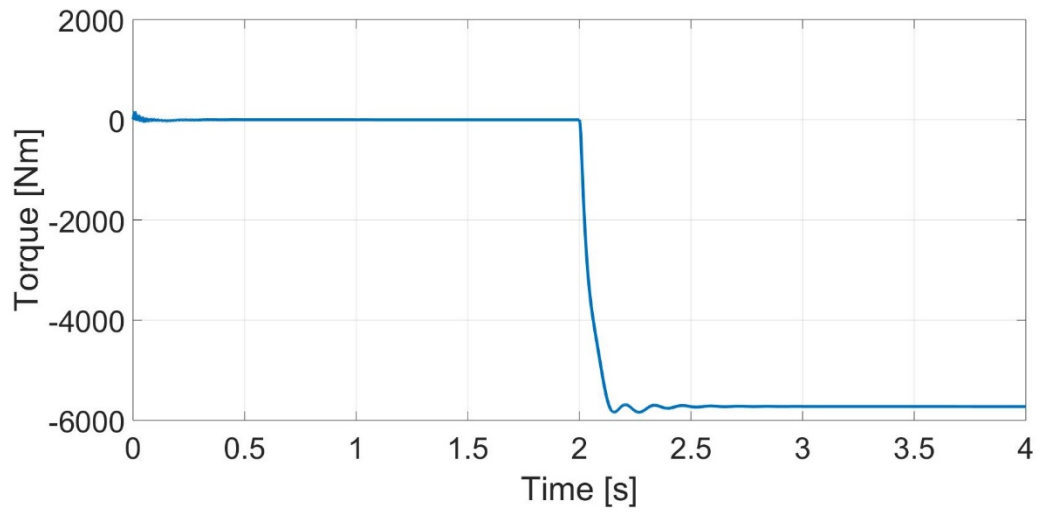


Figure 4.16: Integrated system full load test LSIM torque

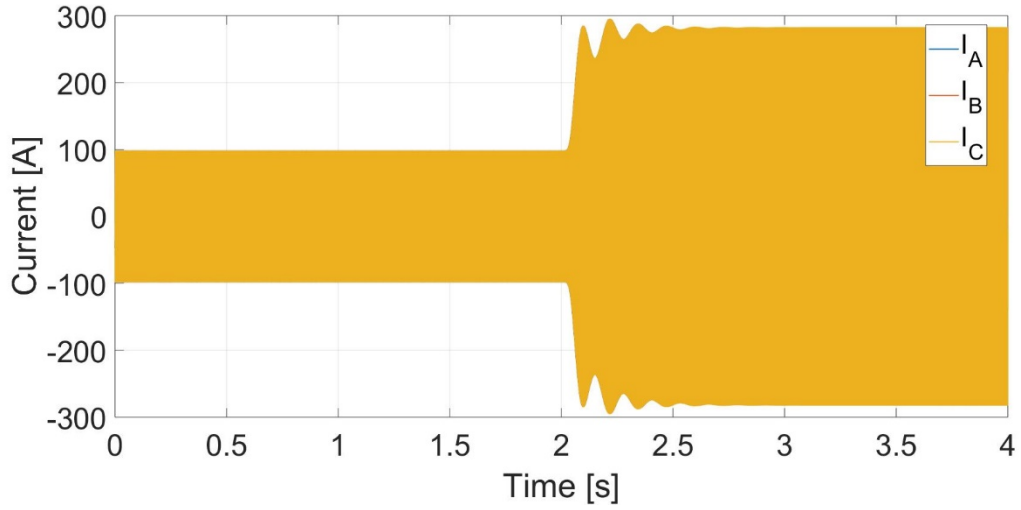


Figure 4.17: Integrated system full load test HSIM current

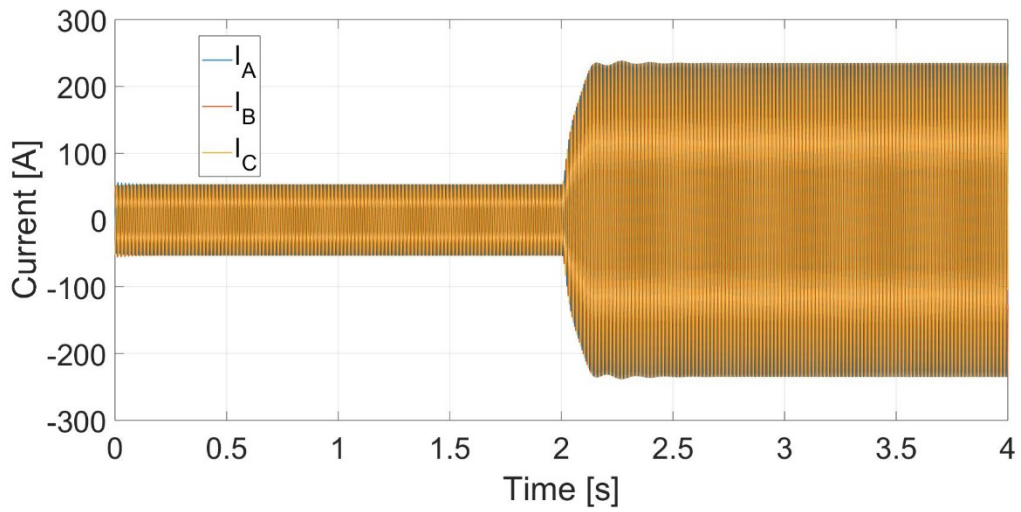


Figure 4.18: Integrated system full load test LSIM current

After full load tests are conducted on the system, trip conditions on both sides of the system are also simulated. These conditions involve testing different response times of the controller and determining a safe rate of driving the system to rest. Tripping of the high speed side of the system is a likely scenario because of its novelty. Through the tuning of

the PI and testing different settings for ramp rates to zero, the system can be driven to a state of rest in 4 seconds based on the current constraint of operating within nominal values. This case can be seen through the control signals in Figure 4.19, Figure 4.20, and Figure 4.21.

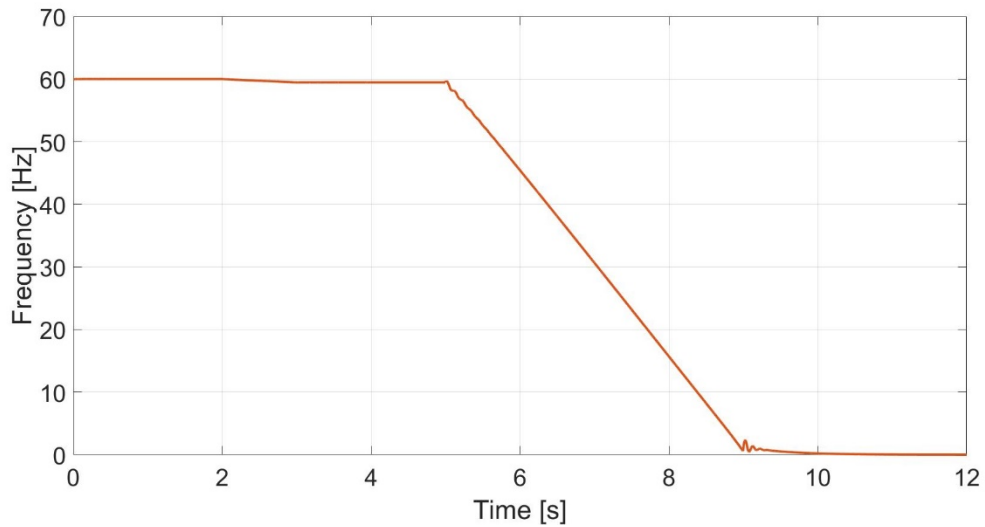


Figure 4.19: HSIM trip frequency reference

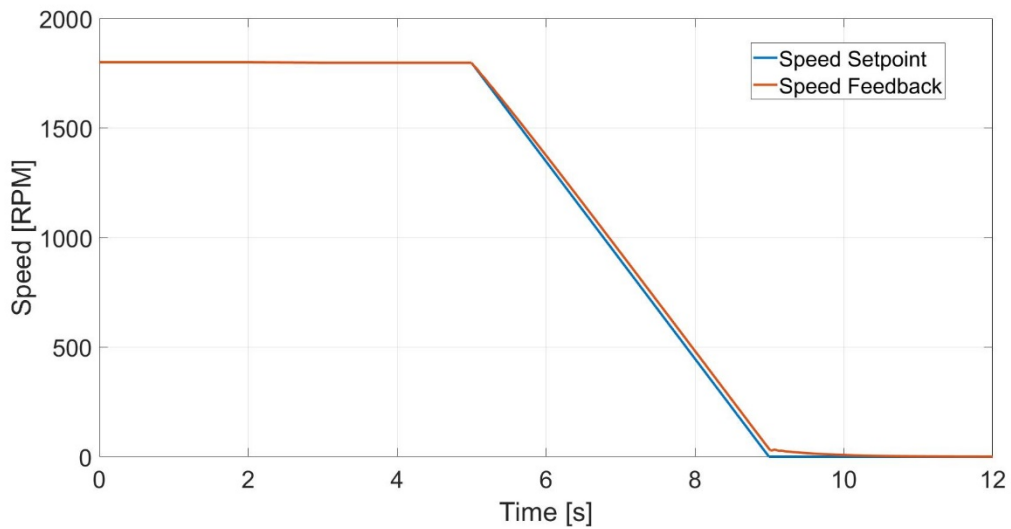


Figure 4.20: HSIM trip speed control



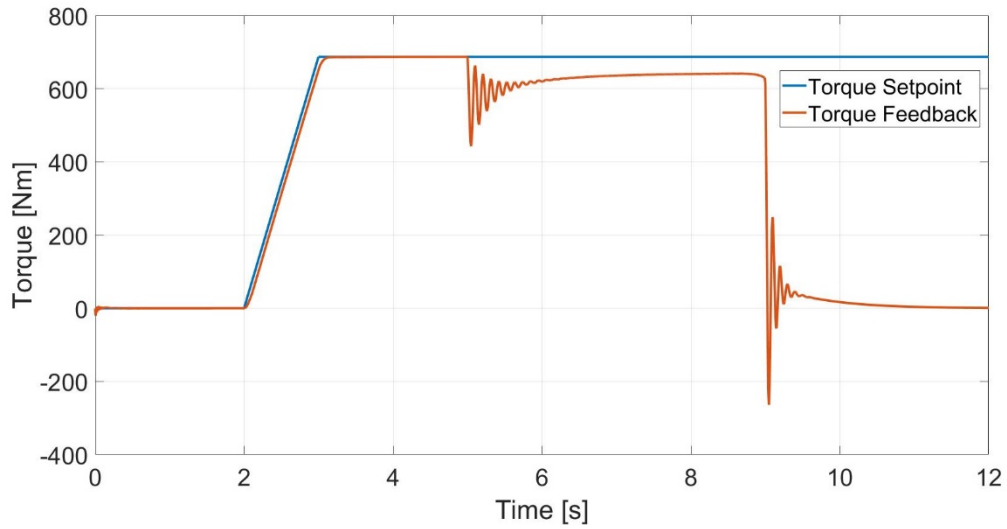


Figure 4.21: HSIM trip torque control

The mechanical response of the motors show the effect of the controls. These behaviors can be seen in Figure 4.22, Figure 4.23, Figure 4.24, and Figure 4.25. The electrical waveforms can be seen in Figure 4.26, Figure 4.27, Figure 4.28, and Figure 4.29.

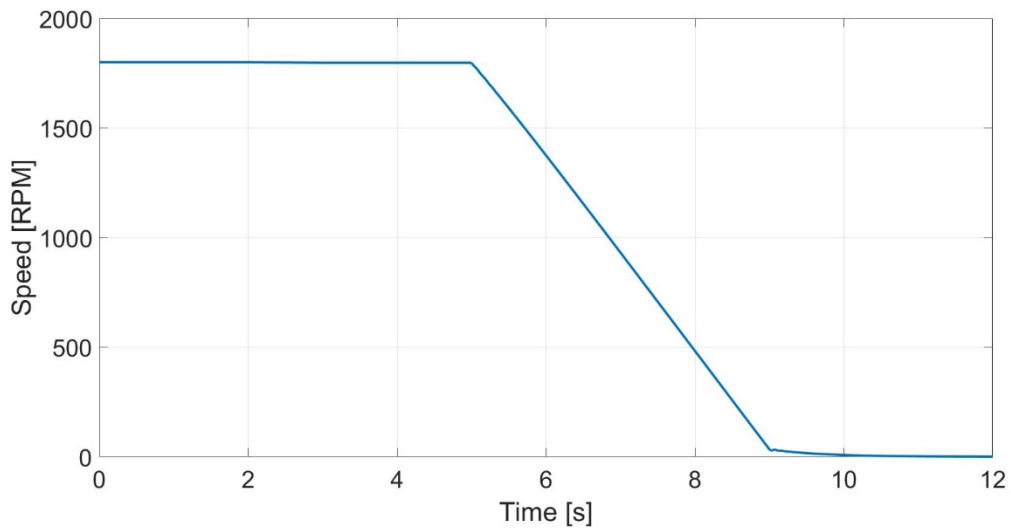


Figure 4.22: HSIM trip LSIM speed

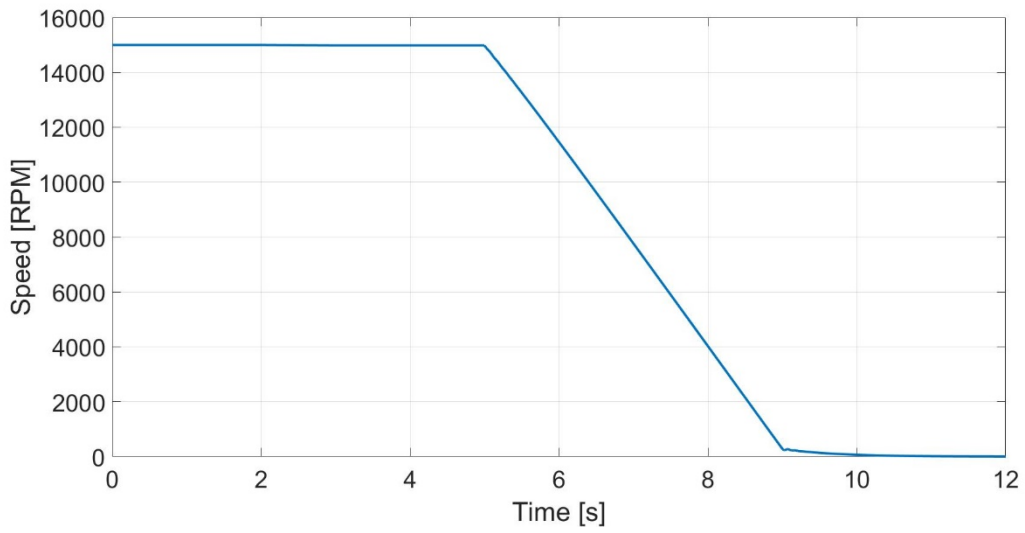


Figure 4.23: HSIM trip HSIM speed

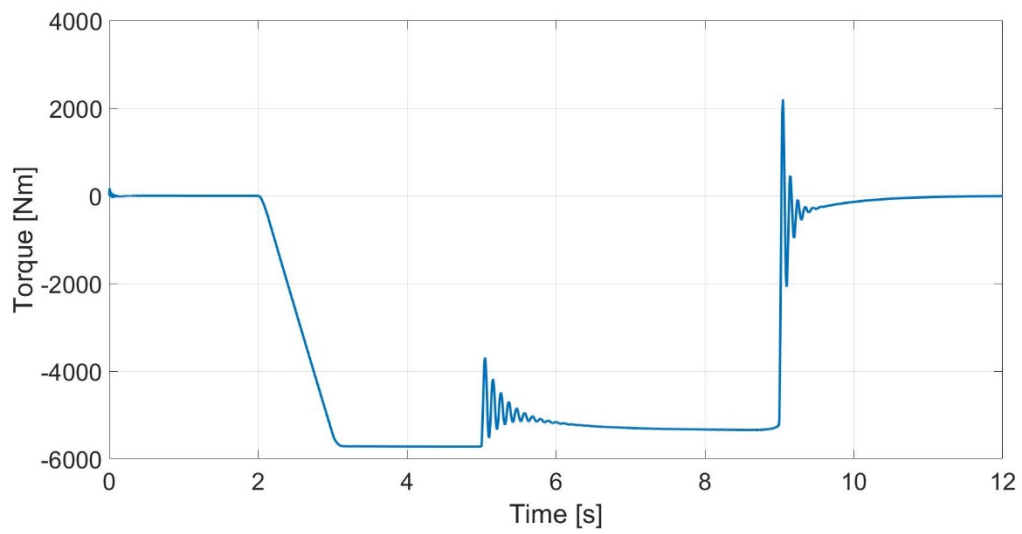


Figure 4.24: HSIM trip LSIM torque

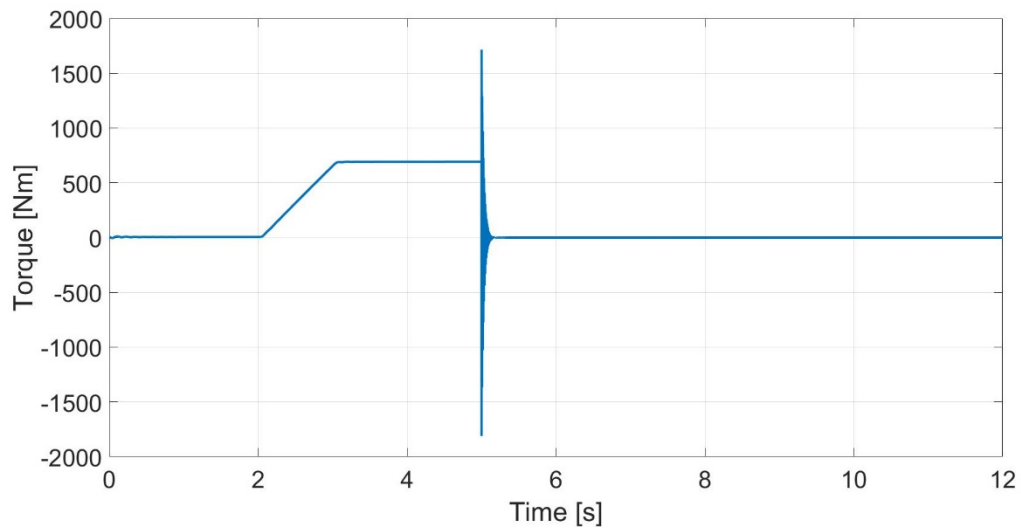


Figure 4.25: HSIM trip HSIM torque

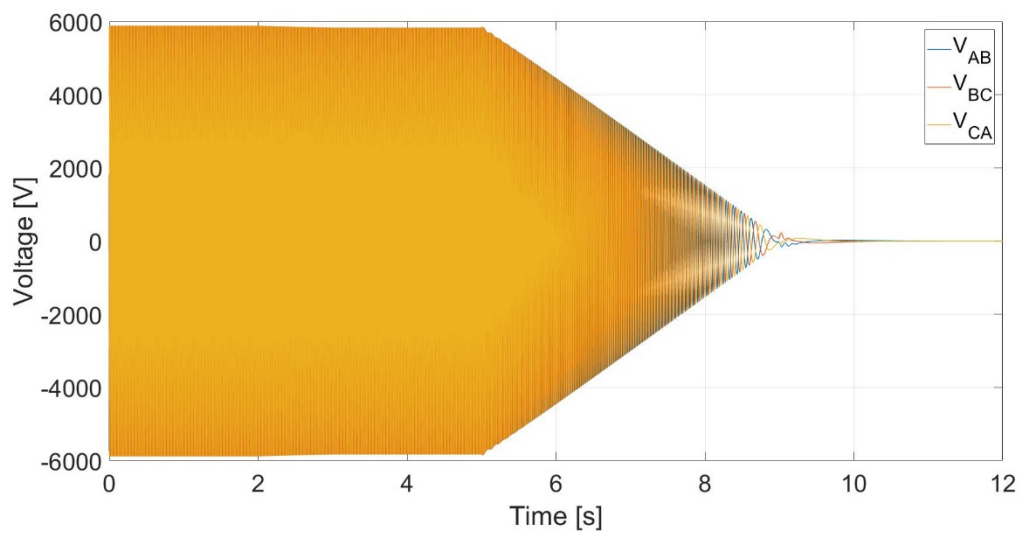


Figure 4.26: HSIM trip LSIM voltage

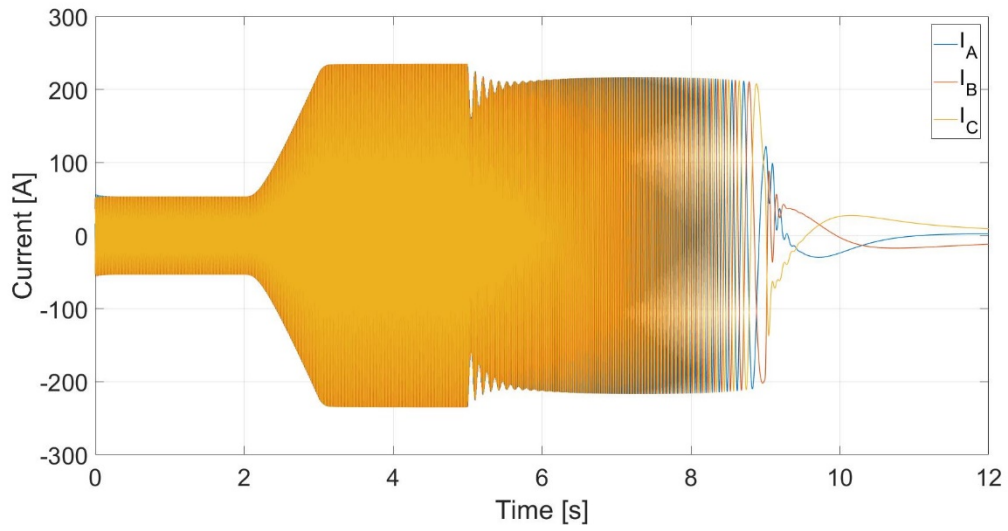


Figure 4.27: HSIM trip LSIM current

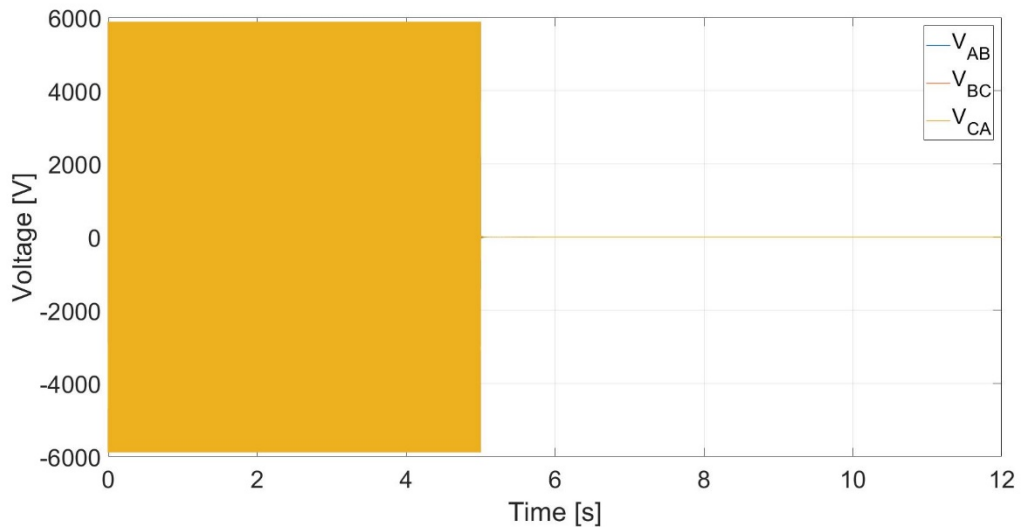


Figure 4.28: HSIM trip HSIM voltage

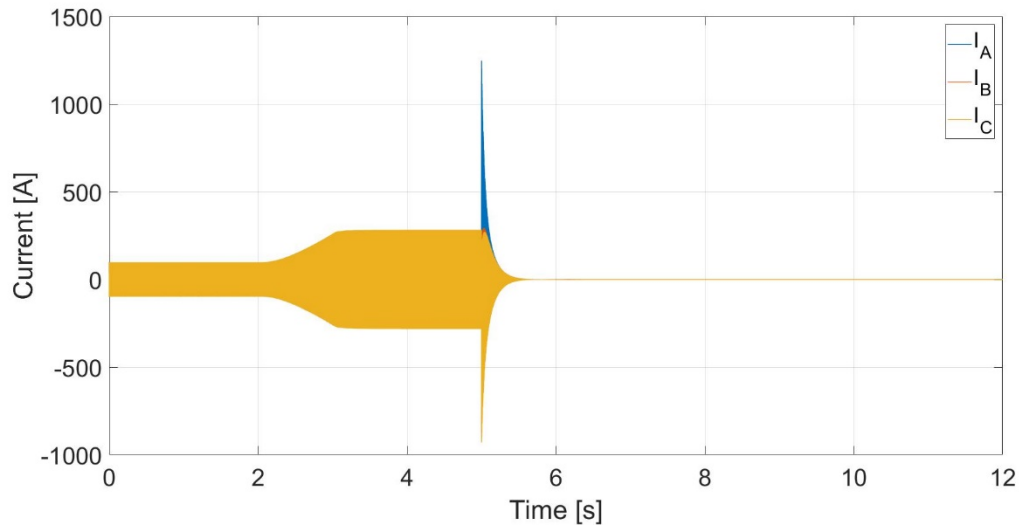


Figure 4.29: HSIM trip HSIM current

### Dynamics

The full load test simulated a successful integrated system operation. The desired ratings were achieved with the prescribed controls. The oscillations in the speed occur due to the controller tuning of the inner speed loop of the LSIM drive. Although these oscillations are not ideal behaviors, the scale at which they occur provides less consequence for the whole system. Also, since the loading of the HSIM is desired, the dynamics of the torque response are much more relevant. The electromagnetic torque plots of the HSIM and LSIM are shown as positive and negative respectively. This designation represents the motoring and generating modes of each motor. The current drawn from the drives of the two motors are also manually kept within the design specifications for the motors through the ramp timing. With an additional current loop, more exact timing of the ramp down can be assessed. This full load test was done with a step load, but initial testing of the actual

equipment can be done with ramped loads to achieve less stress on the electromechanical system.

The HSIM trip test utilizes a ramped load to bring the system to full load operation. This 1 second ramp is smoothly achieved by the designed control system. Once the system is at a full load steady-state, the VSD is tripped and the HSIM is disconnected. In simulation, the large torque and current transients of the HSIM are not entirely realistic. Tripping of the actual system will cause the mechanical potential energy of the HSIM to affect the low speed drive shutdown. Modeling the trip condition through ideal switches leaves certain electrical behaviors unaccounted for, such as induced voltages on the stator from the rotor. However, the LSIM is still driven to continue generating a load on the HSIM rotor shaft to bring the system to rest. This is done by changing the rate at which the shutdown is set to occur. The low speed drive can bring the entire system to rest in about 4 seconds based on the constraint of operation within the device full load current ratings. Increasing this time too much may allow for other equipment failures to occur during the shutdown process. Decreasing this time will burden the LSIM and its drive passed its nominal ratings. The consequences of changing the ramp down time can be observed in Figure 4.30. When setting these parameters for actual testing of the system, caution must be taken to shut the equipment down as quickly as possible, while still maintaining safe operating conditions. The inclusion of a current control loop would allow application of limitations to see how fast the system can be brought to rest.

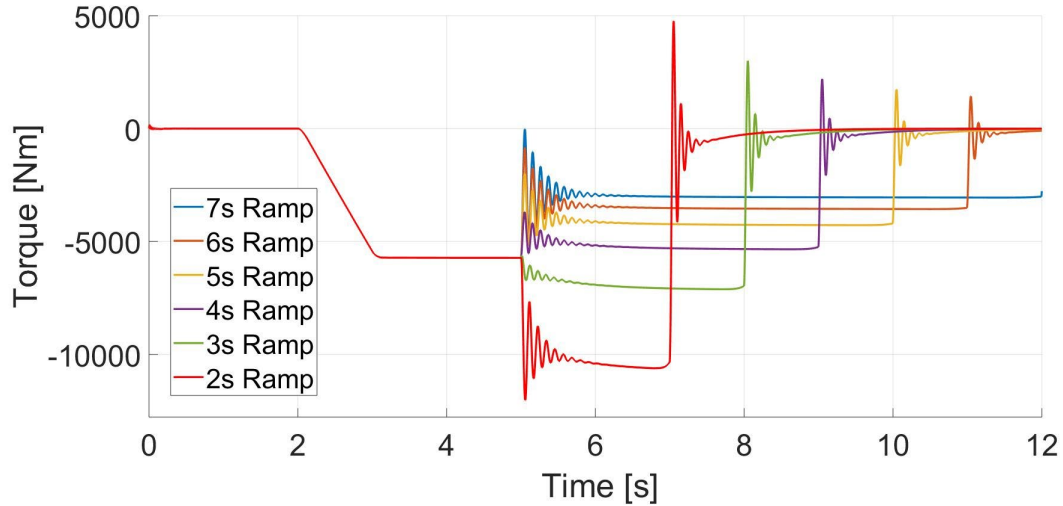


Figure 4.30: HSIM trip LSIM output torque comparison based on ramp to zero speed

### Summary

This chapter gives an overview of the whole system and the modeling efforts done to accurately represent behaviors. The derivation and application of the V/Hz method in a coupled system is expressed through mathematical and control-based means. A PI control method for the low speed drive is given and shown to operate as desired. With the integrated system, a full load can be propounded onto the HSIM through the dynamometer subsystem. Emergency trip tests are also done to evaluate practical considerations for the system protection settings. Adding current limits in the control modeling can allow for stricter determination of ramp rates for the V/Hz method. After integration of the entire system in simulation, the actual prototype devices can be evaluated more efficiently given the software reference. Further testing will lead to improvements that can be made in modeling, accelerating the path to commercialization.

## CHAPTER FIVE

### CONCLUSIONS

Modeling and simulation of the integrated HSI, LSI, gearbox, and the drives provides a useful tool for prediction and validation of a novel system. Individual component models are validated to perform with proposed specifications. Integration of multiple models into a single, time domain based platform allow for simulation of the various interconnected phenomenon of electrical, mechanical, and magnetic domains. Protection and safety concerns are addressed in simulation results, allowing for more efficient testing of the actual system.

The new VSD and HSI will provide significant benefits for the industrial sector after successful evaluations of the prototype. The capabilities of the EIC's MW level dynamometer setup can allow other motor drive systems to be evaluated through comprehensive system tests. This drive integration of WBG devices serves to increase the proven applications and possibilities of the technology. Updates in the standards of motors and drives can be established as this system becomes more commonplace.

Due to project timeline circumstances, the prototype has not been physically tested at the facility. When the system arrives, it will be tested using the simulations presented as reference for operations and commissioning. Startup of the entire system can be simulated to observe interactions between both sides of the system and verify safe operation. The shutdown behaviors exhibited can be used as a benchmark for system protection settings, especially with slew rates for zero speed commands. Other tests can be developed through simulation, such as creating various torque profiles for different loads. Through collected



data of future tests, the models for the devices can be improved to expedite subsequent assessments. Further work will also be done with this VSD and HSIM system in the field of CHP plants. Instead of providing mechanical power, the equipment will be used to operate as a generator. Additional modeling consideration must be done for the VSD to effectively use its AFE.

## APPENDICES

Appendix A  
Excel Validations

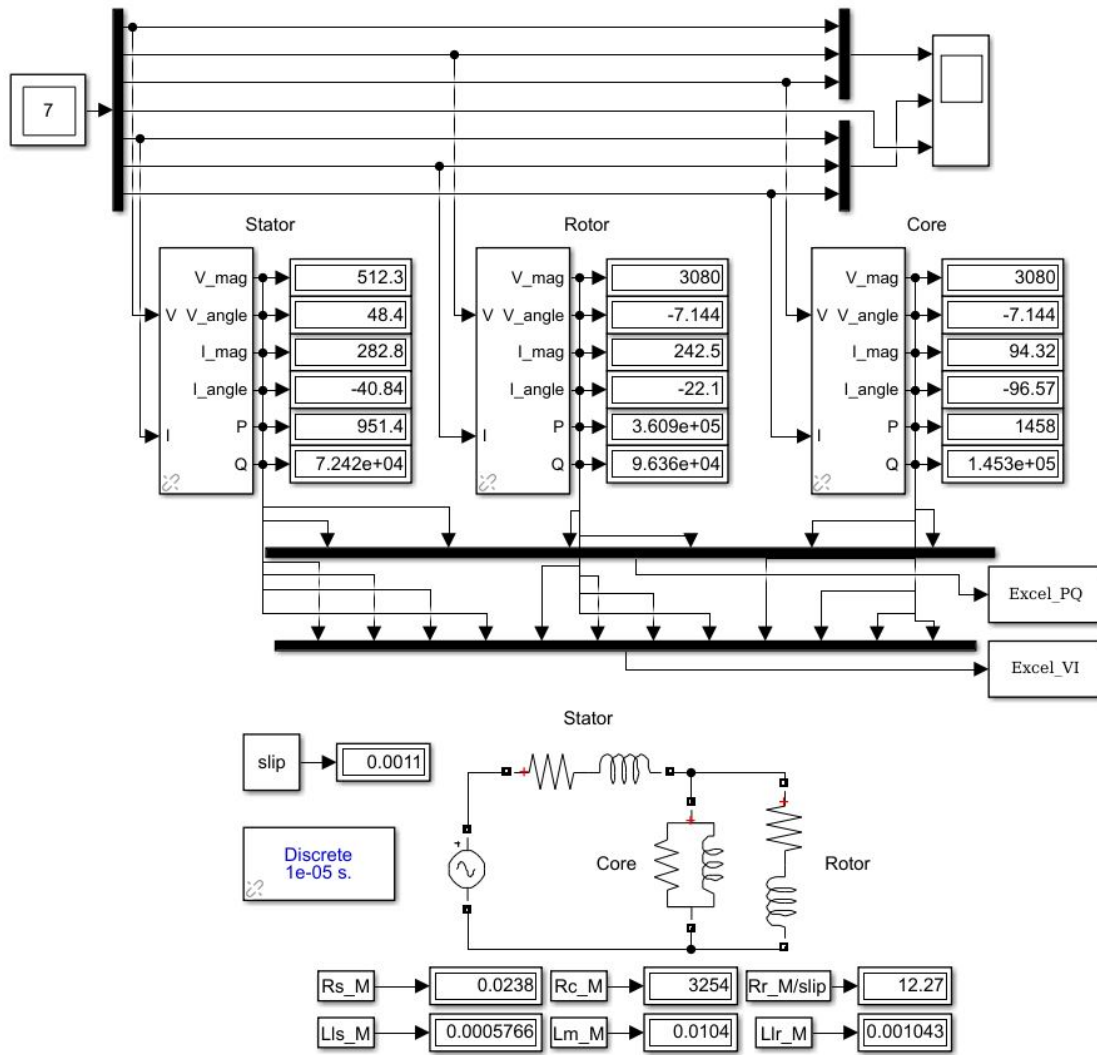


Figure A.1: Model of equivalent circuit model in Simulink

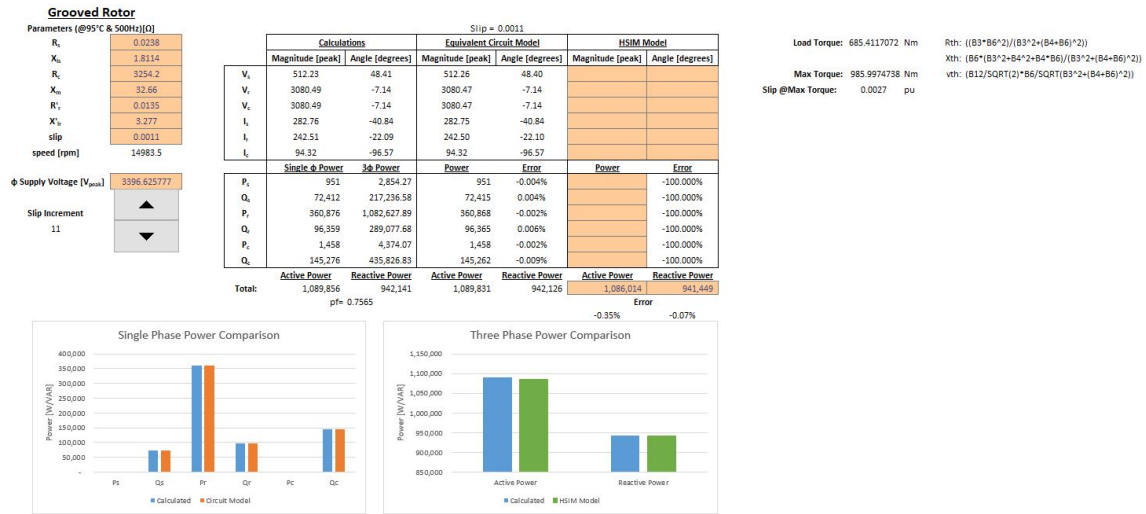


Figure A.2: Spreadsheet for calculations and comparison of equivalent circuit values

## Appendix B

### No-Load Acceleration Tests

Table B.1 No-load acceleration test parameters [12]

|   |                    |       |       |       |       |
|---|--------------------|-------|-------|-------|-------|
| <b>Machine Rating</b>                             | <b>Power [hp]</b>  | 3     | 50    | 500   | 2250  |
|   | <b>Voltage [V]</b> | 220   | 460   | 2300  | 2300  |
|   | <b>Speed [rpm]</b> | 1710  | 1705  | 1773  | 1786  |
| <b><math>\tau_B</math> [N·m]</b>                  |                    | 11.9  | 198   | 1980  | 8900  |
| <b><math>I_B</math> [A]</b>                       |                    | 5.8   | 46.8  | 93.6  | 421.2 |
| <b><math>R_s</math> [<math>\Omega</math>]</b>     |                    | 0.435 | 0.087 | 0.262 | 0.029 |
| <b><math>X_{ls}</math> [<math>\Omega</math>]</b>  |                    | 0.754 | 0.302 | 1.206 | 0.226 |
| <b><math>X_M</math> [<math>\Omega</math>]</b>     |                    | 26.13 | 13.08 | 54.02 | 13.04 |
| <b><math>X'_{lr}</math> [<math>\Omega</math>]</b> |                    | 0.754 | 0.302 | 1.206 | 0.226 |
| <b><math>R'_r</math> [<math>\Omega</math>]</b>    |                    | 0.816 | 0.228 | 0.187 | 0.022 |
| <b><math>J</math> [kg·m<sup>2</sup>]</b>          |                    | 0.089 | 1.662 | 11.06 | 63.87 |

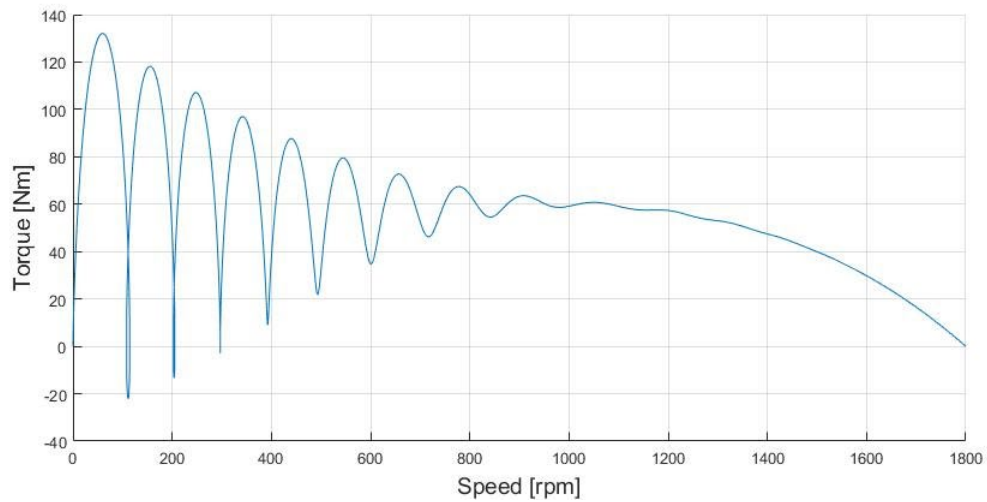


Figure B.1: Torque-speed curve for 3 hp motor

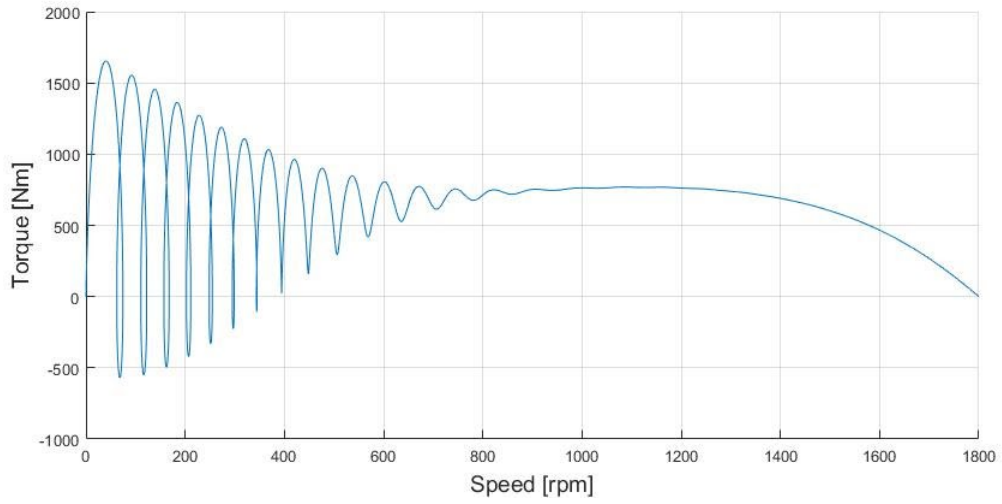


Figure B.2: Torque-speed curve for 50 hp motor

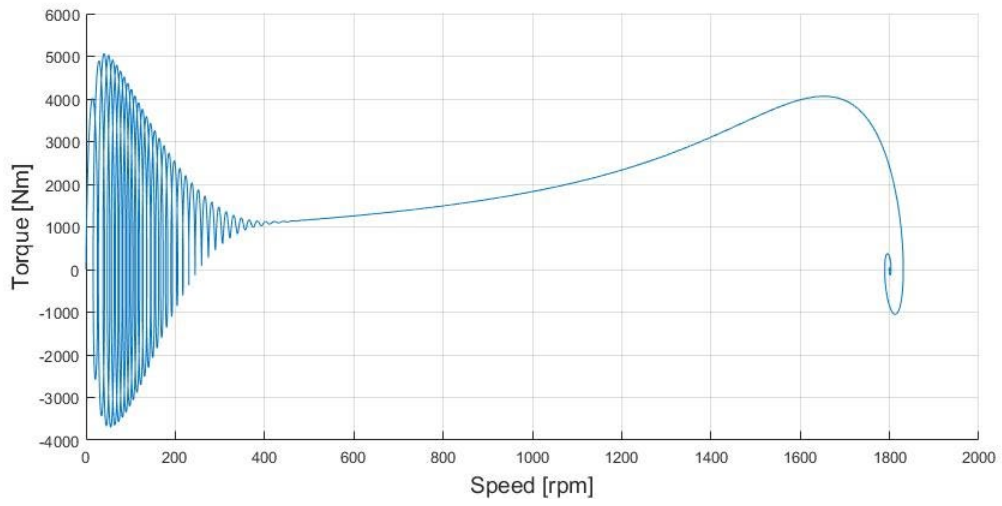


Figure B.3: Torque-speed curve for 500 hp motor

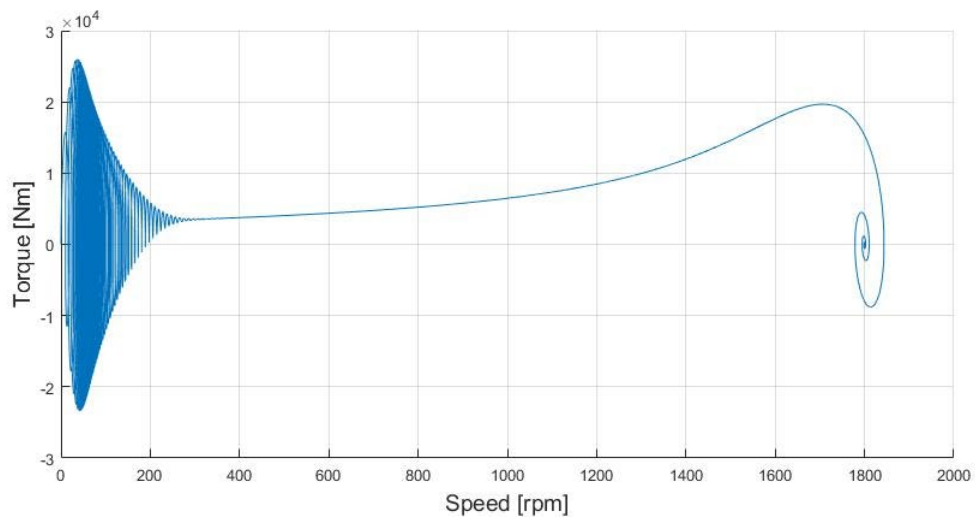


Figure B.4: Torque-speed curve for 2250 hp motor

## Appendix C

### MATLAB Parameter File

```
%%
% Parameters file for PAU_3_Slices.slx & PAU_3_Slices_1100_V.slx
%
% *****
% 3-slice eGRID, High Speed Motor Project
% *****
%%
% Revision History
% 27 Feb 2015 R.Hadidi
% - The source impedance has been updated based on the
% short circuit information provided by the local
% utility.
% - The parameters for step-up and step-down
% transformers have been updated based on their test
% reports.
% 3 March 2015 R.Hadidi
% - Line reactors were added.
% 4 March 2015 R.Hadidi
% - Filter parameters were added.
% - RDN room parameters were added.
% 6 April 2015 R.Hadidi
% - The AFE carrier frequency was changed to 6000Hz.
% - Resistance of the filter inductor was changed to
% 5 m OHM from 150m OHM.
% V2_0 June 2015 IREQ
% - Rectifier Control System + Slice transformer + cube
% model are now inside the library
% "ClemsonControl_lib".
% - PWM carriers for the rectifier 2-level bridges are
% now phase-shifted.
% - New parameters values for the rectifier transformer
% The sampling technique for the inverter PWM
% generators is now "Asymmetrical regular" (double-
% edge).
% - Inverter pulses for slice 5 (6, 7, 8) are identical
% to inverter pulses for slice 1 (2, 3, 4).
%
% October 2015 - Different Vdc_ref settings for each slice is now
% possible
% - Migration to R2015b
% - IGBT deadtime is now modeled
% - 500kW load instead of RDN
% m_nom_inv=0.719; Inverter modulation for Test4
% m_nom_inv=0.839; Inverter modulation index for Open
% circuit Test (Test 3)
%
% August 2017 Dean Millare
% - Create 2 PAU units with 3 slices each
% - Remove impedances to create ideal testing
% - Insert 3-phase inductor between PAUs
% - Adjust scope, measurement, and control system
% blocks to account for new slice topology
% - Created "G" parameters for the "generating" PAU
```



```

%           indented from original parameter
%           > Commented out for testing purposes
%           - Changed Motor parameters for stator and rotor
%           resistance and reactance
February 2018 Dean Millare
%           - No G values for PWM
%           - Four slice Variable Speed Drive
%           - Vdc for 3-slice system is 1100 Vdc
%           - Added IM parameters under "Load" Section
%           - Account for PWM carrier initial phase
%           - Include V/Hz input into Inverter Control
%           - Nominal power set to 1 MW
March 2018 Dean Millare
%           - Added variables for number of slices in drive
%           - Phase shift programmed =
%           (Slice#)*180/(Total#ofSlices)
%           - Parameterized load resistance for load test
%           - Added scopes on model to monitor DC link voltages
%           - Observing all 3 cubes for DC link
%           - Scope to observe individual slice outputs and
%           series combination of slices 3 & 2
%           - Separate frequencies for AFE and power sides
%           - Added scopes to observe control signals for
%           slice 1
April 2018 Dean Millare
%           - Fix Cube C harmonics with higher LPF cutoff
%           frequency value of 2000 instead of 1000
%           - Added RL load (different from R load or L load)
May 2018 Dean Millare
%           - Tested LCL filter on PAU output
%           - Carrier frequencies(inverter & rectifier) set to
%           6kHz
%           - Parameterized rectifier and inverter signal
%           start time
%           - Included variable speed motor parameters
%           - Parameterized phase shift for rectifier control
%           - Parameterized IM model
June 2018 Dean Millare
%           - Identify dead time variable (Td)
July 2018 Dean Millare
%           - Incorporate given inertia value for HSIM
August 2018 Dean Millare
%           - Updated HSIM parameters
%           - Update V/Hz control blocks and parameters
September 2018 Dean Millare
%           - Updated HSIM parameters with grooved rotor
%           - Friction factor accounting for friction and
%           windage
October 2018 Dean Millare
%           - Friction factor made into function of power
%           losses
%           - Modulation index changed for 4160V operation
November 2018 Dean Millare
%           - Updated HSIM power rating from simulation
%           results
%%
clear
clc

```

```

% load IM_Model_Test_High_Speed_IC          % Load initial condition
load IM_Model_Test_High_Speed_IC_2        % Used for
"IM_Model_Test_High_Speed_Closed_Loop"

Fnom = 60;                                % Nominal system frequency (Hz)
    Fnom_G = 60;
F_power = 500;                             % Frequency of machine connected to drive
Slices = 3;                                % Number of slices on high speed drive
    Slices_G = 4;                           % Number of slices on variable speed drive
%
%%
% *****
% Slice Transformer parameters (Active front end)
% *****
% One slice transformer feeds three cubes (A, B & C)
%
Vdc = 1100;                                % DC link voltage (V)
    Vdc_G = 1000;
Pnom_xfo_rec = 1e6;                         % Nominal 3-phase power
    Pnom_xfo_rec_G = 550e3;
Qnom = 750e3;
Vnom_prim_rec = 4.16e3;                     % Nominal primary voltage (Vrms)
    Vnom_prim_rec_G = 4.16e3;
% m_nom_rec = 0.76;                         % Nominal modulation index for rectifier
%     m_nom_rec_G = 0.76;
Vnom_sec_rec = 600;                         % Nominal secondary voltage (V)
    Vnom_sec_rec_G = 600;
%
% Total leakage impedance (Cube A, Cube B and Cube C)
Lxfo_rec_P1 = 0.0609*3*3;                   % Total Leakage inductance - Cube A(pu)
    Lxfo_rec_P1_G = 0.0609*3*3;
Lxfo_rec_P2 = 0.0474*3*3;                   % Total Leakage inductance - Cube B (pu)
    Lxfo_rec_P2_G = 0.0474*3*3;
Lxfo_rec_P3 = 0.0304*3*3;                   % Total Leakage inductance - Cube C(pu)
    Lxfo_rec_P3_G = 0.0304*3*3;

Rxfo_rec_P1 = Lxfo_rec_P1/4;                % Total winding resistance - Cube A (pu)
    Rxfo_rec_P1_G = Lxfo_rec_P1_G/4;
Rxfo_rec_P2 = Lxfo_rec_P2/4;                % Total winding resistance - Cube B (pu)
    Rxfo_rec_P2_G = Lxfo_rec_P2_G/4;
Rxfo_rec_P3 = Lxfo_rec_P3/4;                % Total winding resistance - Cube C (pu)
    Rxfo_rec_P3_G = Lxfo_rec_P3_G/4;
%
Lxfo_prim_rec = 0.000001;                    % Primary leakage inductance
    Lxfo_prim_rec_G = 0.000001;
Rxfo_prim_rec = Lxfo_prim_rec/4;             % Primary winding resistance
    Rxfo_prim_rec_G = Lxfo_prim_rec_G/4;
Lxfo_sec1_rec = Lxfo_rec_P1 - Lxfo_prim_rec; % Secondary 1 leakage inductance
    Lxfo_sec1_rec_G = Lxfo_rec_P1_G - Lxfo_prim_rec_G;
Rxfo_sec1_rec = Rxfo_rec_P1 - Rxfo_prim_rec; % Secondary 1 winding resistance
    Rxfo_sec1_rec_G = Rxfo_rec_P1_G - Rxfo_prim_rec_G;
Lxfo_sec2_rec = Lxfo_rec_P2 - Lxfo_prim_rec; % Secondary 2 leakage inductance
    Lxfo_sec2_rec_G = Lxfo_rec_P2_G - Lxfo_prim_rec_G;
Rxfo_sec2_rec = Rxfo_rec_P2 - Rxfo_prim_rec; % Secondary 2 winding resistance
    Rxfo_sec2_rec_G = Rxfo_rec_P2_G - Rxfo_prim_rec_G;
Lxfo_sec3_rec = Lxfo_rec_P3 - Lxfo_prim_rec; % Secondary 3 leakage inductance
    Lxfo_sec3_rec_G = Lxfo_rec_P3_G - Lxfo_prim_rec_G;
Rxfo_sec3_rec = Rxfo_rec_P3 - Rxfo_prim_rec; % Secondary 3 winding resistance

```

```

    Rxfo_sec3_rec_G = Rxfo_rec_P3_G - Rxfo_prim_rec_G;
%
Rm_rec = 404;                % Magnetization resistance (pu) 1360W at 4.16 kV
    Rm_rec_G = 404;
Lm_rec = 404;                % Magnetization inductance (pu)
    Lm_rec_G = 404;
%
%
%%
% *****
% Cube parameters
% *****
% One cube = One 3-phase 2-level IGBT bridge (rectifier) + DC link + One
%   single-phase H bridge IGBT(inverter)
Pnom_Cube = Pnom_xfo_rec/3; % Cube nominal power
    Pnom_Cube_G = Pnom_xfo_rec_G/3;
Vnom_dc = Vdc;                % Nominal DC link voltage (V)
    Vnom_dc_G = Vdc_G;
Clink = 5.7e-3*5/3;          % PM DC link capacitor (F)(Increase from 6 to 10)
    Clink_G = 5.7e-3;
Vc_Initial = Vnom_dc;        % PM capacitor initial voltage (V)
    Vc_Initial_G = Vnom_dc_G;
%
%
% *****
% Inverter modulation
% *****
m_nom_inv = 1;                % Inverter modulation index
    m_nom_inv_G = 0.839;
%
%*****
% Filter and line reactor parameters
%*****
% Measured and Verified

L_line_reactor = 1e-6;        % Line reactor inductance (H)
    L_line_reactor_G = 120e-6;
R_line_reactor = 1.05e-3;     % Line reactor resistance (ohm)
    R_line_reactor_G = 1.05e-3;
%
%
%%
% Motor Parameters
% =====
%
pf_M = 0.698;                 % pf found through Maxwell 3D simulation
S_nom_M = 1.078e6/pf_M;       % Nominal Power [VA] from simulation results
S_nom_G = 1500*746;           % 1500hp
P_nom_M = S_nom_M*pf_M;
Q_nom_M = S_nom_M*pf_M*tan(acos(pf_M));
V_L_M = Vnom_prim_rec;        % Voltage(line-line) [Vrms]
V_L_G = 4000;
F_M = F_power;                % Frequency [Hz]
F_G = Fnom;
Rs_M = 0.0238;                % Stator Resistance [ohm]
Rs_G = 0.129;
Lls_M = 1.8114/2/pi/F_M;      % Stator Leakage Inductance [H] = 2.48092 [ohm] at
    % 500 Hz referred to stator
Lls_G = 1.772/2/pi/F_G;

```

```

Rr_M = 0.0135; % Rotor Resistance [ohm]
Rr_G = 0.11;
Llr_M = 3.277/2/pi/F_M; % Rotor Inductance [H] = 4.48764 [ohm] at 500 Hz
% referred to stator

Llr_G = 1.861/2/pi/F_G;
Lm_M = 32.66/2/pi/F_M; % Mutual Inductance [H] = 22.8966 [ohm] at 500 Hz
% referred to stator

Lm_G = 61.6/2/pi/F_G;
Rc_M = 3254.2; % Core resistance
Rc_G = 1406;
J_M = 1.39062; % Inertia [kg*m^2] (=33 lb*ft^2)
J_G = 16.986678;
FF_M = 7170/(14983.5*pi/30)^2; % Friction Factor [N*m*s] based on losses
FF_G = 17222/(1784*pi/30)^2;
pp_M = 2; % Pole Pairs
pp_G = 2;
MP_M = 1e+6; % Mechanical Power for Load Flow [W]
MP_G = -1e+6;

%---Initial Conditions---%
s = 1; % Slip
theta = 0; % Theta [deg]
ia = 0; % Phase A current [A]
ib = 0; % Phase B current [A]
ic = 0; % Phase C current [A]
pha = 0; % Phase A shift [deg]
phb = 0; % Phase B shift [deg]
phc = 0; % Phase C shift [deg]

%---Miscellaneous Values---%
Gear = 1800/15000; % Gear Ratio from High Speed to Low Speed [1/N]

%%
% *****
% CONTROL PARAMETERS
% *****
% PWM Carrier Frequency
% =====
Fc_inv = 6000; % Inverter carriers frequency (Hz)
Fc_inv_G = 2000;
Fc_rec = 6000; % Active Front End carrier frequency (Hz)
Fc_rec_G = 6000;

Phase_shift_inv = zeros(1,Slices); % Create a vector for initial phases
Phase_shift_rec = zeros(1,Slices); % of carriers for each slice (deg)
for i = 1:Slices
    Phase_shift_inv(i) = i*180/Slices+90;
    Phase_shift_rec(i) = i*90;
end
clear i

Ts_PWM = 1/(6000*2*4)/50; % PWM generators time step(s)
Ts_Power = Ts_PWM; % SimPowerSystems time step(s)
Ts = Ts_PWM; % Measurement blocks sample time (s)
Td = Ts_PWM*12; % Dead Time for Inverter Control
Sampling_acq = 50; % Decimation for acquired values
Ts_Control = Ts_Power*200; % Control system sample time(s)
%
```

```

% Measurement filters
% =====
Fn_filter_rec = 2000;           % Increased frequency of LPF
    Fn_filter_rec_G = 1000;
Zeta_filter_rec = 1;
    Zeta_filter_rec_G = 1;
FilterPhaseShift60Hz = -6.47;   % Filter phase shift at 60 Hz (deg.)
    FilterPhaseShift60Hz_G = -6.47;
Fn_Notch_rec = 2*F_power;       % Notch filter at second harmonic of frequency
    Fn_Notch_rec_G = Fnom_G*2;
Zeta_Notch_rec = 1.0;
    Zeta_Notch_rec_G = 1;
%
% VDC regulator (VDCreg)
% =====
% Gains:
Kp_VDCreg = 3                   % Proportional gain
    Kp_VDCreg_G = 3;
Ki_VDCreg = 400*.09;           % Integral gain
    Ki_VDCreg_G = 36;
% Limits:
Limits_VDCreg = [ 2, -2];       % Idref output [Upper Lower] limits (pu)
    Limits_VDCreg_G = [2,-2];
%
% Current regulator (Ireg)
% =====
% Feedforward coefficients:
Kbase = (Pnom_Cube/Pnom_xfo_rec); % Power base conversion
    Kbase_G = Pnom_Cube_G/Pnom_xfo_rec_G;
Rff_rec_P1 = Rxfo_rec_P1*Kbase; % Feedforward R (cube A)
    Rff_rec_P1_G = Rxfo_rec_P1_G*Kbase_G;
Lff_rec_P1 = Lxfo_rec_P1*Kbase; % Feedforward L (cube A)
    Lff_rec_P1_G = Lxfo_rec_P1_G*Kbase_G;
Rff_rec_P2 = Rxfo_rec_P2*Kbase; % Feedforward R (cube B)
    Rff_rec_P2_G = Rxfo_rec_P2_G*Kbase_G;
Lff_rec_P2 = Lxfo_rec_P2*Kbase; % Feedforward L (cube B)
    Lff_rec_P2_G = Lxfo_rec_P2_G*Kbase_G;
Rff_rec_P3 = Rxfo_rec_P3*Kbase; % Feedforward R (cube C)
    Rff_rec_P3_G = Rxfo_rec_P3_G*Kbase_G;
Lff_rec_P3 = Lxfo_rec_P3*Kbase; % Feedforward L (cube C)
    Lff_rec_P3_G = Lxfo_rec_P3_G*Kbase_G;
% Gains
Kp_Ireg = 0.1*10;              % Proportional gain
    Kp_Ireg_G = 1;
Ki_Ireg = 8;                   % Integral gain
    Ki_Ireg_G = 8;
% Limits
Limits_Ireg = [ 2, -2];        % Vdq_conv output [Upper Lower] limits (pu)
    Limits_Ireg_G = [2,-2];
%
% V/Hz Inverter Control
% =====
%
BL_rec = 0.01;                 % Start time for rectifier control
BL_inv = 0.5;                  % Start time for inverter control

%---High Speed IM---%
Time_M = [0 BL_inv BL_inv+6 999]; % Time Vector [Begin Start Steady-State End]
V_Magnitude_M = [ 0.075 0.075 1 1]; % Voltage Output [Begin Start End End] (pu)

```

```

F_Magnitude_M = [0 0 F_power F_power]; % Frequency Output [Begin Start End End]
V_Hz_M = V_Magnitude_M(3)/F_Magnitude_M(3);

%---Variable Speed IM---%
Time_G = [0 BL_inv BL_inv+6 999];
V_Magnitude_G = [0 0 1 1];
F_Magnitude_G = [0 0 Fnom_G Fnom_G];
V_Hz_G = V_Magnitude_G(3)/F_Magnitude_G(3);

%%
% Current Limit Flags
% =====
%
VSD_I_lim = 220*sqrt(2); % Peak current limit of VSD
Trip_I_lim = VSD_I_lim*2; % Trip current limit of VSD
%
%%
% End of file

```

Appendix D

Motor Data

Table D.1 HSIM parameter (95°C, 500Hz)

|                            | <b>Grooved Rotor</b> | <b>Smooth Rotor</b> |
|----------------------------|----------------------|---------------------|
| <b>R<sub>s</sub> [Ω]</b>   | 0.0238               | 0.0238              |
| <b>X<sub>ls</sub> [Ω]</b>  | 1.8114               | 1.9998              |
| <b>R'<sub>r</sub> [Ω]</b>  | 0.0135               | 0.0163              |
| <b>X'<sub>lr</sub> [Ω]</b> | 3.277                | 3.43                |
| <b>R<sub>c</sub> [Ω]</b>   | 3254.2               | 945.6               |
| <b>X<sub>m</sub> [Ω]</b>   | 32.66                | 30.1                |
| <b>Slip [-]</b>            | 0.0011               | 0.0014              |

Table D.2 HSIM simulated full load test

|   |   |         |
|---|---|---------|
| <b>Slip [-]</b>                         |   | 0.0011  |
| <b>Output Power [kW]</b>                |   | 1078    |
| <b>Torque [Nm]</b>                      |   | 687     |
| <b>Stator</b>                           | <b>Phase Resistance [<math>\Omega</math>]</b> | 0.02346 |
|   | <b>Current [A]</b>                            | 220     |
|   | <b>Iron Loss [kW]</b>                         | 2.28    |
|   | <b>Teeth Loss [kW]</b>                        | 3.56    |
|   | <b>Copper Loss [kW]</b>                       | 3.4     |
|   | <b>Stray Load Loss [kW]</b>                   | 1.09    |
| <b>Rotor</b>                            | <b>Core Loss [kW]</b>                         | 8.55    |
|   | <b>Cage Loss [kW]</b>                         | 3.79    |
| <b>Friction &amp; Windage Loss [kW]</b> |   | 5.76    |
| <b>Total Loss [kW]</b>                  |   | 36.22   |
| <b>Motor Efficiency [%]</b>             |   | 96.75   |
| <b>Power Factor [-]</b>                 |   | 0.698   |



Table D.3 HSIM locked rotor test (95°C, 500Hz, 2082V)

|   |   |         |
|---|---|---------|
| <b>Slip [-]</b>                         |   | 1       |
| <b>Output Power [kW]</b>                |   | 0       |
| <b>Torque [Nm]</b>                      |   | 32      |
| <b>Stator</b>                           | <b>Phase Resistance [<math>\Omega</math>]</b> | 0.02346 |
|   | <b>Current [A]</b>                            | 250     |
|   | <b>Iron Loss [kW]</b>                         | 0.45    |
|   | <b>Teeth Loss [kW]</b>                        | 0.59    |
|   | <b>Copper Loss [kW]</b>                       | 4.41    |
|   | <b>Stray Load Loss [kW]</b>                   | 1.41    |
| <b>Rotor</b>                            | <b>Core Loss [kW]</b>                         | 36.01   |
|   | <b>Cage Loss [kW]</b>                         | 18.35   |
| <b>Friction &amp; Windage Loss [kW]</b> |   | 5.79    |
| <b>Total Loss [kW]</b>                  |   | 67      |
| <b>Motor Efficiency [%]</b>             |   | 0       |
| <b>Power Factor [-]</b>                 |   | 0       |

Table D.4 LSIM simulation motor parameters

|   |       |
|---|-------|
| <b>Power [hp]</b>   | 1500  |
| <b>Voltage [V]</b>  | 4000  |
| <b><math>R_s</math> [<math>\Omega</math>]</b>                 | 0.129 |
| <b><math>X_{ls}</math> [<math>\Omega</math>]</b>              | 1.772 |
| <b><math>R'_r</math> [<math>\Omega</math>]</b>                | 0.11  |
| <b><math>X'_{lr}</math> [<math>\Omega</math>]</b>             | 1.861 |
| <b><math>R_c</math> [<math>\Omega</math>]</b>                 | 1406  |
| <b><math>X_m</math> [<math>\Omega</math>]</b>                 | 61.6  |
| <b><math>J</math> [<math>\text{kg}\cdot\text{m}^2</math>]</b> | 16.99 |

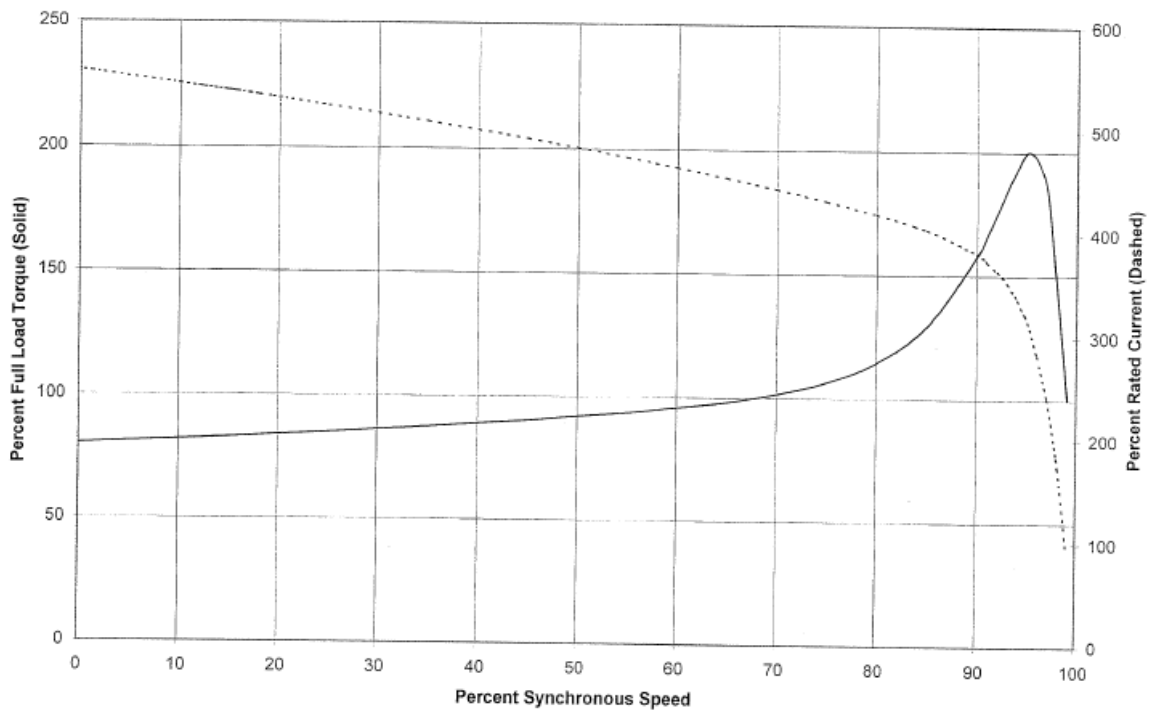


Figure D.1: Percent full load torque and current vs. percent speed

Table D.5 LSIM data

|                            |       |
|----------------------------|-------|
| Full Load Speed [RPM]      | 1784  |
| Full Load Current [A]      | 193   |
| Locked Rotor Current [A]   | 1070  |
| No-Load Current [A]        | 36    |
| Frequency [Hz]             | 60    |
| Full Load Efficiency [%]   | 95.3  |
| Full Load Power Factor [-] | 0.876 |
| Full Load Torque [Nm]      | 5987  |
| Starting Torque [Nm]       | 4790  |
| Breakdown Torque [Nm]      | 11975 |

## REFERENCES

- [1] US Department of Energy (DOE), "Next Generation of Electric Machines: Megawatt Class Motors," *Funding Opportunity Announcement (FOA) number DE-FOA-0001208*, 2015.
- [2] IEEE Std 1547-2005, *IEEE Standard Conformance Test Procedures for Equipment Interconnecting Distributed Resources with Electric Power Systems*, 2005.
- [3] UL Std 1741, *Standards for Inverters, Converters, Controllers and Interconnection System Equipment for Use with Distributed Energy Resources*, 2010.
- [4] H. Karmaker, P. Guedes-Pinto, E. Chen, J. Keck, E. Ledezma and J. C. Fox, "High Speed MW-rated Induction Motor Drive System," in *2017 IEEE International Electric Machines and Drives Conference (IEMDC)*, Miami, 2017.
- [5] J. Leonard, J. C. Fox, R. Hadidi, B. Gislason and M. McKinney, "Experimental PWM Method Validation of a 9-level 4.16 kV Series Connected H-bridge Grid Simulator," in *2016 IEEE Power and Energy Conference at Illinois (PECI)*, Urbana, 2016.
- [6] R. Hadidi, J. Leonard, C. Fox, P. Giroux and R. Gagnon, "Experimental Model Validation of a Multi-Megawatt Grid Simulator to Reduce Risk of Grid Integration Testing," in *15th Wind Integration Workshop*, Vienna, 2016.
- [7] Rockwell Automation, "AC Drives Using PWM Techniques," June 2000. [Online]. Available: [https://literature.rockwellautomation.com/idc/groups/literature/documents/wp/drives-wp002\\_-en-p.pdf](https://literature.rockwellautomation.com/idc/groups/literature/documents/wp/drives-wp002_-en-p.pdf). [Accessed 3 December 2018].
- [8] "AC Drive Theory and Application," May 2008. [Online]. Available: <https://www.eaton.com/ecm/groups/public/@pub/@electrical/documents/content/ap04014005e.pdf>. [Accessed 10 January 2019].
- [9] P. C. Sen, *Principles of Electric Machines and Power Electronics*, Hoboken: John Wiley and Sons, Inc., 2014.
- [10] NEMA Standards Publication MG 1-2009, *Motors and Generators*, Rosslyn: National Electrical Manufacturers Association, 2009.
- [11] IEEE Std 112-2017, *IEEE Standard Test Procedure for Polyphase Induction Motors and Generators*, 2017.
- [12] P. C. Krause, O. Wasynczuk and S. D. Sudhoff, *Analysis of Electric Machinery and Drive Systems*, Hoboken: John Wiley & Sons, 2002, pp. 149-153.
- [13] S. Hegde, S. Angadi and A. Raju, "Speed control of 3-phase induction motor using volt/hertz control for automotive application," in *2016 International Conference on Circuits, Controls, Communications and Computing (I4C)*, Bangalore, 2016.
- [14] Siemens, "AboveNEMA Motors Instruction Manuals," 2014. [Online]. Available: [https://www.industry.usa.siemens.com/drives/us/en/electric-motor/anema-motors/specification/Documents/InstrManual\\_Horiz\\_ODP\\_WPI\\_WPII\\_ANIM-03520pv.pdf](https://www.industry.usa.siemens.com/drives/us/en/electric-motor/anema-motors/specification/Documents/InstrManual_Horiz_ODP_WPI_WPII_ANIM-03520pv.pdf). [Accessed 2018].

- [15] MathWorks, "Asynchronous Machine," [Online]. Available: <https://www.mathworks.com/help/physmod/sps/powersys/ref/asynchronousmachine.html>.
- [16] Z. Zhang, Y. Liu and A. M. Bazzi, "An Improved High-Performance Open-loop V/f Control Method for Induction Machines," in *2017 IEEE Applied Power Electronics Conference and Exposition (APEC)*, Tampa, 2017.
- [17] J. Rodriguez, S. Bernet, B. Wu, J. O. Pontt and S. Kouro, "Multilevel Voltage-Source-Converter Topologies for Industrial Medium-Voltage Drives," *IEEE Transactions on Industrial Electronics*, vol. 54, no. 6, pp. 2930-2945, 2007.
- [18] J. Rodriguez, J.-S. Lai and F. Z. Peng, "Multilevel Inverters: A Survey of Topologies, Controls, and Applications," *IEEE Transactions on Industrial Electronics*, vol. 49, no. 4, pp. 724-738, 2002.
- [19] US Department of Energy (DOE), "Combined Heat and Power (CHP)," *Funding Opportunity Announcement (FOA) number DE-FOA-0001750*, 2018.
- [20] R. Khanna, A. Barchowsky, A. A. Amrhein, W. E. Stanchina, G. F. Reed and Z.-H. Mao, "A Linear Model for Characterizing Transient Behaviour in Wide Bandgap Semiconductor-based Switching Circuits," *International Journal of Automation and Power Engineering*, vol. 5, 2016.
- [21] Cree, "Design Considerations for Designing with Cree SiC Modules Part 1. Understanding the Effects of Parasitic Inductance," 2015. [Online]. Available: <https://www.wolfspeed.com/power/tools-and-support/application-notes>. [Accessed 27 July 2017].
- [22] Z. Zhang, J. Dix, F. Wang, B. J. Blalock, D. Costinett and L. M. Tolbert, "Intelligent Gate Drive for Fast Switching and Crosstalk Suppression of SiC Devices," *IEEE Transactions on Power Electronics*, vol. 32, no. 12, pp. 9319-9332, 2017.
- [23] IEEE Std 1566-2015, *IEEE Standard for Performance of Adjustable-Speed AC Drives Rated 375kW and Larger*, 2015.
- [24] IEEE Std 519-2014, *IEEE Recommended Practice and Requirements for Harmonics Control in Electric Power Systems*, 2014.
- [25] UL 347A-2015, *Standard for Medium Voltage Power Conversion Equipment*, 2015.
- [26] IEC 61800-4, 2002, *Adjustable Speed Electrical Power Drive Systems-Part 4: General Requirements-Rating Specifications for AC Power Drive Systems Above 1000 VAC and Not Exceeding 35 kV*, 2002.
- [27] IEC 61000-3-6, 2008, *Harmonic Emission Limits for Customers Connected to MV, HV and EHV*, 2008.
- [28] D. Millare, R. Hadidi, M. H. McKinney, J. Leonard and J. C. Fox, "Calculations for Asymmetrical Fault Synthesis for Evaluating Ride-Through of Grid Connected Solar Inverters," in *2018 9th IEEE International Symposium on Power Electronics for Distributed Generation Systems (PEDG)*, Charlotte, 2018.

- [29] Clemson University and TECO Westinghouse Motor Company, "Fully Integrated High Speed Megawatt Class Motor and High Frequency Variable Speed Drive System," 2016.
- [30] G. Holmes and T. A. Lipo, "Overmodulation of an Inverter," in *Pulse Width Modulation For Power Converters: Principles and Practice*, Hoboken, John Wiley & Sons, 2003, pp. 349-370.